Title

A RAMAN SCATTERING METHOD FOR HIGH PRECISION COMPARATIVE MEASUREMENTS OF THE OXYGEN CONCENTRATION IN AIR

Authors

Tans, P.P.
Lashof, D.A.

Publication Date

1985-05-01

LBL-19977
UC-37

Lawrence Berkeley Laboratory
UNIVERSITY OF CALIFORNIA

Physics Division

A RAMAN SCATTERING METHOD FOR HIGH PRECISION COMPARATIVE MEASUREMENTS OF THE OXYGEN CONCENTRATION IN AIR

P.P. Tans and D.A. Lashof

May 1985

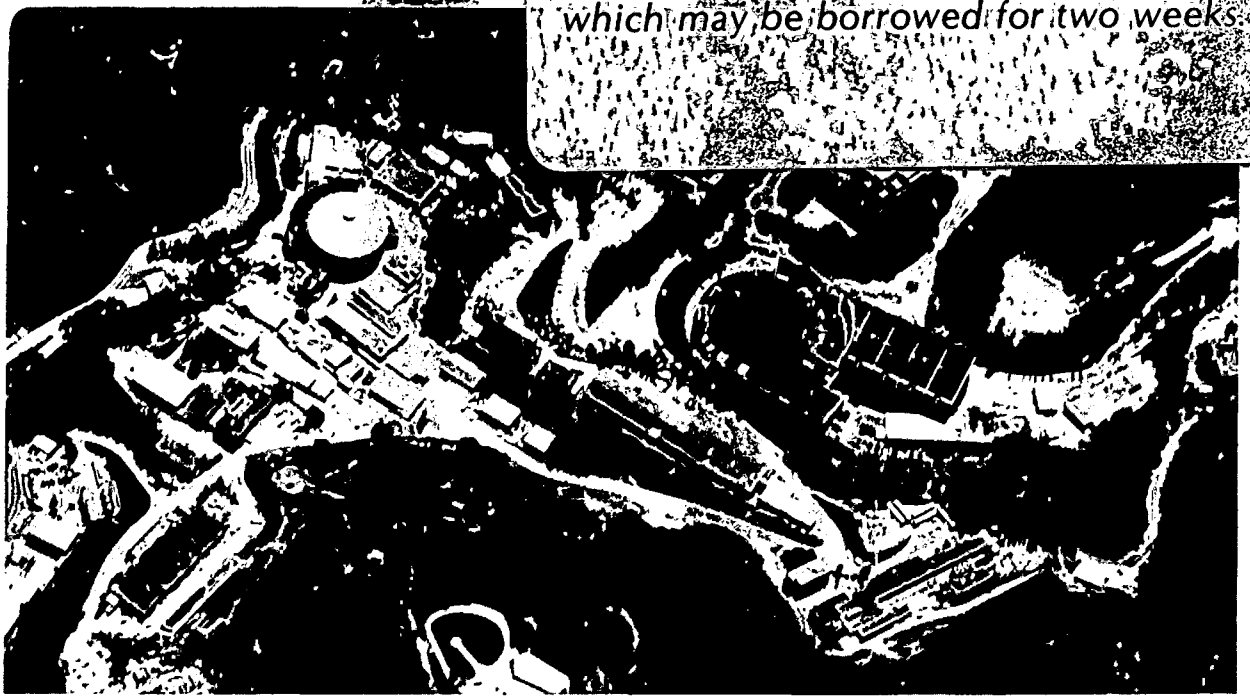

Prepared for the U.S. Department of Energy under Contract DE-AC03-76SF00098

DISCLAIMER

A RAMAN SCATTERING METHOD FOR HIGH PRECISION COMPARATIVE MEASUREMENTS OF THE OXYGEN CONCENTRATION IN AIR.

Pieter P. Tans and Daniel A. Lashof

Lawrence Berkeley Laboratory
University of California
Berkeley, California 94720

ABSTRACT

We describe a method designed to determine relative concentrations of oxygen in air to a few parts per million. The method is based on the comparison of Raman scattering intensities from air in two cells, both of which are placed inside the cavity of an Ar ion laser. The scattered light is channeled through fiber optic light guides into the detectors which consist of dielectric interference filters and photomultiplier tubes. The systematic errors effecting the long-term stability of the intensity comparison are analysed and our efforts to overcome these errors are described.

OUTLINE

ACKNOWLEDGEMENTS

We have enjoyed many helpful discussions with the members of the LBL astrophysics group, especially Frank Crawford, Jordan Kare, Don Morris, Richard Muller and Jim Welch. Richard Muller generously allowed us to work outside of the mainstream of his group and encouraged us to pursue our own research interests. John Yamada built may of the electronic and mechanical subsystems with great care. Stewart Bloom contributed many ideas as a co-investigator during the first stages of this project. The first tests were done in his laboratory at the Lawrence Livermore National Laboratory. We are grateful to the Chevron Research Corporation of Richmond, CA for providing to us on long-term loan some crucial equipment, such as a spectrometer and the laser. The main supporter of this work has been Lester Machta of the NOAA Air Resources Laboratory through grant number NA 81 RAG 00250 to the Lawrence Berkeley Laboratory.

This manuscript has been authored by a contractor of the U.S. government under contract number DEAC03-76SF00098. Accordingly, the U.S. government retains a non-exclusive royalty-free licence to publish or reproduce the published form of this contribution or allow others to do so for U.S. government purposes.

I. PURPOSE OF THE MEASUREMENT

Our interest in making precise measurements of the oxygen concentration in air arises from the desire to improve our understanding of the global carbon cycle. The burning of fossil fuels and the clearing of tropical forests result in the release of large amounts of carbon dioxide to the atmosphere. As a result, the globally averaged CO_2 concentration is rising by a little more than one part per million (ppm) per year. There is a general consensus among scientists that the amount of CO_2 in the atmosphere is an important determinant of the earth's climate, because CO_2 is a strong absorber of infrared radiation.

There are large uncertainties in several key components of the predictions of future CO_2 levels and the ensueing climate changes.[1] These uncertainties fall naturally into three categories. First, at what rate is mankind going to burn its fossil fuels and how will we manage our agricultural and forest lands? The second category concerns the global carbon cycle. How are the natural systems reacting to the input of CO_2 into the atmosphere; which fraction of the CO_2 finds its way elsewhere and on what timescale? The third category assumes a certain level of atmospheric CO_2 and tries to predict, sometimes with very elaborate computer models, the consequences for the earth's climate systems.

Our measurements directly address an important unsolved problem in the carbon cycle, namely whether the total amount of carbon locked up in terrestrial plants is presently increasing or decreasing. Careful accounting of world-wide coal, oil and natural gas production shows that the present rate of fossil fuel combustion amounts to about 5 gigatons of carbon per year[2]. During the past decade, various estimates have been made of the additional carbon added to the atmosphere due to human land use patterns. These have varied between a net global release of carbon from plant biomass of 8 gigatons per year to a net uptake of 1 gigaton.[3-6]. The problem with such estimates is the

incredible inhomogeneity and diversity of plant communities, soils and climates. Since the increase being measured in the atmosphere corresponds to roughly 2 gigatons of carbon per year, there must be additional sinks for between 11 and 2 gigatons, depending on the role of the biosphere. One significant CO_2 sink is dissolution in the world's oceans, but most oceanographers find it very hard to believe that the oceans could take up much more than 2 to 3 gigatons per year[7]. Since no other large carbon sinks are known, they suggest that the storage of carbon in temperate latitudes forests must at least compensate for losses in the tropics.

Sufficiently precise measurements of the global oxygen concentration would settle this question by circumventing the heterogeneity found at the ecosystem level. We can state the idea of the oxygen measurements in a schematic way as follows. If all the generated CO_2 were to dissolve in the oceans, the atmosphere would lose one oxygen molecule for every carbon atom. If, on the other hand, plants assimilate the CO_2 through photosynthesis, the carbon is bound in tissue and the oxygen released again to the atmosphere. Since oxygen is only slightly soluble in water, almost all of the free oxygen on the surface of the earth is present in the atmosphere. Therefore, after correcting for the (known) oxygen consumption during fossil fuel combustion, changes in the amount of atmospheric oxygen depend upon how the storage of carbon in plants is evolving. In this way, very precise oxygen measurements can tell us to what extent both uptake processes, dissolution of CO_2 in the oceans or photosynthesis in plants, are effective in absorbing the CO_2 generated by man's activities. A great advantage of this method is that the atmosphere is very homogeneous and well mixed on the timescale of interest, so that it integrates the combined effects of all the various sources and sinks. Thus, oxygen measurements with a precision on the order of 1 ppm would be instrumenmtal to improving our ability to predict future atmospheric CO_2 concentrations. This type of measurement was first attempted by Machta and Hughes with a modified Beckman oxygen analyser[8].

Their method achieved a precision of 15 ppm, which was not considered quite sufficient for the problem at hand.

II. DESCRIPTION OF THE APPARATUS

A. Choice of Raman Scattering

The expected change in the global atmospheric oxygen level is on the order of a few parts per million (ppm) per year, out of a total concentration of about 21%, or 210,000 ppm. The amount of oxygen in a volume of any air sample will be proportional to the total density of that sample, therefore, any oxygen measurement will have to be normalized to the sample density in order to obtain a concentration. Thus, the determination of the air density in the sample has to be at least as precise as the oxygen measurement. Since the measurements have to address minute long term changes in the atmospheric composition, it is also important to choose a method that allows, at least in principle, the maintenance of comparison standards.

Spontaneous Raman scattering meets the above criteria. It was first suggested for this type of measurement by Schwiesow and Derr[9]. The incident (laser) light excites rotational-vibrational levels in the air molecules. Different molecules have different rotational-vibrational energies. The Raman light is inelastically scattered from these molecules; it has lost some of its energy in the excitation of the molecule. The precise amount of energy lost is characteristic of the molecule. As a consequence, the frequency shift of the Raman scattered light is also molecule-specific. With spontaneous Raman scattering one can look at the light scattered from the beam simultaneously at several frequencies. We have chosen to look at oxygen, nitrogen and carbon dioxide. Nitrogen serves as a natural density calibration of the measurements since it is both abundant and stable in the atmosphere.

The other outstanding feature of Raman scattering is that it does not affect the sample in any way. The air is highly transparent at 514 nm, the frequency of incident light. There is no heating of the sample and no molecules are destroyed or made

reactive. This makes it possible to maintain standards indefinitely in cells that never have to be opened.

The only serious drawback of Raman scattering is its low cross-section, about 4.5×10^{-31} cm^2/sterrad for oxygen and nitrogen at 514 nm. This leads to integration times on the order of one day to be able to reach a precision of one part per million in the oxygen concentration.

B. Changes in Oxygen as a Ratio of Ratios

Raman scattering cannot be used to determine the absolute concentration of a molecular species to great precision. The cross section is not known better than to two decimal places. It is also very difficult to determine in absolute terms the solid angle collected, the transmission of all optical elements and the quantum efficiency of the detector. Since we are interested only in small differences, not absolute amounts, we can compare the amount of oxygen in a sample to that of a standard. Because we need to normalise for density, we measure the ratio of oxygen to nitrogen in a sample and compare that to the ratio of oxygen to nitrogen in a standard.

This is achieved by putting the standard and the sample in the beam simultaneously. The detectors then receive signals of almost equal magnitude when the sample and the standard are interchanged rapidly by an optical chopper. The chopping is fast enough to ensure that the precision is not limited by 1/f noise in the detector-amplifier-discriminator chain.

C. Optical Fibers

Accomplishing this measurement requires a stable method for alternately directing light from the standard and sample into the separate detectors for each molecular species. The reason for constructing this device from optical fibers will become clear by

analysing why our earlier attempt with more conventional optics failed. That set-up was built and tested as shown in fig. 1. The 45° beamsplitter (S) divides both incoming beams into two equally intense beams, one that is analysed for oxygen, and the other that is analysed for nitrogen. The choppers ensure that either the incoming beam from the standard (unprimed) is admitted to the beamsplitter or the beam that comes from the sample (primed).

We measure the ratio

$$\frac{O_2/O_2'}{N_2/N_2'}$$

When we flow the same air through both the STD and UNK location, that ratio (which is close to 1.0) should remain stable for many days. If we define T and R as, respectively, the transmissivity and the reflectivity (T+R= 1) of the beamsplitter (S) we see from fig. 1 that the above defined ratio depends, among other things, on T^2/R^2. In this case, then, taking a ratio of two signals does not result in a cancellation of errors when the reflectivity of the beamsplitter changes. We found that we were measuring small changes of the reflectivity of the beamsplitter as a function of temperature and humidity, instead of small relative changes in gas concentrations.

The fiberoptic beamsplitter and/or lightmixer is depicted schematically in fig. 2. The laser beam steering optics, the spherical reflecting mirrors for Raman scattered light and the Canon lenses have not been changed from the initial set up. Light scattered from the beam in both locations is focussed by a camera lens, followed by an achromat, into a line image on the face of a lucite lightguide. The lucite sheet is 20 cm long and slightly tapered. The light is very much defocussed when it leaves the lucite and enters the optical fibers, thus uniformly illuminating them. The glass fibers at this end are in the form of 40 fused fiber bundles, with each bundle containing about 400 fibers. The bundles coming from the UNK and STD locations are

then brought together and intermixed in a checkerboard pattern, which abuts a rectangular lucite lightguide. The lucite bar has a length of 58 cm, allowing light from both entrance locations to mix before entering a new set of glass fibers. These fibers are initially intimately mixed but separate out into 4 separate bundles, each going to a different passband filter and detector. A special effort has been made at each stage to let the light "forget where it came from". Each of the four separate bundles at the back end has been internally scrambled, so that light from, say, the upper left corner of the lucite mixing bar ends up spread out over the entire output face of each of the four bundles.

This device is inherently stable because of a combination of design features. First, it relies on transmission only, which implies that each lightguide carries two or more signals, the ratio of which is taken when the data are analyzed. Second, there are a large number of individual fibers which are very uniformly illuminated because of the large mixing distances incorporated in the lucite light guides. We can put the idea in mathematical terms by adopting the following notation:

$\frac{d\sigma}{d\Omega}(O)$, $\frac{d\sigma}{d\Omega}(N)$	Differential Raman scattering cross sections
N_2, O_2	Concentration of N_2 and O_2
$T_f(O)$,$T_f(N)$	Transmission of front end optics, including Solid angle acceptance
$T_b(O)$, $T_b(N)$	Transmission of back end optics (after rectangular lucite mixing bar) including the filter and the quantum efficiency of the detector.

Primed quantities again refer to the "unknown" and unprimed to the "standard" side. The tuning fork choppers (CH in fig. 2) alternately transmit unknown or standard at a frequency of about 36 Hz. The counting rate for oxygen in the standard (for example) is proportional to:

$$R(0) = \frac{d\sigma}{d\Omega}(0) * O_2 * T_f(0) * T_b(0)$$

We record the ratios of 4 channels:

$$\frac{R'(0)/R(0)}{R'(N)/R(N)} = \frac{\frac{d\sigma}{d\Omega}(0) * O'_2 * T'_f(0) * T'_b(0)}{\frac{d\sigma}{d\Omega}(0) * O_2 * T_f(N) * T_b(N)} * \frac{\frac{d\sigma}{d\Omega}(N) * N_2 * T_f(N) * T_b(N)}{\frac{d\sigma}{d\Omega}(N) * N'_2 * T'_f(N) * T'_b(N)}$$

$$= \frac{O'_2/O_2}{N'_2/N_2} * \frac{T'_f(0)/T'_f(N)}{T_f(0)/T_f(N)} * \frac{T'_b(0)/T'_b(N)}{T_b(0)/T_b(N)}$$

In the ideal apparatus, the latter two groups of factors containing the transmissions will be identical to 1. For instance, if the lucite mixing bar had "infinite" length it would not make any difference whether the light entering the fibers at the back end had originated from standard or unknown. Then we would have $T'_b(0)=T_b(0)$ and $T'_b(N)=T_b(N)$. In actual practice, these groups of factors are slightly different from 1. Stability is achieved because corresponding transmission factors change together, so that their ratio is not affected. Thus, if a front end fiber on the unknown side breaks, for example, $T'_f(0)$ and $T'_f(N)$ will both be reduced by (almost) the same factor. This is realized to the extent that the optics and the fibers are uniformly illuminated. This problem is analysed further in the section on systematic errors.

D. Counting Statistics

The number of photons per second Raman scattered by oxygen entering our optics will be equal to:

$$n_{ph} * \frac{d\sigma}{d\Omega}(0) * \Omega * L * O_2$$

with:

n_{ph} = $2.5*10^{18}$ photons/sec for one watt of laser power

$\frac{d\sigma}{d\Omega}(0)$ = $4.3*10^{-31}$ cm^2/sterrad

Ω = 0.45 sterrad, including reflection off the spherical mirror

L = 2.5 cm, the length of laser beam imaged

O_2 = $0.21*2.7*10^{19}$ molecules/cm^3 for one atm of air pressure

This equals $5.3*10^6$ photons per second per watt of laser power per atmosphere of gas pressure. We obtain the number of single photon counts per second produced by the photomultiplier by multiplying by the transmission of the lenses, Rayleigh blocking filters (Schott OG 530), lucite, optical fibers, bandpass filters (0.3), and the quantum efficiency of the PMTs (0.08). All these combine to an overall efficiency factor of about $4*10^{-3}$, so that we have $2.5*10^4$ counts sec^{-1} $watt^{-1}$ atm^{-1}. The counting rate for nitrogen is only a little higher than for oxygen because, although there is four times as much in the sample, we devote only half as many output fibers to nitrogen and the detector quantum efficiency is lower at the wavelength of nitrogen.

The typical laser power (intracavity, light going in both directions) is about 100 watts, and the gas pressure in the sample tubes is 10 ato, so that we have $25*10^6$ counts per sec for oxygen.

For an ideal apparatus the precision is limited by photon statistics. We employ fast photomultipliers with high counting rates because they give a better signal to noise ratio than large area photovoltaic detectors, despite the lower quantum efficiency of the photomultipliers. The Raman scattering of a photon is a random event. Likewise, absorption in the optics or the liberation of a photoelectron at the photocathode is determined by chance. Ideally, the arrival of pulses at the photomultiplier output is governed by Poisson statistics, in which case the standard deviation of the total number of counts (n) is equal to the square root of the total number $(n)^{1/2}$. The uncertainties in each of the four counting channels are independent and contribute to the total measurement error in the ratios. Let $\sigma(x)$ stand for one standard deviation of the variable x. Using the notation introduced above tR'(0) is then the number of counts for oxygen in the "unknown" location after t seconds. We denote that by n'(0).

$$Q = \frac{tR'(O)/tR(O)}{tR'(N)/tR(N)} = \frac{n'(O)/n(O)}{n'(N)/n(N)}$$

The uncertainty in Q can be obtained by standard methods:

$$\sigma^2(Q) = \left|\frac{\partial Q}{\partial n'(O)}\right|^2 \sigma^2(n'(O)) + \left|\frac{\partial Q}{\partial n(N)}\right|^2 \sigma^2(n(N)) + \cdots\cdots$$

$$\left|\frac{\sigma(Q)}{Q}\right|^2 = \frac{\sigma^2(n'(O))}{n'^2(O)} + \frac{\sigma^2(n(N))}{n'^2(N)}$$

$$= \frac{1}{n'(O)} + \frac{1}{n(N)} + \frac{1}{n(O)} + \frac{1}{n'(N)}$$

Because the counting rates for unknown and standard are very nearly the same, we have

$$\left|\frac{\sigma(Q)}{Q}\right| = \sqrt{\frac{2}{n(O)} + \frac{2}{n(N)}} = \frac{1}{(t)^{1/2}}\left(\frac{2}{R(O)} + \frac{2}{R(N)}\right)^{1/2}$$

With the oxygen counting rate $25*10^6$ sec $^{-1}$, nitrogen $40*10^6$ sec $^{-1}$, and the fraction of time spent on unknown and standard 0.35 each, the theoretical precision attainable in one second is $6.1*10^{-4}$. The precision increases with the square root of time, as the total number of counts is proportional to time. A determination of relative oxygen concentrations to a precision of 5 ppm (corresponding to 1 ppm absolute since oxygen comprises 1/5 of the atmosphere) would take

$$\left|\frac{6.3*10^{-4}}{5*10^{-6}}\right|^2 = 15{,}000 \text{ sec}$$

or about 4 hours of integration time.

E. Beam Position Feedback

As will be explained in the section on systematic errors, it is important that the laser beam does not change its average position by more than about 5 μm (micrometer) between runs. This is accomplished by an active feedback system that continually

centers the beam on two quadrant detectors (Q in fig. 2) located on both sides of the gas cells containing the samples.

Initially we attempted to control the beam position in a straight extended laser cavity, without the two 90° bends. We hoped that we could adjust the beam position by turning the curved mirror at the far end of the laser cavity (M1, fig. 2) in combination with the flat reflector in the back of the laser. Upon trying to calibrate the amount of beam movement against mirror tilt, however, we found that the response was non-linear and that horizontal and vertical control were coupled. This coupling was probably due to refraction by the laser plasma. Gas lasers have spatial profiles of the refractive index due to gain and dispersion of the laser transition. This can, among other things, significantly influence the direction of beam propagation. We need to control four degrees of freedom, two for parallel beam displacement and two for beam tilt. The amount of coupling between horizontal and vertical beam movement was not constant over time and it effectively reduced the number of degrees of freedom we could control to three, making full control impossible.

In order to overcome this problem we decided to decouple the laser beam position in the scattering region from its position in the plasma region by bending the beam twice over 90° (fig. 2). The addition of extra mirrors gave us the opportunity to control the beam position in the scattering region while at the same time optimizing laser power by positioning the beam independently in the plasma discharge. Laser power and beam position signals are obtained from the two quadrant detectors mounted directly behind mirrors M1 and M2 (fig. 2). The beam is translated by moving M2 and M3 together. Beam tilt is handled by M1 and M2 together. In addition, laser power is maximized with a feedback on mirror 3. While it is beneficial to maintain maximum laser power when the laser is left unattended for many hours, more importantly, we found power feedback to be necessary for the position feedback to work at all. The vertical and horizontal degrees of freedom of

position are only fully decoupled with the power feedback working. This feedback is computer controlled in the following way: M3 is moved 50 steps in each direction and laser power is measured after each step. A cubic is then fit to the power data, and the mirror is moved to the maximum of the fit curve. The horizontal optimization is followed by a vertical adjustment. Power optimization immediately follows position adjustments, and the entire proces is repeated evey few minutes throughout the measurement.

We have taken a power spectrum of beam position fluctuations with the feedback system turned off. It was very highly peaked toward the lowest frequencies because the variability was dominated by very slow drifts of the beam position, of up to 100 μm over a period of several hours. With the feedback system, the power spectrum becomes flat, but noisier at the high frequency end because of the intentional mirror movements. The quadrant detectors are used as null detectors, measuring intensity changes in opposing segments. Because the beam spot is small the detector electronics do not have to be exceptionally stable. Thus the feedback system is able to hold the centroid of the laser beam position, averaged over several hours, to about 1 μm with respect to the quadrants.

F. Computer Control of the Experiment

Beam control, timing, and data collection are controlled by an LSI-11/23 computer via a CAMAC interface crate. The timing base for data collection is set by an 8-channel timing pulse generator which triggers drive pulses to run the choppers (exactly out of phase) and establishes timing windows which enable the scalers used to accumulate photon counts. The actual phase relationship between the choppers is forced to match the phase relationship between the drive pulses by a feedback loop which stabilizes the time difference between the drive pulse and a zero-velocity pickup to within 50 microseconds.

Since the same detectors (and scaler channels) are used for both unknown and standard signals, the scalers must be read and cleared every chopper half-cycle. While the scalers are accumulating photon counts, the computer is kept busy monitoring the laser beam. Each cycle the quadrant detectors are read in order to determine the average beam position. Once per second a shutter is closed in the laser beam and dark-noise is counted for two cycles. Every few minutes all three mirrors are moved to correct the laser beam position based on the average readings of the quadrant detectors since the last adjustment. Following this correction, power is optimized as described above. Finally, every ten minutes all the data that has been accumulated during this period is written to disk, completing one update. The data collected each update includes the total number of standard counts, and the difference between the number of unknown and standard counts, from the oxygen, nitrogen, and carbon dioxide channels. Dark-noise, beam position, and beam power data are also recorded.

G. Data Treatment

All data is stored digitally, either as the actual number of counts recorded by the scalers or, in the case of beam position, power, and polarization data, as the value generated by an analog-to-digital converter. This allows all corrections to be made in a non-destructive fashion, after data collection is completed. The only exception to this rule is the correction for the dead-time of the photomultiplier-descriminator chain. This correction (on the order of 0.1%) is applied in real-time so that the instantaneous counting rates can be used.

After a run of typically 25 to 50 updates (4-8 hours) background subtractions are applied, and the data are analyzed to determine the average ratio of ratios and the precision of the measurement. The dark-noise subtraction is calculated using the data obtained with the shutter closed at one second intervals. Other background subtractions are based on calibration

measurements in which we obtain the count rates on the detectors with the target cells evacuated or filled with pure gases. We also plan to calibrate the instrument with standards made by mixnig pure gases--precisely weighing the mixture after each addition so that the final composition is known.

Storing intermediate data at ten minute intervals allows analysis for trends and correlations. Observed standard deviations are calculated and compared with what is expected from Poisson statistics. A power spectrum is also calculated to check for time dependence of the measured ratio-of-ratios. Finally, correlation coefficients are calculated between all the recorded variables and some of their ratios to aid in determining the source of any systematic errors.

H. Target Call Design

The cells containing the gases that are being compared inside the laser cavity are an important aspect of the overall design. They have gone through a number of revisions before we arrived at the design presented here. The following requirements are necessary. The optical quality of the beam windows has to be superb to prevent the loss of laser power. All materials used in the construction should resist oxidation and be non-porous to minimize outgassing, adsorption and desorption, especially since we want to consider some of these cells as standards, never to be opened after they have been pressurized.

Furthermore, there are some requirements that are highly desirable. Raman scattering is a very weak process and if extreme care is not taken in designing a low background cell, inelastically scattered light from the walls and fluorescence from the beam window can make a significant contribution. For that reason, a dull (black) finish is important in making apertures more effective in shielding the collection optics from any light not scattered by the gas itself. High pressure improves the signal to noise ratio and reduces integration times

by boosting the scattering from the gas while leaving the background largely unaffected. The viewing windows should also be of high optical quality and equal dimensions so that the apparent beam position as viewed through the window does not change.

The target cell design of fig. 3 approximates these conditions reasonably well. The central cylinder which is seen end-on contains anti-reflection coated viewing windows on both sides. The beam enters the cell through the long side arm, traverses the central body parallel to the viewing windows and exits through the opposing side arm.

The spots where the beam traverses a window are extremely bright sources of elastically scattered light, as well as bright sources of a continuum of fluorescent light. Both side arms contain a system of apertures designed to ensure that any light originating at the beam window must bounce at least twice in a diffuse manner before it can pass through a viewing window. The reflection off the inside of the beam window is channeled into a light trap. This design has a continuum background contributing about one thousandth of the Raman intensities to the oxygen and nitrogen channels at a gas pressure of 10 atm.

The cells and the apertures are machined and welded out of aluminum. After the basic construction, they are hard anodized to give them a hard non-porous oxide surface layer. The aluminum alloy 6061 turns naturally black upon hard anodizing. The windows are clamped on with metal C-ring seals. The valve is a Nupro stainless steel bellows valve. It is clamped on metal-to-metal with high pressure fittings from Autoclave Engineering Inc.

The beam windows are made out of fused silica which has very low stress birefringence that could otherwise rotate the plane of polarization of the beam. In addition fused silica has the lowest fluorescence of a number of glasses that we tested. The surface flatness of the windows is better than $\lambda/20$ and the parallelism is 1 arcsec.

On top of the sample chamber is a small window through which the polarization of the laser beam can be monitored by means of the elastically scattered (Rayleigh) light. (see section III B)

I. Sample Collection and Storage

The air samples are first collected into Whitey high pressure cylinders. A schematic of the sample collection system is shown in fig 4. High pressure is deemed an advantage because the bulk of the stored air increases, while the container surface area remains the same. An additional advantage is that it is relatively easy to transfer small quantities of gas cleanly from a high pressure cylinder into the laser target cells.

It is of paramount importance that the gas stored in the high pressure cylinder is dry. Any condensed water will greatly facilitate corrosion by acting as an electrolyte. At 100 atm. of total pressure enough CO_2 will dissolve in condensed water to give it a pH of 4.63 . This is the reason for including a cryogenic drying stage before the compressor. It consists of 60 ft of 3/4" stainless steel tubing wound into a coil that is immersed into a dry ice alcohol bath. Inside the coil is a stainless steel strip twisted with a pitch of about half a turn per inch to increase air turbulence and heat transfer. The air will have a dewpoint of -65^0C before it reaches the compressor. The concentration of water vapor is then 5 ppmv. At a pressure of 125 atm. the dewpoint will then be -22^0C. To combat any further chances of corrosion, the cylinders have either been electropolished or plated with a 0.5 to 1 mil thick layer of gold.

The compressor is a completely oil-free breathing air compressor, manufactured by RIX industries. To exclude the possibility of forming nitrogen oxides during compression the compressor runs very slowly, with the compression taking place in three stages with cooling in between. If the temperature of the gas is kept below 300 ^0C at all times, the equilibrium

concentrations of NO and NO_2 can never be higher than 1 ppm. This is a conservative approach that does not have to take into account the kinetics of the reactions. We did not measure the temperature of the gas directly during the last compression stroke. We measured instead the temperature of the last compression cylinder of the compressor. It reaches 100 ^{0}C. The Whitey sample cylinder becomes lukewarm, about 35 ^{0}C.

An air sample is taken by pumping air into one end of a cylinder that has a relief valve at its other end. After the relief valve opens at about 1800 psi we continue pumping air through the cylinder for a period equal to 5 times the initial filling time, thus thoroughly flushing the cylinder at high pressure.

We are also experimenting with Spectraseal cylinders from Airco. These are aluminum cylinders that have been internally hard anodized. In addition they have gone through a proprietary passivation process at Airco. The storage of CO, NO, SO_2, NO_2 in air in calibration gas mixtures in these cylinders is superior to other materials and surface treatments.

III. ANALYSIS OF SYSTEMATIC ERRORS

Introduction: Spatial Distribution and the Polarization of the Scattered Light.

The intensity of the Raman scattered light is anisotropic. More importantly, the angular distribution depends on the molecular species; it is slightly different for oxygen and nitrogen gas. The result is that the ratio of the light scattered by oxygen to that scattered by nitrogen that is incident on the collection optics depends on the solid angle accepted by the optics and on the direction of polarization of the laser light. Given a certain desired repeatability, this leads to a requirement for stability of the beam position and polarization with respect to the viewing optics. We will first derive an expression for the angular distribution of the Raman light that employs tabulated optical properties of oxygen and nitrogen. Then we derive in sub-sections A, B, C and D the specifications that our apparatus will have to meet in this regard. The remaining sub-sections deal with other systematic effects. In subsection A we only discuss the effect of beam movement on the solid angle of acceptance of the optics. Its effect on the apparent orientation of the polarization is treated in B.

The intensity of Raman scattered light depends on the viewing angle of the observer with respect to the polarization of the incoming light that will be scattered. We define laboratory coordinates so that the incoming beam is along the y-axis and is polarized in the z-direction. The observer is located on the x-axis (see fig 5). Apart from a multiplicative factor, the distribution of scattered light from a single molecule is given by

$$I_z(\theta,\phi) = (-\alpha_{zy}\sin\phi + \alpha_{zz}\cos\phi)^2 + (-\alpha_{zx}\sin\theta + \alpha_{zy}\cos\theta\cos\phi + \alpha_{zz}\cos\theta\sin\theta)^2 \quad (1)$$

Our treatment will be somewhat similar to that of Porto[10], where

further references can also be found. The scattered light propagates along the e_3-axis and the two terms in eq (1) correspond to polarizations along the e_1 and e_2 axes (see fig 5). The subscript z on I_z signifies that the laser beam is polarized in the z-direction. The factors α_{ij} (i,j=x,y,z) make up the polarizability tensor in laboratory coordinates. (Actually, the derivative of the polarizability with respect to the vibrational coordinate for vibrational-rotational scattering.) The polarizability tensor expressed in coordinates fixed in the molecule reduces to diagonal form by choosing the principal axes as the coordinate system. The three remaining components are then α_1, α_2, and α_3, the principal values of the tensor, with the principal axes of the molecule labeled as 1,2,3. For a particular orientation of the molecule, an element α_{zy} of the polarizability in laboratory coordinates is given by

$$\alpha_{zy} = \Sigma\alpha_i \cos(i,z)\cos(i,y) \qquad (i=1,2,3) \tag{2}$$

When calculating the polarizability in laboratory coordinates of an assembly of independent molecules randomly oriented in space we have to average the intensity from each over all possible orientations. We have to calculate averages like $\overline{\alpha_{zy}^2}$ and $\overline{\alpha_{zy}\alpha_{zz}}$. Denoting cos(i,x) by X_i, this means evaluating expressions of the type

$$\overline{\alpha_{zx}\alpha_{zy}} = \alpha_i^2\overline{Z_i^2X_iY_i} + \alpha_1\alpha_2\overline{Z_1Z_2(X_1Y_2+X_2Y_1)}+\ldots..$$

The most general rotation of one coordinate system to another is via Euler's angles. The bar denotes averaging over

$$\int_0^{2\pi} d\xi \int_0^{2\pi} d\phi \int_0^{\pi} \sin\theta d\theta$$

All averages of fourth power products of the direction cosines of the above type are zero except the following[11]:

$$J_1 = \overline{X_1^4} = \overline{X_2^4} = \overline{X_3^4} = \overline{Y_1^4} = \ldots\ldots\ldots = 1/5$$

$$J_2 = \overline{X_1^2Y_1^2} = \overline{X_2^2Y_2^2} = \ldots\ldots\ldots = 1/15$$

$$J_3 = \overline{X_1^2 X_2^2} = \overline{X_1^2 X_3^2} = \ldots\ldots\ldots = 1/15$$

$$J_4 = \overline{X_1 Y_1 X_2 Y_2} = \overline{X_1 Y_1 X_3 Y_3} = \ldots\ldots = -1/30$$

$$J_5 = \overline{X_1^2 Y_2^2} = \overline{X_1^2 Y_3^2} = \overline{X_1^2 Z_2^2} = \ldots = 2/15$$

An average like $\overline{\alpha_{zx}^2}$ is then equal to

$$(\alpha_1^2 + \alpha_2^2 + \alpha_3^2)/15 - 2(\alpha_1\alpha_2 + \alpha_2\alpha_3 + \alpha_3\alpha_1)/30$$

Following convention, we define the isotropic and the anisotropic parts of the scattering tensor in the principal axis representation as follows:

(3) $$\alpha = (\alpha_1 + \alpha_2 + \alpha_3)/3$$

(4) $$\beta^2 = ((\alpha_1 - \alpha_2)^2 + (\alpha_2 - \alpha_3)^2 + (\alpha_3 - \alpha_1)^2)/2$$

The frequency dependence of the scattering tensor has not been explicitly included in our notation. The isotropic part (α) of the scattering tensor gives rise to the so called trace scattering which does not change the polarization of the incoming radiation. It is the part that acts like a completely spherically symmetric molecule. It does not contribute to the rotational side branches because that involves a change in angular momentum and polarization. The anisotropic part (β^2) contributes both to the Q-branch and to the side branches.

Averaging (1) over molecular orientations and multiplying by 45 gives the total scattered intensity as a function of angle for z-polarized light as:

(5) $$I_z(\theta,\phi) = (45\alpha^2 + 4\beta^2)((\cos^2\phi) + (\sin^2\phi\cos^2\theta)) + 3\beta^2((\sin^2\phi) + (\sin^2\theta + \cos^2\phi\cos^2\theta))$$

The two polarizations, e_1 and e_2, are given in separate inner parentheses in eq.(5).

In practice the actual laser beam polarization will never be exclusively along the z-axis. Although the gain per pass is negative for the x-polarization due to the 6% reflection for that polarization at each interface of the 6 Brewster windows, a certain amount of x-polarization is continually being generated

inside each window due to stress birefringence. In addition the alignment of the windows with respect to one another is not perfect. Therefore we have to consider the case where the laser polarization consists of two components, in the z- and x-direction, that have some arbitrary phase relationship with respect to each other. Then all cases of linear and elliptical polarization will be included. Of course, the z-polarization will dominate due to its amplification inside the laser cavity.

Neglecting time dependence, the electric field amplitude in the laser beam is described by:

$$E = e_z E_z + e_x E_x \tag{6}$$

where e_z and e_x are unit field vectors along the z- and x-axes and E_z and E_x are complex amplitudes, to allow for a phase difference between them. The total power in the beam is proportional to $E_z{}^2 + E_x{}^2$.

The amplitude scattered in the e_3 direction, polarized along the e_1 direction (see fig. 5), is given by:

$$\begin{aligned} E_1 = {} & (\alpha_{xx}E_x + \alpha_{zx}E_z)\,(-\sin\theta) + \\ & (\alpha_{xy}E_x + \alpha_{zy}E_z)\,(\cos\theta\cos\phi) + \\ & (\alpha_{xz}E_x + \alpha_{zz}E_z)\,(\cos\theta\sin\phi) \end{aligned} \tag{7}$$

The intensity, I_1, equals $E_1\,E_1{}^*$, the amplitude times its complex conjugate, averaged over all molecular orientations:

$$\begin{aligned} I_1(\theta,\phi) = {} & (\alpha^2 + \tfrac{4}{45}\beta^2)(|E_x|^2\sin^2\theta + |E_z|^2\cos^2\theta\sin^2\phi - \\ & \qquad 2\cos\eta|E_x||E_z|\sin\theta\cos\theta\sin\phi) \\ & + \tfrac{3}{45}\beta^2(|E_x|^2 + |E_z|^2)\cos^2\theta\cos^2\phi \\ & + \tfrac{3}{45}\beta^2(|E_x|^2\cos^2\theta\sin^2\phi + |E_z|^2\sin^2\theta + \\ & \qquad 2\cos\eta|E_x||E_z|\sin\theta\cos\theta\sin\phi) \end{aligned} \tag{8}$$

The angle η represents the phase difference between E_x and E_z. The expression for the intensity polarized in the e_2-direction is

$$(9)\qquad I_2(\theta,\phi) = (\alpha^2 + \tfrac{4}{45}\beta^2)|E_z|^2\cos^2\phi + \tfrac{3}{45}\beta^2\left((|E_x|^2 + |E_z|^2)\sin^2\phi + |E_x|^2\cos^2\phi \right)$$

The total intensity is equal to the sum I_1+I_2. In the special case $E_z=0$, we have pure x-polarization of the laser beam and the sum simplifies to :

$$(10)\qquad I_x(\theta,\phi)=I_1+I_2 = (\alpha^2 + \tfrac{4}{45}\beta^2)|E_x|^2\sin^2\theta + \tfrac{3}{45}\beta^2|E_x|^2(1+\cos^2\theta)$$

The first term in eq.(10) is now seen to be the familiar radiation distribution pattern of a dipole oscillating along the x-axis, while the second term is characteristic of two dipoles, 90^0 out of phase, one oscillating along the y-axis, and the other along the z-axis (right and left circularly polarized light). The intensity distribution displays cylindrical symmetry around the x-axis. The scattered intensity distribution for z-polarized laser light that we obtained in eq. (5) is identical to the distribution from x-polarized light except that the symmetry is about the z-axis. This is not readily apparent in our coordinate system, because it is centered on the x-axis. The z-polarized laser scattering pattern can be obtained from that for the x-polarized laser, however, by rotating the coordinate system about the y-axis. The components of the vector field amplitudes transform among each other as a spin-1 system.

The total intensity, $S(\theta)$, that we collect is the integral of I over the solid angle subtended by the optics:

$$(11)\qquad S(\theta) = \int_0^{2\pi} d\phi' \int_0^{\theta} \sin\theta' d\theta' (I_1(\theta',\phi') + I_2(\theta',\phi'))$$

By integrating over the azimuthal angle ϕ the cross terms in eq. (8), which contain $\cos\eta$, cancel out because $\int_0^{2\pi} d\phi \sin\phi = 0$. The case of rotated linear polarization is then no different from elliptical polarization. For the following we will define:

$$(12)\qquad \begin{aligned} E_x^2 &= f \\ E_z^2 &= 1-f \end{aligned}$$

so that f is the fraction of the total laser power that is

polarized in the "wrong" direction. Then

$$S(\theta) = \pi\int_0^{\theta}\sin\theta' d\theta'\Big[(\alpha^2 + \tfrac{4}{45}\beta^2)(2f\sin^2\theta' + (1-f)\cos^2\theta' + (1-f)) + \tfrac{3}{45}\beta^2(\ (1+f) + \cos^2\theta' + 2(1-f)\sin^2\theta' + f\cos^2\theta')\Big] \quad (13)$$

Retaining only the leading powers in θ leads to:

$$S(\theta) = \frac{3}{8}\Big(\frac{1+\rho_t}{1+2\rho_t}(\theta^2 - \tfrac{1}{3}\theta^4 + \tfrac{62}{720}\theta^6) + \frac{\rho_t}{1+2\rho_t}(\tfrac{1}{2}\theta^4 - \tfrac{1}{6}\theta^6)\Big) - \frac{3}{8}f\frac{1-\rho_t}{1+2\rho_t}\Big(\theta^2 - \tfrac{5}{6}\theta^4 + (\tfrac{62}{720} + \tfrac{1}{6})\theta^6\Big) \quad (14)$$

Where

$$\rho_t = \overline{\alpha_{zy}^2}/\overline{\alpha_{zz}^2} = \frac{3\beta^2}{45\overline{\alpha^2} + 4\overline{\beta^2}} \quad (15)$$

and we have normalized eq. (14) by the total amount of scattering over 4π. The total scattering over 4π can be obtained by integrating eq.(10):

$$\int_0^{2\pi} d\phi \int_0^{\pi} \sin\theta d\theta I_x(\theta) = \frac{8\pi}{3}(\alpha^2 + \tfrac{10}{45}\beta^2) \quad (16)$$

In the special case f=0, we obtain, to sixth order in θ:

$$S_z(\theta) = \frac{3}{8}\frac{1+\rho_t}{1+2\rho_t}\theta^2 - \frac{1}{16}\frac{2-\rho_t}{1+2\rho_t}\theta^4 + \frac{1}{32}\frac{1-\rho_t}{1+2\rho_t}\theta^6 \quad (17)$$

For our opening angle of θ = 0.28 radians, adjacent terms in the expansion of $S_z(\theta)$ differ from each other by factors of 25 to 40.

Experimentally, the molecular anisotropies have usually been measured at the Q-branch frequency (no change in rotational quantum number) by taking the ratio of the scattered intensity along the x-axis of two polarizations, y and z, which correspond in our notation to e_1 and e_2 for that direction (fig. 5). The depolarization ratio ρ_q is then defined as

$$\rho_q = \overline{\alpha_{q,zy}^2}/\overline{\alpha_{q,zz}^2} \quad (18)$$

This is equivalent to

$$(19) \qquad \rho_q = \frac{3c_q\beta^2}{45\alpha^2 + 4c_q\beta^2}$$

The factor c_q is the fraction of the total depolarized intensity of the entire rotational-vibrational band (O-, Q-, and S-branch) that contributes to the Q-branch. For linear molecules (except hydrogen) $c_q = 0.25$,[12] so that

$$(20) \qquad \rho_t = \frac{4\rho_q}{4\rho_q + 1}$$

When, as in our case, the frequency passband of the collection optics is such that most of the rotational-vibrational band contributes to the signal, one has to take for ρ a value closer to ρ_t than to ρ_q (see section F, filter transmission).

A. Beam Positioning with Respect to the Light Collection Optics

Expression (17) can now be used to calculate the theoretical effect of horizontal beam movements on the measured ratio of scattering intensity from oxygen and nitrogen. It is sufficient to consider the special case f=0 (eq. 12) for this calculation since changes in the relative contributions of I_z and I_x are of second order importance compared to the effects of solid angle acceptance. Insertion of the measured values[12] of ρ_q (eq. 18, 19) for O_2 (0.047) and N_2 (0.022) in (20) and using the result in (17) will tell us how the measured relative intensities vary with solid angle of collection. More precisely, we need to know

$$(21) \qquad \frac{1}{Q}\frac{d}{d\theta}Q = \left[\frac{S_{z,N}(\theta)}{S_{z,O}(\theta)}\right]\frac{d}{d\theta}\left[\frac{S_{z,O}(\theta)}{S_{z,N}(\theta)}\right]$$

where the quotient Q has been defined earlier in section II D (Counting statistics) and the subscripts O, N stand for O_2 and N_2. The stability of our measurement actually depends on the difference of this quantity between sample and standard. We cannot assume, however, that the beam behaves in exactly the same way in both places; it can translate, but also tilt. Therefore, we will here and in the remainder of this report assume that the

variations in both locations are independent. This introduces a factor of $(2)^{1/2}$ in all estimates of how the ratio-of-ratios is affected by changes in the average beam position.

When the beam moves in the horizontal plane with respect to the collecting optics, the received flux is affected directly because of the change in solid angle that is captured. The change in solid angle is the same for oxygen and nitrogen so that any change in their ratio must be due to differences in the angular distribution of the scattered light from the two species. By sustituting eq. 17, $\rho_{t,N} = 0.089$, $\rho_{t,O} = 0.179$, and $\theta = 0.28$ radian we obtain:

$$(22) \qquad \frac{1}{Q}\frac{dQ}{d\theta} = 0.073\theta + 0.294\theta^3 - \ldots\ldots$$

A change in the horizontal beam position is related to the angle of acceptance θ by

$$\frac{dx}{d\theta} = \frac{-h}{\sin^2\theta}$$

h is the radius of the entrance pupil (30 mm) and x is the distance of the beam to the entrance pupil (104 mm). The result is that if we want to keep relative changes in the ratio of oxygen to nitrogen below 1 ppm, we have:

$$0.28(0.073+0.023)\sin^2(0.28)\Delta x/30 < 10^{-6}$$

or $$\Delta x < 15\ \mu m$$

This criterion is relaxed considerably by a solid angle cancellation effect. When the beam moves away from the collecting lens, the beam image produced by the spherical mirror (R in fig. 2) moves closer. This reduces the sensitivity of the measured intensity ratio to horizontal beam movement by about a factor of 4 to 5 since the spherical mirror contributes roughly 40% of the total collected intensity. The total amount of horizontal movement of the beam that we allow with regard to this effect is then about 60 μm.

A vertical beam movement changes a number of things in the collection geometry. The distance of the beam to the center of

the entrance pupil increases, the projection of the lens assembly normal to the chief ray decreases, and the angle of the polarization of the laser beam with respect to the chief ray will vary. The last effect will also be treated below in the next section.

In contrast to horizontal beam translation, which produces an effect that is linear in the small deviations Δx considered, vertical translation causes effects that are quadratic in Δz. As a result the ratio is not appreciably affected by small vertical beam drifts, despite the fact that the spherical mirror does not produce a cancellation effect. Only the third effect, that on polarization, has to be considered since there are several other mechanisms that can have a large impact on the polarization. In that case a small additional change due to a beam drift Δz produces changes in Q that are proportional to Δz.

B. Beam Polarization and Birefringence

The direction of the laser polarization is determined by the orientation of the Brewster windows of the plasma tube and the target cells and the wavelength selector prism in the cavity. Small deviations can be introduced by mechanical (thermal, for instance) orientation changes of one or more of these optical elements. The direction of polarization (and laser power) is also affected by stress birefringence of any optical element in the cavity. Also a change in the vertical beam position is equivalent to turning the polarization of the laser, because one is looking at the beam from a different angle (see fig.5).

The loss per interface at each Brewster window is close to 6% for the horizontal polarization. There are 6 windows plus the wavelength selective prism inside the cavity, so that for a single pass the loss for x-polarized light is 0.58 ($1-(1-0.06)^{14} = 1-0.42$). For our Spectra Physics model 171 ion laser we measured at our operating current (30 amp) a single pass gain of about 50%, while internal losses, other than from the

windows, are about 20%. It is clear that there is a net attenuation for the x-polarization at each pass, while there is a large amplification for the z-polarization, which has almost no window losses. However, horizontally polarized light is continually being generated from the vertical polarization inside the glass due to stress birefringence. The laser gain is so high that it can tolerate a large amount of generated x-polarization, which is quickly lost, and still have an overall positive gain.

In practice this means that there is considerable uncertainty as to the exact state of polarization of the beam and that the polarization may vary over time. When we substitute the value of 0.28 for θ in eq. 14 we obtain for the dependence of the collected Raman scattered light on small changes in f (eq. 12, and $f << 1$)

$$(23) \qquad \frac{1}{S(0.28)} \frac{dS(0.28)}{df} = - \frac{(1-\rho_t)(1-0.0392)}{1+(1+0.0392)\rho_t}$$

By developing (23) as a power series in ρ we find that the ratio of oxygen to nitrogen changes as a function of f as:

$$(24) \qquad 0.961f[2.039(\rho_{t,O} - \rho_{t,N}) - 2.119(\rho_{t,O}^2 - \rho_{t,N}^2) + 2.202(\rho_{t,O}^3 - \rho_{t,N}^3) - \ldots\ldots]$$

If we retain terms to third order in $(\rho_{t,O} - \rho_{t,N})$, this equals

$$0.137f$$

We measure f continually through the window on top of each target cell. We can therefore correct the measured Raman scattered ratio for changes in the laser polarization. This correction is not perfect however. The chief ray of our Raman collection optics will be off the x-axis by a small angle ε'' and the laser polarization detector will be off the z-axis by some small angle ε'. These are independent and equivalent effects.

We will first consider the case in which the measurement of f is in error because $|\varepsilon'| > 0$. We measure $|E_x'|^2$, where the prime indicates that the coordinate system has been rotated around the y-axis by a small angle ε', positive or negative. For

$|\varepsilon'| << 1$ we have for the measured f':

$$f' = |E_x'|^2 = f + \Delta f' = (\varepsilon' E_z + E_x)(\varepsilon' E_z^* + E_x^*)$$
$$= |E_x|^2 + \varepsilon'^2 |E_z|^2 + 2\varepsilon' \cos\eta |E_x||E_z| \quad (25)$$

The error in the measurement of f is denoted by $\Delta f'$. The phase difference between E_x and E_z is given by η. If E_x and E_z are $\pi/2$ out of phase ($\eta = \pi/2$, elliptical polarization) then

$$\Delta f' = \varepsilon'^2$$

In this case the effect is negligable because from the alignment precision we estimate $\varepsilon' = 0.002$. If E_x and E_z are not out of phase the effect is more serious. We then have (for $f << 1$):

$$\Delta f' = \varepsilon'^2 + 2\varepsilon' (f)^{1/2} \cos\eta$$

For most actual values of f and η the second term dominates. We will see below that E_x, caused by stress birefringence, is in fact mostly 90^o out of phase.

If the optical axis of the Raman collection optics is off the x-axis by a small angle ε'', the value of $f'' = |E_x''|^2$ that matters to the scattering is slightly different from $f = |E_x|^2$ that we defined with respect to the coordinates of the optical table. We can again define the error in f by $f'' = f + \Delta f''$ and by the same procedure we find that

$$\Delta f'' = \varepsilon''^2 + 2\varepsilon'' (f)^{1/2} \cos\eta$$

The Raman results are corrected for changes in f. What remains are the errors $\Delta f'' - \Delta f'$, which we can express as:

$$\Delta f'' - \Delta f' = \varepsilon''^2 - \varepsilon'^2 + 2(\varepsilon'' - \varepsilon')(f)^{1/2} \cos\eta \quad (26)$$

The fraction f is measured by looking down on the Rayleigh scattered light along the z-axis. There are several scattered components that are picked up. First of all there are small depolarization factors for the Rayleigh scattered light (0.0291 for O_2 and 0.0108 for N_2) which cause the incident z-polarized laser light to be seen from above. The z-polarization can also be seen directly due to the finite size of the aperture. This last effect is very small, however, because our opening angle is only 1/20 radian. The x-polarization is seen very strongly through direct un-depolarized scattering. The intensity that is picked up, $S_R(\theta)$, normalized to the total Rayleigh scattering over 4π, is

$$(27)\quad S_R(\theta) = \frac{3}{8}\frac{1}{1+2\rho}\{(1-f)[2\rho(\theta^2 - \frac{\theta^4}{3}) + \frac{\theta^4}{2})] + f(1+\rho)(\theta^2 - \frac{\theta^4}{3})\}$$

Eq. 27 has been derived by integrating (13) over a small solid angle around the x-axis, with the roles of $|E_z|^2 = 1-f$ and $|E_x|^2$ interchanged. This is the same as an integral around the z-axis for the original E_z and E_x. The terms have been arranged so that the origin of each is transparent. The $\theta^4/2$ term is due to direct viewing of a z-oriented dipole through a finite aperture situated exactly above it on the z-axis. The term with 2ρ derives from the radiation of two dipoles, one along the x-axis and one along the y-axis. The relative strength of each of these dipoles is ρ, the depolarization ratio. The last term represents the radiation from the x-polarized component of the laser directly from an x-dipole and also from a dipole along the y-axis with a relative strength of ρ.

For $\theta=1/20$ radian $\theta^4/3 = 8.3*10^{-4}\theta^2$, so that by far the biggest term is the depolarized scattering from the z-polarization, if $f << 2\rho$ (= 0.0291 for air) as expected. The signal caused by $2\rho|E_z|^2$ is DC. By rotating a polarizer in front of the detector the part of the signal caused by $|E_x|^2$ is modulated as a sine wave with a peak amplitude proportional to $f(1-\rho)$.

Synchronous detection will easily pick up f trom the noise on the DC signal that is caused by laser power fluctuations. Because we are looking at Rayleigh light the cross section is relatively large, 10^{-27} cm^2/sterrad. The AC signal when f is down to 10^{-5} is still 10^{-12} watt, which is two orders of magnitude above the noise equivalent power (detectivity) of a good small area photovoltaic detector.

The main cause for the appreciable, for our purposes, magnitude of E_x is birefringence of the optical elements in the laser cavity. Stress in glass causes the index of refraction to be slightly different for light polarized parallel to the

direction of stress compared with light polarized perpendicular to the stress. Not only intentionally applied stresses, but also residual internal stresses after annealing of the glass give rise to this effect. The stress optical coefficient for fused silica is $3.5*10^{-6}mm^2/N$. The residual stress birefringence is usually specified as nanometers of optical path difference per cm of glass traversed.

The detailed calculation of what happens to the laser polarization when the beam travels through the Brewster windows under 10 atm of pressure is presented in appendix A. The result for one window, assuming that the only stresses are due to pressure, is depicted in fig. 6 by solid arrows. The effect of the opposite window of the same target cell is represented by the dashed arrows in fig 6. The beam has a Gaussian intensity profile, $\exp(-2r^2/R^2)$. The $1/e^2$ intensity contour (r=R) for a perfectly centered beam has been drawn in. The largest effect takes place on the fringes of the beam, where the generated x-amplitude reaches on the order of 5% of the z-amplitude. The x-amplitude is retarded by a little over $\Pi/2$ on one side and advanced by almost $\Pi/2$ on the other side. When we integrate $|E_x|^2$ over the beam profile we obtain $f=6*10^{-4}$. This occurs inside the target cell, even if the incident polarization is perfectly vertical and the beam is centered. If the beam changes shape, or just merely its radius, f is affected. Indeed, f depends quadratically on the beam radius.

Upon traversing the Brewster window on the opposite side of the cell, the part of the beam that has a phase advance now generates an x-component with a phase retardation, so that perfect z-polarization gets (almost) restored outside of the target cell. Almost, because the x-component has suffered 2 reflections, diffraction tends to "wash out" what happens in the fringe regions due to the much greater amplitude in the center region, and the calculations are based on the assumption that the z-component is not affected (appendix A).

If the beam is off-center horizontally by 0.5 mm, f is

larger by about $4.5*10^{-4}$. This effect grows quadratically with the offset. When the beam is also offset on the opposite window by 0.5 mm, the effect is again (almost) cancelled outside of the cell. If the beam is tilted with respect to the y-axis, the offsets will not be quite the same on both sides.

Regardless of any stresses caused by pressurizing the target cells, there will always be some effect due to the residual stress birefringence that remains after fine annealing. Whether such a stress causes the generation of an x-component depends on the orientation of the stress axes with respect to the electric field vector of the light. The proportionality is $\sin 2\theta$, where θ is the angle between the stress axes and the polarization axes. The specification for the residual stress birefringence in our fused silica is less than 5 nm/cm, for any polarization direction. As a maximum then, the window could generate an x-amplitude of up to $5*0.5d*2\Pi/\lambda$ (appendix A). The thickness of the glass is d, and λ is the wavelength of light in nanometers (514nm). $|E_x|$ is then 0.035 and $E_x{}^2 = 1.2*10^{-3}$.

When the return beam traverses the same piece of glass, the x-amplitude would get doubled if there were no intervening reflection losses. In general, the x-amplitude will build up until the loss per pass equals the gain. The loss per pass for the x-amplitude (not intensity) due to the reflections at all the Brewster windows is 35%, while (in this hypothetical case) 3.5% is added (see previous paragraph) per pass. Therefore the amplitude will, on the average, increase to 0.035/0.35=0.1 . This crude estimate assumes continuous loss and gain, while in fact both of these occur in discrete steps. In some places the amplitude could be higher than 0.1, while in others it would be lower.

The effect of residual birefringence can be very considerable. Our estimate above is an upper limit for a single window based on the tolerance specifications for the glass. This estimate is for a single window. The other glass elements in the beam also contribute to the x-amplitude. In principle it is

possible to minimize the effect, however, by rotating the Brewster windows such that the residual stress is either aligned with, or perpendicular to the electric field vector.

C. Target Cell Windows and Alignment.

The beam position feedback system keeps the beam centered on the crosshairs of the quadrant detectors located on either side of the sample and standard positions (fig 2). However, the target cell beam windows displace the beam inside the cells, while the viewing windows cause an additional apparent displacement. We are really interested in making sure that the apparent position of the beam, as viewed through the collection optics, does not change significantly between target cells. That leads to a number of specifications for the windows which will be discussed in what follows.

A fused silica beam window causes a parallel vertical beam displacement of (see fig 7):

$$d_v = t\left(\frac{\sin(\alpha-\alpha')}{\cos\alpha'}\right) = 0.439t \tag{28}$$

with

d_v = parallel vertical displacement
t = thickness of window
n = index of refraction of fused silica (1.4616)
α = Brewster's angle (55.62^0)
α' = same, but after refraction

It follows that if the thickness varies by 0.001" between windows, the beam offset varies by 11 μm. The actual variation is about that much.

If the angle of incidence increases by one degree in the vicinity of Brewster's angle, the beam offset goes up by 0.013t. The thickness is 0.375", so that a 1^0 angle change near Brewster's angle produces a beam translation of 125 μm. The beam window seats are machined to a precision of 5 arcmin, which

introduces a beam offset uncertainty of about 10 μm in the vertical direction per window.

If we call θ the rotation angle around a vertical axis, the horizontal shift (d_h) is given by

(29) $$d_h = t(\cos\alpha + \sin\alpha\tan\alpha')\theta/n = \theta t\left(\frac{\cos(\alpha-\alpha')}{\cos\alpha'}\right)/n$$

A rotation of the window by 5 arcmin then produces a horizontal displacement of the beam by the same amount, 10 μm.

If the faces of the window are not exactly parallel, the beam direction will differ between the two sides of the glass. The beam enters the glass at an angle of incidence α, is refracted to α', then encounters the other side at an angle of (α - γ), due to a wedge angle of γ, and is refracted to α - γ' (see fig 8). The resulting beam deviation is δ = γ - γ' . We have $\sin(\alpha - \gamma') = n*\sin(\alpha' - \gamma)$. If we let $\sin\gamma = \gamma$, $\sin\gamma' = \gamma'$, and $\cos\gamma = \cos\gamma' = 1$, since $\gamma \ll 1$, we obtain

$$\gamma' = n(\cos\alpha'/\cos\alpha)\gamma$$

(30) $$\delta = \gamma(n\cos\alpha'/\cos\alpha - 1)$$

$$= 1.14\gamma \qquad \text{for } \alpha = \text{Brewster's angle}$$

and $$= 0.4616\gamma \qquad \text{for normal incidence}$$

The quadrant detectors are about 1 meter apart. If we place the wedge exactly halfway between them (worst case) and center the beam on the quadrants, the beam will be displaced at the location of the wedge by an amount equal to δ/4 times 1 meter. The wedge specification of the windows is less than 1 arcsec, so that the maximum displacement caused by this mechanism due to a single window is less than 1.5 μm.

The largest amount of wedge is introduced by the pressure inside the target cells. The beam traverses the glass at an angle of 34.38^0, the complement of Brewster's angle. It enters and leaves the window at a distance of 3.2 mm on either side of the centerline. Because the window bulges outward under pressure, the outer and inner surface subtend an angle with respect to each other at the places of the beam crossing. The deflection of the window under pressure is given by eq. (A9) in

appendix A. Taking the derivatives at +3.2 mm and -3.2 mm, multiplying them by 1.25 to include the effect of shear gives a difference of 17 arcsec between the normals to the window at the places where the beam enters and leaves the glass. The propagation is restored to its original direction upon exiting from the target cell because the other window forms a prism with the reverse orientation. As a result, the beam receives a parallel displacement of 20 μm.

Increasing the gas pressure to 10 atm changes the index of refraction of air from 1.0003 to 1.003 . This introduces a beam deflection inside the target cell of 4.0×10^{-3} radian, leading to a change in height of the beam of 0.48 mm between the viewing area and the beam window. The height of the quadrant detectors is adjusted so that the beam height is correct in the viewing region at 10 atm gas pressure.

Next to be considered are the viewing windows. They are manufactured of Schott LF5 glass, with index n=1.583 . The horizontal beam position as perceived by the receiving optics shifts by an amount

$$x = t(1-1/n)$$

The tolerance on window thickness is 0.002 inches, so that the apparent beam position varies between windows by 19 μm for direct light and 38 μm for light reflected by the spherical mirror on the opposite of the target cell. This reflected light goes through the back window twice and the deviations accumulate.

If the window is rotated around a horizontal axis by an angle θ, the beam will seem displaced vertically by an amount

$$\Delta z = t\theta(1-1/n)$$

For θ = 15 arcmin, Δz = 10 μm.

Wedge causes a shift of

$$\Delta z = d(n-1)\gamma$$

with γ = the wedge angle and d = the distance of the window from the beam. The tolerance on the wedge is 3 arcmin, so that $\Delta z \ll 15$ μm.

The viewing windows also have a broadband anti-reflection coating on both surfaces. First all the windows were coated on one side and the reflectivities became 1.05 % at 559 nm (oxygen) and 1.18 % at 584 nm (nitrogen). The coating on the second surface produced reflectivities of 0.68 % at 559 nm and 0.90 % at 584 nm. Uncoated LF5 glass has reflectivities of 5.25 and 5.15 % respectively. Thus the coatings increased the transmission of the windows from 0.895 to 0.9827 at 559 nm and from 0.897 to 0.9792 at 584 nm. It is clear that the observed ratio of oxygen to nitrogen depends on the type of glass and the coatings of the windows used, as well as of the optics further downstream. This could conceivably impart a "signature" to each individual target cell, although the difference in transmission between windows of the same batch was smaller than the measurement precision.

D. Finite Beam Size and Fiberoptics Entrance Aperture

So far we have considered effects on the detected Oxygen-to-Nitrogen ratio as if all the light was scattered from a single point. In fact, what matters is the integral of the apparent ratio over the entire area of the beam which contributes to the detected scattered intensity. This is determined by the the beam's intensity profile, the effective apertures of the collection optics, and the transmission of the optics and filters. The Canon lens (f/1.2, 85 mm focal length) and the achromatic close-up lens (Melles Griot LAO 267) form an image of the laser beam on the front face of the tapered lucite sheet (fig. 2). The image magnification is 1.55 x. The lucite face is concave, to follow the curvature of field of the close-up lens. The sheet is 196 mm long and is tapered in both height and width. From the front to the back the height decreases from 7 mm to 3 mm and the width first expands from 41 mm to 44 mm and then narrows to 40 mm. The amount of taper and the width have been optimized to match the angular acceptance of the filters. The result is that the filters at the end of the fiberoptics will in principle (neglecting the efficiency factor of the filter)

transmit within their bandpass all the light that gets into the lucite front end, regardless of where the light enters and at what angle. Because the filters accept a larger solid angle than what is incident on the lucite it is possible to enlarge the entrance area and have the lucite taper down to the face of the fiberoptics.

The beam has a Gaussian profile ($I(r)=\exp(-2r^2/R^2)$) with a beam radius (R) of about 0.8 mm. However, R can vary by as much as a few tenths of a mm. If the image of the vertical midplane of the beam is sharp on the lucite sheet, the portions of the beam that are closer or farther from the lens will not form a sharp image. Also the solid angle accepted depends on whether one is looking at a part of the beam closer by or further away from the entrance pupil of the Canon lens. There is some chromatic aberration introduced as well by the Canon lens and also by the target cell viewing windows.

Scattered light from a certain fraction of the tail of the Gaussian intensity profile will spill over the top and bottom of the lucite, because it is imaged outside of the aperture that is formed by the lucite face. How much is spilled depends on the beam radius, the sharpness of focus and the precision of alignment. A change in any of these factors could influence the ratio of oxygen to nitrogen detected. To first order, "unknown" and "standard" will be affected in an identical way by changes in the beam radius. But the cancellations that obtain will not be perfect because sharpness of focus and local alignment are also involved.

In eqs.(22),(24) and (26) we calculated how the observed ratio of ratios (Q) is affected by small changes in the position of the scattering point with respect to the viewing optics. This can be summarized in the following formula:

$$(31)\quad \frac{dQ}{Q}(x,z) = \frac{0.0960h}{x_o^2 + h^2}x + 0.14\left(\frac{z^2}{x_0^2} - \frac{x^2}{z_p^2} - 2(f)^{1/2}\cos n\left(\frac{z}{x_0} + \frac{x}{z_p}\right)\right)$$

where:

x_0 = distance to entrance pupil of Raman optics (104 mm).

z_p = distance to entrance pupil of polarization pickup (100 mm).

h = radius of entrance pupil of Raman optics (30 mm).

The other symbols refer to figure 9, or have been defined earlier. Eq.(31) has been obtained by expanding Q(x,z) in a Taylor's series around (0,0) and retaining the leading terms. The first term is due to changes in the solid angle acceptance of the collection optics, with positive x in the direction of the lenses. The next three terms are due to discrepancies between what is measured for f from above and what f looks like from the side (eq. (26)):

$$\varepsilon''^2 - \varepsilon'^2 + 2(\varepsilon'' - \varepsilon')(f)^{1/2}\cos\eta$$

The longitudinal chromatic aberration caused by the viewing windows can be taken into account in the following way. Light scattered from an oxygen molecule appears to come from a point closer to the collection optics than if it were scattered from a nitrogen molecule. The effect is proportional to $t(1/n_N - 1/n_O)$ where t is the viewing window thickness and n_N, n_O stand for the indices of refraction at 584 and 559 nm. respectively. We were unable to obtain quantitative information about the chromatic aberration of the Canon lenses from the manufacturer. Due to the aberration from the viewing windows alone, the beam viewed via oxygen appears 5 μm closer than if viewed via nitrogen. For light that is reflected by the spherical mirror on the opposite side of the target cell the effect is 15 μm, because it passes through a window three times, each time adding to the displacement in the same direction.

The effect is modelled by including in the expression for the beam intensity an offset term:

$$I = \exp(-2((x - \Delta x)^2 + (z - \Delta z)^2)/R^2)$$

The integral of the intensity incident on the lucite is then differentiated with respect to Δx, the horizontal offset, and multiplied by the chromatic offset averaged over front and back, Δx_c (= 10 μm). This leads to a term in the integral of dQ/Q for

the received ratio of

$$(32) \qquad \frac{4(x - \Delta x)\Delta x_c}{R^2}$$

with Δx horizontal beam offset

Δx_c longitudinal chromatic aberration

We have seen that every point in the beam gives rise to a slightly different value for Q, the ratio of ratios. We have to make sure that the height of the lucite aperture is sufficiently large that phenomena such as a change in beam radius do not produce a significant effect. Therefore we will integrate deviations in Q over the beam between the limits that get through the lucite aperture.

Fig. 9 illustrates how we carry out the integration by calculating how each point on the lucite is illuminated. By definition, the point (x,z) = (0,0) in the beam is focussed onto z_1=0 on the face of the lucite. Other points in the beam, situated within the shaded cones $-0.27x < z < +0.27x$ (determined by the acceptance solid angle and magnification) also contribute to the intensity at z_1=0, albeit in a defocussed way. All contributions have to be weighted by the defocussing effect and the beam intensity distribution. The calculation is the same for other points z_1 on the lucite.

The full integral over the face of the lucite entrance sheet is then:

$$(33) \qquad \int_{-2.3}^{2.3} dz \frac{dQ}{Q}(1.55z) = \int_{-2.3}^{2.3} dz \frac{2}{\pi R^2} \int_{-4}^{4} dx \frac{2}{\pi(0.27x)^2} * \int_{-0.27x}^{+0.27x} dz' \exp\left(\frac{-2[(x-\Delta x)^2 + (z - \Delta z + z')^2]}{R^2}\right)(\text{eq.31}+\text{eq.32})[0.27x^2 - z'^2]^{1/2}$$

All dimensions are in mm. To limit the number of free parameters the beam offsets Δx, and Δz have been assumed to be the same for the Raman optics along the x-axis as for the Rayleigh pickup

along the z-axis. That assumes in fact that when the positioning of the beam is perfect with respect to one, it is also perfect for the other. We do not have to perform an integration along the y-axis (the laser beam axis) because the dependence on y of these effects is more than an order of magnitude lower.

The results show that the height of the lucite aperture, 7.1 mm (= 1.55*4.6) is indeed sufficient to rule out significant effects due to the finite size of the beam. The dependence on R between 0.6 and 1.0 mm, and on the sharpness of focus on the lucite (if less than 1 mm) is generally smaller than 1 ppm. In effect the integral of eq. 33 doesn't significantly alter the result obtained by evaluating eq. 31 at the value of Δx and Δz.

The interaction between the dependence on f and the beam offsets does give rise to some concern if the values of f are on the order of 0.01 and η is not 90^0, as is evident directly from eq. 31.

E. Incomplete Mixing of the Fiberoptics

The overall transmission factors from the sample and standard locations to the various filters are not identical. As a result the ratios of the counting rates are slightly different from 1 when the same air is present in both target cells. We will consider the uniformity of transmission in the various optical elements in order.

The illumination of the lucite entrance sheet is extremely uniform along its width because a horizontal line image of the laser beam is formed there. In the vertical there is great non-uniformity, with all the light entering near the middle and almost nothing at the edges. We tested the pieces by pointing a He-Ne laser beam at a diffuser situated against the front of the lucite. The diffuser generates an angular spread of the entering light rays with a half-width of about 7.5^o , which is comparable to that from the Raman scattering. At the other end of the lucite sheet we monitored the output by moving a photodetector

with a 10 μm wide horizontal slit along the vertical direction. The intensity at the output end differed in no place by more than 1-2% regardless of whether the He-Ne beam was pointed at the center or at the edge of the front face.

As we mentioned before, the fiberoptics that brings the "standard" and the "unknown" side together consists of a total of 40 fused fiber bundles, with each bundle containing about 1600 fibers. The transmission through each of these bundles and the widths of the cracks between adjacent bundles are far from uniform. When the He-Ne laser is scanned across the front the total light output from the back oscillates, depending on whether a part of the laser beam falls into a crack. These transmission minima vary between 60% and 90% of the average maximum. The maxima themselves vary among each other by 5-10%, except one which is only 70% of the others.

From the beam spot diameter and the variation in the minima we estimate that the effective width of the cracks, including broken or defective fibers along the edges, is between 0.1 and 0.3 mm. The width of each (square) fiber bundle is 2 mm on the side. The overall transmission on one side is 77%, on the other it is 81%.

The central mixing bar, with dimensions 585x16x10 mm, was tested in the same way as the entrance sheet with the diffuser and the He-Ne beam. The laser beam was pointed at a corner, at the middle of an edge, and at the middle of the bar (I,II,III in fig 10). We measured the output through a 1 mm round aperture moving along the middle or along an edge at the other end (A, B in fig 10). Light from any one point will irradiate the entire back end, but we see from fig 10 that the area exactly opposite the illuminated spot may receive, as a typical figure, 50% more than the average. This increase falls off over a distance of 2-4 mm. The overall transmission of the lucite bar is 92%.

The second set of fiberoptics takes the light from the lucite bar and divides it into 4 output bundles, each of which leads to a different filter and photomultiplier. We tried to

make sure that each bundle samples the lucite bar uniformly and also that light from each area of the bar does not leave the bundle from just a few spots, but from fibers sprinkled over the entire output end. We tested its uniformity by illuminating the front end through a 25 mil wide slit. We monitored all 4 outputs while moving the slit. The result is plotted in fig 11. About half of the fibers are devoted to oxygen, to increase its counting rate relative to nitrogen.

The slit (area 6.4 mm) illuminates about 2000 fibers simultaneously so that the variations in the transmission of the oxygen channel should be $1/(1000)^{1/2} = 3\%$ in the case of perfect randomization of the fibers and identical and flawless fibers. The actual performance is about 4 times worse than that. The standard deviation of the transmission for the different slit positions is 13%, relative to the average, for the O_2 channel. It is 18% for the N_2 channel. These numbers are based on 25 independent samples or slit positions.The overall transmission is about 50%, with 23% coming out of the O_2 channel, 11% from N_2 and 8% each from the other two.

What is the order of magnitude of the imbalance in the transmission that we can expect for our fiberoptic system? First of all, the illumination of the central lucite bar is very insensitive to beam movement and chromatic aberration due to the defocussing provided by the entrance sheets. Therefore, we feel that there are no significant differences in the transmission of the front end for O_2 and N_2 scattered light, except for the surface reflections being different for the two wavelengths. These wavelength dependent effects are exactly the same on both sides, however.

The "unknown" and "standard" side illuminate the central mixing bar in a checkerboard pattern with a total of 40 2x2 mm squares. Because the lucite is not infinitely long there is still a recognizable modulation of the light intensity at the back end when the input comes from the "unknown" only. Based on the data shown in figure 10, this modulation will be on the order

of 2-3%.

The modulation "samples" the transmission curves of fig 11 with the result being slightly different transmission factors for light coming originally from "unknown" or "standard" for each of the 4 output channels. The spatial frequency of the modulation matches the resolution of fig 11 rather well. Therefore we can take 20 samples of the curves in fig 11, each of which has a standard deviation of 13% in the case of oxygen. The standard deviation of the sum is then $13/(20)^{1/2} = 2.9\%$. If the transmission of the light coming from "unknown" is high by 2.9% it will be too low by 2.9% for "standard". For nitrogen the figure is $18/(20)^{1/2} = 4.0\%$.

The standard deviation for the expected offset of the ratios is then 10% ($= (8^2+5.8^2)^{1/2}$), if the input to the last fiber stage were 100% modulated, that is, if the inputs from "unknown" and "standard" were incident on totally separate fibers. The actual offset from 1 to be expected for Q is the product of the modulation intensity (0.02-0.03) and the non-uniformity of the last stage (0.10), 0.002-0.003. This represents a constant offset, that should not be affected, to a very good approximation, by laser beam drifts, temperature, or humidity.

F. Filter Transmission

The transmission characteristics of the filters at normal incidence are shown in fig 12, together with the intensities of the O-, Q-, and S-branches of the fundamental ro-vibrational Raman bands that they are to transmit. Our filters are 4-period interference filters manufactured by Spectrofilm Inc. It should be remembered that the depolarization of the Q-branch ($\rho_Q = 0.047$ for O_2 and $\rho_Q = 0.022$ for N_2) is different from that of the side branches which is 0.75. As a result the spatial distribution of the light intensity of the side branches differs from that of the Q-branch. Indicated on fig 12 is the location of the centers of the Q-branches of the "hot band" and the molecules containing a

rare isotope, $N^{14}N^{15}$ and $O^{16}O^{18}$. The hot band arises when the lower state is not the vibrational ground state but the first excited state.

The transmission of the filter for the light of interest is influenced by two factors: the bandpass characteristic moves when the filter temperature changes and the bandpass shifts to shorter wavelengths at larger angles of incidence (we define normal incidence here as zero). The intensity of the light as a function of frequency can change also. When the sample gas temperature is higher the Boltzmann distribution over the rotational states widens and the population of the first excited vibrational level (hot band) increases.

The signal-to-noise ratio is maximized when the Q-branch is contained within the filter passband, but is located on the short wavelength side of a relatively narrow band filter (fig 12). The light coming from the optical center line will go through the filter at normal incidence. However, the endface of the fiberoptics presents a finite field of view to the collimating lens and there will be light coming from the fibers several mm away from the optical center line. After collimation that light will traverse the filter at an angle and as a result the Q-branch will now be located on the long wavelength side of the (shifted) passband. Our first priority is not signal-to-noise however, but stability, especially with respect to any temperature effects. This is best accomplished by choosing a very wide and flat-topped bandpass (the 4-period filters in fig 12).

We will look in more detail at the shift of the bandpass and the angles of incidence that apply in our case. The wavelength shift of the filter as a function of the angle of incidence (ψ) is given by

$$\lambda = \lambda_n(1-(\sin\psi/n)^2)^{1/2} \qquad (34)$$

with: λ_n wavelength at normal incidence

n effective index of refraction (= 2.1 for these filters)

After collimation by the Nikkor 50 mm f/1.8 camera lens the light

from every fiber will approach the filter as a parallel bundle but at an angle that is different for each fiber. The uniformity of the filter is very good across the face. The transmission through the filter can be calculated for each fiber as the convolution of the O-, Q-, and S-branch intensities with the filter passband that is shifted by the appropriate amount for each fiber. The algorithm that computes this, for various temperatures of the sample gas and the filter, is given in appendix C (program BDPASS).

Table 1. Filter Transmission

	narrow band		wide band	
	O_2	N_2	O_2	N_2
Q branch location (A)	5593	5846	5593	5846
bandwidth (FWHM) (A)	47	39	185	135
Bandcenter (A)	5614	5860	5622	5869
Tilt angle (^{o})	6.5	4.	0.	0.
Transmission (t)	0.31	0.44	0.53	0.55
Depolarization (ρ)	0.149	0.124	0.182	0.083
t for rare isotope	0.16	0.20	0.50	0.51
ρ for rare isotope	0.389	0.124	0.182	0.083
Dependence on temp. of filters (/K):				
(dt/dT)/t (ppm)	-6000	-3200	-450	-1600
$d\rho/dT$ (ppm)	850	190	10	70
Dependence on temp. of gas (/K):				
1/t(dt/dT) (ppm)	-238	-127	-28	-36
$d\rho/dT$	88	-53	-11	-14

We have calculated the transmission for a number of filters in this way, with the transmission profiles as supplied by the manufacturer. In the computation the entire filter can be tilted with respect to the optical axis, moving the bandpass with

respect to the Raman lines, in order to optimize the transmission. Some results of these calculations are shown in table 1. It is clear from the table that the required stability for our measurements is hard to obtain with the narrow band filters.

If the temperature of the unknown gas increases by 1 degree relative to the standard the ratio of ratios changes by -238 + 127 = -111 ppm because the relative change in the oxygen counting rate is -238 ppm and in nitrogen -127 ppm (table 1). To combat this problem, the difference between the temperatures of the two gases being measured must be kept below about 0.01 degree. This requirement is much relaxed for the wide band filters where the gas temperature dependencies are -28 and -36 ppm/K respectively.

The dependence of the transmission on the filter temperature is also considerable, and there are other factors that can have a similar effect on the position of the bandpass, such as ageing and moisture uptake. To first order, the transmission of standard and sample will be affected equally, so that their ratio does not change. However, since the distribution of light originating from standard and from unknown is not perfectly uniform upon leaving the fiber output bundles (see Section III E) there is still a small effect.

To estimate its magnitude, let us compare half of the fibers that comprise the inner core of the output bundle at the output end with the outer half of that bundle. Taking the oxygen bundle as our example, the inner half consists of roughly 12,000 fibers. If the fiber distribution were truly randomized one would expect 6000 ± 77 (1.3%) to originate on areas of the lucite bar where "unk" is slightly favored. From Section III E we know that the actual randomization of the output bundle is four times worse than what is theoretically possible, so that 52½% of the fibers of the inner half might be looking at areas favored by "unk" and 47½% at areas favored by "std". This situation would then be vice versa for the outer half of the output bundle. The

average displacement of the filter transmission characteristic for the inner half is 7 cm^{-1} and 21 cm^{-1} for the outer half. With a transmission curve shift with temperature of 0.75 cm^{-1}/K the transmission changes by about -5×10^{-4} and $-10 \times 10^{-4}/K$ respectively for the two halves. The total transmission is 0.50 so that these changes are -0.1% and -0.2% respectively. The ratio of UNK to STD then changes as

$$\frac{(0.5 + 0.025)(1 - 0.001) + (0.5 - 0.025)(1 - 0.002)}{(0.5 - 0.025)(1 - 0.001) + (0.5 + 0.025)(1 - 0.002)}$$

or $1 \times 10^{-4}/K$ if the output of the lucite bar were fully spatially modulated with respect to UNK and STD. In section III E we showed that modulation to be only about 0.02 to 0.03 so that the effect of temperature variations of the oxygen filter would be 2-3 ppm/K in the ratio of UNK to STD. For the nitrogen filter a similar estimate leads to the same result.

Finally, the filters transmit a small fraction (between 10^{-3} and 10^{-4}) of the light they are not supposed to transmit. This effect can easily be measured by, for instance, putting pure Ar (no Raman scattering) or pure O_2 gas in the cells and collecting the counts on all detectors. Appropriate corrections can then be made.

G. Dark Current, Background, and Detector Non-linearity

Dark current is the number of photon counts per second that is registered when there is no light hitting the photocathode. A major cause is thermionic emission from the photocathode. The photomultipliers for O_2 and N_2 (RCA 31024A) have dark currents of several thousand counts per sec. The one for CO_2 (RCA 31034A), which has a much lower photon rate, is cooled and has a dark current of about 180 per second.

The dark current has to be subtracted to obtain the real photon rate. The dark current is sufficiently unstable that we

have to monitor it, in order to be able to make a reliable subtraction. Once a second the laser is cut off by a shutter during which time the dark noise in all detectors is measured. The dark current is not influenced by the photon rate. We tested this by varying the light intensity while running the two tuning fork choppers in exact coincidence. The photomultipliers are then in the dark every half-cycle and receive double the amount of light during the other half of the cycle. The instability of the dark current is also independent of the photon rate. The dark counting rate and instability generally increases with the length of time that the photomultipliers have high voltage applied to them. This still occurs when they are kept in the dark with the voltage on. The dark current on the PMT devoted to oxygen typically increases from 3000 counts per second to 3500; the typical increase on the nitrogen PMT is from 13,000 to 18,000 per second.

We define background as counts due to real photons that do not originate from the gas molecules we are looking at. There is some fluorescence in the beam windows where they are traversed by the laser beam. We have tested a number of glasses for fluorescence and high purity fused silica was the lowest. On our spectrometer with a resolution of 1 nm it showed up as a broad continuum in the red and infrared. The elastic scattering is extremely bright where the laser crosses the windows, but it is possible to see the glass fluoresce as a faint red line if one blocks the scattered laser wavelength with long-pass laser safety goggles.

Additional fluorescence takes place on the walls of the target cell that get hit by elastically scattered laser light. This source of fluorescence increases with increasing gas pressure as the target cell gets brighter through the increased scattering from the gas molecules.

The glass fibers and the lucite light guides constitute another source of fluorescence. The light traverses about 2 m of material. If during this time only 0.001 of the Rayleigh light

would be converted to longer wavelengths, that would be a large signal on the Raman detectors. The Rayleigh cross section is 2000 times as large as the Raman cross section of the scattering gas. Each filter accepts only a fraction of the wavelength continuum of the downshifted fluorescent light and also the solid angle of acceptance has to be taken into account. We found that this source of fluorescence contributes 10-20% of the oxygen and nitrogen signals, while it swamped the CO_2 detector. It disappeared by placing a sharp cut-off long pass filter (Schott OG530) in front of the fiberoptics. A tiny fraction still survives; it is generated by fluorescence in the target cell viewing windows,the Canon lens, and the cut-off filter itself. Another part is due to the Rayleigh light that still gets through the Schott filter (less than 10^{-4}).

The background, since it is broadband, is satisfactorily monitored by a filter with a bandpass in between that of oxygen and nitrogen. It can be subtracted after a calibration with different gases at various pressures, including vacuum.

Crosstalk we define as photons at the wavelength of oxygen appearing at the nitrogen detector and vice versa. The effect is small since the interference filters behind the fiberoptics have excellent rejection for wavelengths outside of the bandpass. The effect shows up when calibrating the system with different gases. Fluorescence in the fiberoptics shifting oxygen light to nitrogen wavelengths would be indistinguishable from crosstalk, however. For the backgrounds and crosstalk on the O_2 channel we measure 310 + 14/psi counts per second with Ar gas and 310 + 33/psi with N_2 gas for one of the target cells (UNK). The other target cell had 920 + 31/psi for Ar and 920 + 62/psi for N_2 gas.

Detector non-linearity obviously can effect the ratio of two different counting rates. First of all the dead time effect increases with high counting rates. After the discriminator has been triggered the signal needs to go below a certain level before it can be triggered again. If a pulse comes before that

has happened it will not be counted. We measured the dead time per pulse for both photomultiplier-amplifier-discriminator combinations by splitting the pulse into two cables one of which has an adjustable length (delay) and then recombining them again. All counting rates are corrected for dead time effects (dead time about 2 nsec). Another non-linearity is that at high counting rates the gain of the tube decreases so that a larger fraction of the pulses will not reach above the discriminator level. There is a tendency for tube "fatigue" after prolonged periods of counting at high rates. We monitor this by counting all pulses at two discriminator levels, one higher than the other.

To get a more quantitative idea of how remaining non-linearities and things like background and dark current affect the measurement of the ratio of light intensities, we will adopt the following simple model of the relationship between counting rate (N) and photons (P) hitting the detector:

(34) $$N = D + qP + nP^2$$

with
- D dark count
- P = U + B (unknown + background) or S + B (standard + background)
- q "quantum efficiency" (including amplifier and discriminator)
- n coefficient of nonlinearity of response

If we assume that U-S << S; nP << q; B << U,S; and D/q << U,S, then we have to a good approximation:

(35) $$\frac{N_u}{N_s} = \frac{U}{S}\,1 + \frac{D}{qS}\,\frac{S-U}{S} + \frac{nS}{q}\,\frac{U-S}{S} + \frac{B_u - B_s}{S}$$

The ratio of the counting rates is a faithful representation of the Raman light intensities (U, S) if the difference in illumination from U and S can be kept small, and if the correct background subtractions are applied. The magnitude of D/qS is about 2×10^{-3} for the O_2 detector and 6×10^{-3} for N_2; nS/q is about 3×10^{-3}. In our determination of N_u/N_s we apply the darknoise, background and non-linearity corrections first, before

taking the ratio.

The error that is made in the final ratio depends on the errors in our darknoise measurement, non-linearity correction (drift of PMT dead-time) and stability of the backgrounds, because these contributions are subtracted from the total counting rate before a ratio is taken. We subtract the same dark noise from both unknown and standard. The dark count is actually noisier, by a factor of 2.5 to 3, than what would be expected from counting statistics alone. We have verified that the dark count during the "unknown" and "standard" sub-periods is the same, within the noise that is inherent in the dark count. Therefore, the error due to the assumption of equal dark count during both sub-periods is small, only about 1/10 of the error due to the counting statistics of the actual oxygen and nitrogen Raman signals. The error due to the absolute amount of the darknoise subtraction is negligible, since the uncertainty in the darknoise is multiplied by the percentage unbalance of the unknown and standard signals, which can easily be made less than 0.5% (eq. 35). Likewise, an error in the dead time correction of 5% would lead to an error of only $0.05 \times 3 \times 10^{-3}$ times the percentage unbalance, or less than 1 ppm. The dead time has been checked a number of times and does not appear to change. The background subtraction is important and has to be known accurately, since balancing the total counting rates from unknown and standard does not help--each target cells has its own background. The backgrounds are on the order of 1/1000 of the Raman counting rates of O_2 and N_2.

H. Temperature of Front End Optics

The front end optics at each side consists of the target cell windows, Canon lens, OG 530 Schott glass filter, Melles Griot lens, lucite entrance sheet and the first fiber bundle. The transmission of all these elements depends somewhat on temperature and this temperature dependence is not necessarily

the same for different colors. The Schott glass filters, in particular, are designed to have a sharp wavelength cutoff, the location of which is influenced slightly by temperature. In addition there is the possibility of moisture buildup on all optical surfaces, possibly to a thickness of some 50 molecular layers. Such a film is not visible to the naked eye, but since the index of refraction of water is intermediate between air and glass, it would form an interference layer a fraction of a wavelength thick. Due to the different (proprietary) multi-layer coatings on the optical surfaces and their unknown thicknesses and refractive indices we are not able to calculate either the effect of temperature on transmission or the effect of a layer of water even if we knew its thickness.

We have measured the effects of temperature on what we believe are the most sensitive elements: the OG 530 filter and the Canon lens which has a total of 16 coated optical surfaces. We wound electrical heating tape around the assemblies of both unknown and standard side, with and without the Schott filter in place. (Normally the filter is screwed onto the Canon lens.) We increased the temperature of the optical elements by about 15 degrees in this way.

We found an interplay between transmission changes with temperature of the filter and the lens, which have different response rates. Also, both lenses did not react in the same way. The response of the filter is immediate and it shifts the absorption edge toward longer wavelengths. Fig. 13 gives the measured transmission profile of the OG 530 (thickness 6mm). The oxygen line is affected more than the nitrogen line because it is closer to the absorption edge. The change in the oxygen to nitrogen ratio on the unknown side was 600 ppm/°C. For the standard it was 900 ppm/°C, although on this side we did not measure the temperature, we only put the same current through the heating tape. These changes are close to what we can expect from fig. 13 when we consider the manufacturer's specification that the transmission edge (50% point) shifts by 1.2 Angstroms per

degree. The slope of the extinction curve at the halfway point is 0.005/A so that the extinction should increase by 0.006/°C. The transmission is exponential with thickness, x, ($T=e^{-kx}$), so that the decrease in transmission from 0.500 to 0.494 corresponds to an increase in k, the absorption coefficient, by 1.7%. If the extinction coefficient at the wavelengths of oxygen and nitrogen would increase by the same 1.7% per degree C, the transmission for oxygen would decrease by 9.0×10^{-4} and for nitrogen by 1.7×10^{-4}. The ratio of oxygen to nitrogen is then changed by 730 ppm/°C . The temperature dependence of the present OG 530 filters is so severe that they will be removed from the system. Controlling the temperature to the degree required would be impractical.

The temperature response of the Canon lenses is delayed by 30-45 minutes and it is less severe than for the filters. We do not know why the lenses respond more slowly than the filters, but it could be explained if the response of the lenses is due to a small amount of internal water vapor which takes some time to equilibrate. After equilibrium had been reached, the transmission of the lens on the "standard" side increased by 2.4×10^{-4}/K for N_2 and 2.2×10^{-4}/K for O_2. The transmission of the lens on the "unknown" side decreased by 4.0×10^{-5}/K for N_2 and by 3.8×10^{-5}/K for O_2. Therefore, if we control the temperature of the lenses to 1/20 of a degree the measured ratios of O_2 to N_2 will not change by more than 1 ppm.

I. Sample Storage

Samples may be stored for a considerable period of time between being collected and being analyzed, and ideally, it should be possible to maintain standards indefinitely without any observable change in composition. To this end, great care is taken to minimize the possiblity of oxidation reactions within the cylinders by passivating internal surfaces and excluding liquid water from the samples (Section II.-I). Nonetheless, it

is impossible to prevent all interactions between the containers and the stored air. Some adsorption of gas molecules on the internal surfaces of the cylinders must be expected. An upper limit can be placed on this effect by assuming that the effective internal surface area is 10 times the geometric area, and that a complete monolayer of gas is adsorbed. The surface area-to-volume ratio is most unfavorable for the smallest cylinders that we use: 300 ml Whitey stainless steel sample cylinders. We pressurize these to about 1800 psi, so they initially contain about 37 liters of gas at STP, or about 1.5 moles. The internal surface area is about 400 cm^2 assuming it is perfectly smooth; allowing a factor of 10 increase in surface area due to irregularities, and taking the size of an adsorption site to be 14 A^2,[13] there are $3x10^{18}$ sites, or room for $5x10^{-6}$ moles of gas. Because of the flushing proceedure during sample collection, the cylinder walls presumably reach equilibrium with the sample before the final volume of air is sealed into the cylinder, thus the initial concentration should not be effected by adsorption. The fraction of surface sites which are occupied, however, may be effected by the temperature and pressure of the cylinder. In the worst case, all the sites could initially by occupied by oxygen, and this saturation could decrease to 50% if the pressure decreased to 500 psi as the gas was used up. This would cause a rise in the O_2 concentration of a few ppm. An effect of this magnitude is very unlikely to occur, however. Although there may be a significant difference between the heat of adsorption of oxygen and nitrogen, it is unlikely that the percent of sites which are occupied would change significantly over the working pressure range. At all pressures above a few micro-torr, essentially complete saturation would be maintained. Thus, although a significant quantity of gas will be adsorbed on the cylinder walls, the adsorbed population should remain essentially constant, and therefore, the gas concentration in the cylinder should not be effected.

Another potential problem in sample storage is dissolution of gas in the bulk metal of the container wall. The dissolution

of nitrogen in iron has been measured at 700°C and 1 atm. pressure[14]. Because diatomic gases dissociate upon dissolution, the equilibrium concentration scales with the square root of pressure. For small temperature changes, the enthalpy of solution is roughly constant, and the equilibrium solute concentration scales exponentially with temperature. If it is roughly valid to extrapolate from 700°C to room temperature and from iron to steel, then the mass of dissolved nitrogen would be on the order of 10^{-8} times the mass of the cylinder. The small cylinders weigh about 1 kg and contain about 50 g of gas when full. Since the cylinders are considered empty when the remaining gas weighs about 10 g, the gas dissolved in the walls of the cylinder can never represent more than 1 ppm. Once gas is dissolved in the cylinder walls, it is possible for it to diffuse out of the cylinder, driven by the 100 atm. pressure gradient. An upper limit on this diffusion rate is provided by data from Hydrogen, however, which indicates that it would be far more than 10 years before 1 ppm could escape.

IV. STATUS AND PROSPECTS

In the proceeding sections we have discussed a wide variety of effects which can influence the measured oxygen-to-nitrogen ratio of a sample compared to a standard in our Raman scattering apparatus. Of these factors, some, such as incomplete mixing of the fiber optics, produce a fixed offset between the actual and measured concentration ratios. These do not pose a problem because they can be calibrated out, to a large extent, using standards of known composition. While absolute accuracy will be limited by the accuracy with which standards can be prepared, the precision with which comparative measurements can be made will not be limited by such offsets.

Another set of potential causes of error have led to design constraints which must be met in order to keep the induced errors below a tolerable level. In our case, the design goal is a precision of 1 ppm. This has led us to implement an active feedback system in order to keep the laser beam position well within the required 60 μm tolerance for horizontal beam movement. Moderately tight tolerances on the optical alignment, including the target cell windows, were also required to meet this specification. Similarly, the interference filters must be maintained at a constant temperature to within 0.3°C, and the difference between the temperatures of the two target cells must be kept below 0.1°C.

Furthermore, the OG530 filter will have to be abandoned, and the temperature of the Canon lenses apparently must be held constant to 0.05°C. Without such temperature control, the ratio-if-ratios can drift on the order of 100 ppm over a day or longer. After we had implemented the polarization measurement and made corrections to the counting rates accordingly, we found that there could still be a residual long term drift of the above magnitude. Putting the entire front end in a temperature controlled environment is now the highest priority. Since there was not enough time to implement this in Berkeley it will be done

after the experiment is moved to Boulder. The dark box enclosing the scattering regions will be thermally insulated and we will blow dry, dust-free air over the optics. The air will be heated a few degrees above ambient with the temperature controlled by a feedback signal based on the temperature of the lenses.

Two important sources of error cannot be eliminated, but must be monitored and corrected for. These are laser polarization and background counts due to photons which do not originate from the gas molecules. Laser polarization within each target cell is continuously monitored as described in section III-B. We have found that the x-polarized fraction has a magnitude of up to one-thousandth of the main z-polarization, although the value may change by a factor of 5 during a run. Thus we must make corrections on the order of 100 ppm, and our precision is limited by how accurately this correction can be made. Currently the accuracy of the polarization measurement during a single update (10 minutes of counting) is limited by electronic noise equivalent to 11 ppm in the ratio-of-ratios. This is well below the statistical precision per update. Since we do not presently know the power spectrum of this noise it is not clear how much better the polarization measurement becomes when overaged over a typical run of 100 updates. The electronic noise is well above the inherent noise of the detector, and thus optimizing the circuit design and construction could reduce the residual error to below 1 ppm.

Correcting for backgrounds represents a somewhat different problem. We can precisely measure the background rates at any given time by evacuating the target cells or filling them with pure gases. Counting statistics are not a problem because the background rates are only about one-thousandth of the total counts. Our present set of background measurements is not reliable since the target cells were found to have small leaks. For instance, our measurements with Ar were probably contaminated with some air. The background is also sensitive to the presence of dust particles in the beam, as is the polarization

measurement. Dust we have eliminated by inserting glass-fiber particle filters into the gas manifold leading to the target cells. In addition to eliminating dust and obtaining leak-free target cells, the background correction will be improved by continuous monitoring using one of the output legs with a filter which lies between oxygen and nitrogen. This may allow us to obtain a stable correlation between the rates on the background channel and the background rates on the oxygen and nitrogen channels.

Laser power has been somewhat disappointing with the target cells in the cavity. We lose about a factor of 2 in beam power when we insert the target cells into the laser cavity, and the power drops by another factor of 2 as we increase the pressure in the target cells to 10 atmospheres in order to increase the counting rate. This decrease in intra-cavity power is apparently due to stresses on the beam windows; we were able to place the target cells in the beam with the windows loosely attached (unsealed) without an appreciable degradation of laser power. At 10 atm pressure we have about 20 Watts of laser power left. This leads to counting rates of $2 - 3 \times 10^6$ per second for the O_2 and N_2 detectors, and statistical precision of 100 ppm/update. With this laser power, the best we can achieve during a run of about 100 updates is then a precision of about 10 ppm. Since 10 ppm is the precision of the ratio of O_2 in the sample vs. the standard, this would enable comparative measurements of the atmospheric oxygen concentration to 2 ppm. As of this time we are short of this goal because of long-term drifts, apparently due to the effect of temperature on the front-end optics. Because intra-cavity power is significantly degraded by stress induced birefringence in the target cell windows we are considering eventually abandoning intra-cavity operation in favor of a light trapping scheme used by Hill and Hartley[15]. In this approach a high power intensity is built up by injecting the external laser beam, at a slight angle, into a cell defined by a flat mirror on one side and an elliptical mirror on the other. With appropriately chosen curvature and mirror separation the

propagation direction will collapse to the major axis of the elliptical mirror after a few bounces. This approach would be relatively insensitive to birefringent elements in the cavity, and may allow us to significantly improve the statistical precision of our measurements.

We have taken air samples from the coast of California during 1984. They are stored at high pressure in Whitey stainless-steel cylinders. In November 1984 sample collection was begun at Cape Grim, Tasmania, in collaboration with Dr. Roger Francey of CSIRO, and in early 1985 sampling was started at the South Pole GMCC station. These samples are waiting to be analysed when the temperature control of the scattering region and associated optics has been implemented. We expect the temperature control to be in place about 2 months after rebuilding the apparatus in Boulder.

To tie the samples to absolute concentrations we have on order a set of 4 standards from the Van Swinden Laboratory in the Netherlands. The oxygen content in these standards will be determined gravimetrically to ±30 ppm (2 σ) and they will span a range of a few hundred ppm around ambient.

V. APPENDICES

A. The Polarization of the Laser and Window Stresses

The maximum stress on the surface of the glass at 10 atm. is about 4.5 N/mm^2. With a stress optical coefficient of $3.5*10^{-6} mm^2/N$ such a stress would give rise to about one third of a wavelength of retardation if this stress were uniform throughout the glass. Fortunately, the stress decreases and then changes sign as the beam probes further into the glass. A retardation is then cancelled by an advance. There is no net effect if the beam goes exactly through the center of the window. Furthermore, it is the difference in stress between the radial and tangential directions that causes the birefringence. Nevertheless it is clear from this order of magnitude estimate that these stresses have to be considered carefully.

Fig A1 displays the behavior typical for stressed optical glass. $n_{\parallel}$ and $n_{\perp}$ are the indices for the electric field vectors parallel and perpendicular to the direction of the stress (σ), respectively. The stress optical coefficient is defined as

(A1) $$K = K_{\parallel} - K_{\perp} = (n_{\parallel} - n_{\perp})/\sigma$$

Positive means that for tensile stress the $\parallel$ polarization will have a higher index than the $\perp$ polarization, although for both the index will be less than for unstressed glass. The parallel polarization will be retarded with respect to the perpendicular polarization.

It is sufficient to consider the case of tensile and shear stresses in the plane perpendicular to the direction of propagation, because that is where the polarizations are. Stress along the propagation axis cannot affect the two polarizations differently.

We will first look at the the pair of shear stresses along the z- and x-axes (fig A2). This is equivalent to a pure tensile stress along the t-axis and compression along the c-axis, at 45°

to the original z- and x-axes. The light, originally polarized along the z-axis, decomposes into two components:

$$E_z = \frac{1}{(2)^{1/2}} E_t + \frac{1}{(2)^{1/2}} E_c \tag{A2}$$

The change in the index of refraction equals

$$\begin{aligned} &\text{for } E_t: && \Delta n_{t\parallel} + \Delta n_{c\perp} = n_\parallel - n_\perp \\ &\text{for } E_c: && \Delta n_{c\parallel} + \Delta n_{t\perp} = n_\perp - n_\parallel \end{aligned} \tag{A3}$$

since the effects add linearly and the stress in the c-direction is compressive so that the index change reverses sign. The magnitude of $n_\parallel - n_\perp$ equals $(K_\parallel - K_\perp)\sigma = K\sigma$, the stress optical coefficient times the stress. After having traversed a certain distance E_t has accumulated a retardation ϕ, expressed as a phase factor $e^{-i\phi}$. At the same time E_c has accumulated a phase factor $e^{i\phi}$.

Transforming back to x- and z-coordinates now gives us

$$\begin{aligned} E_z' &= (1/2)^{1/2} E_z (e^{-i\phi} + e^{i\phi}) = E_z \cos\phi \\ E_x' &= (1/2)^{1/2} E_z (e^{-i\phi} - e^{i\phi}) = -iE_z \sin\phi \end{aligned} \tag{A4}$$

The shear stresses have turned the originally linear polarization into elliptical polarization.

When the glass is subjected to pure tensile stresses in the z-direction (σ_z) and the x-direction (σ_x) the changes in index are:

$$\begin{aligned} &\text{for } E_z: && K_\parallel \sigma_z + K_\perp \sigma_x = \tfrac{1}{2}(K_\parallel + K_\perp)(\sigma_z + \sigma_x) + \tfrac{1}{2}K(\sigma_z - \sigma_x) \\ &\text{for } E_x: && K_\parallel \sigma_z + K_\parallel \sigma_x = \tfrac{1}{2}(K_\parallel + K_\perp)(\sigma_z + \sigma_x) - \tfrac{1}{2}K(\sigma_z - \sigma_x) \end{aligned} \tag{A5}$$

Pure tensile stresses along the polarization directions do not mix the polarizations, but produce a retardation per cm of E_z with respect to E_x of $K(\sigma_z - \sigma_x)$. Any combination of tensile and shear stresses in 3 dimensions can be transformed to a set that is aligned with the polarizations and the direction of propagation of the light.

We will now take a look at the stress patterns that develop when the window is subjected to a pressure of 10 ato. We

consider the case of a circular plate freely supported on a circle along the edge. The support is the metal C-ring making the vacuum seal with the target cell. The window is clamped from above with a ring that has a 2.1 mm wide contact area with the glass, situated exactly above the C-ring. This way of clamping exerts very little bending moment on the glass.

The window and the notation for the various coordinates is sketched in fig. A3. The stress pattern parallel to the glass surfaces is given by:[16]

$$\sigma_r = -\frac{3W}{4mt^3}(3m+1)\left(1-\frac{r^2}{a^2}\right)z' \qquad \text{(A6)}$$

$$\sigma_t = -\frac{3W}{4mt^3}(3m+1)\left(1-\frac{m+1}{3m+1}\frac{r^2}{a^2}\right)z'$$

with

W	total applied load (1100 N), in z-direction
t	thickness (9.5 mm)
a	radius (19 mm)
r	distance from center
m	inverse of Poisson's ratio (1/0.17)
z'	depth normal to surface (z'=0 is midplane)

The subscript r is for stress in the radial direction, t is for tangential direction. A positive sign means tension, negative stands for compression. The tension and compression are maximum in the center, falling off toward the edges. They are zero in the neutral plane.

In addition to these tensile and compressive stresses there are also shear stresses. They are given by

$$\tau_{zr} = \frac{Wr^2}{a^2}\frac{3}{rt^3}\left(\frac{t^2}{4} - z'^2\right) \qquad \text{(A7)}$$

The shear stresses are largest at the neutral plane and the directions are indicated as in fig. A1 .

For completeness we will give the total deflection in the center:

$$d = -\frac{3W(m^2-1)a^2}{16\,Em^2t^3}\left(\frac{5m+1}{m+1} + \frac{4m}{m-1}\frac{t^2}{a^2}\right) \qquad \text{(A8)}$$

with d displacement, positive in +z' direction

E Young's modulus (75000 N/mm)

The first term is due to pure bending without shear and the second is the additional displacement through shear. In our case t/a=1/2 so that the second term contributes a little more than 20% to the total displacement. The deflection as a function of radius for the case of pure bending is:

$$(A9) \quad d = \frac{3W(m^2-1)}{8\ Em^2t^3} \left[\frac{(5m+1)a^2}{2(m+1)} + \frac{r^4}{2a^2} - \frac{(3m+1)\ r^2}{m+1} \right]$$

The laser beam traverses the windows at an angle of 34.4°, after refraction from Brewster's angle of incidence. Fig. A4 depicts the situation and the coordinates used in two windows of one target cell. The x',y',z' coordinates are fixed in the window and differ from the laboratory x,y,z coordinates by a rotation around the x-axis. The normal to the window surface subtends an angle of 55.6° (Brewster) to the beam, that is traveling along the laboratory y-axis. The polarization that is labeled v (for vertical) has an angle of 34.4° to the y'-axis in the glass. The other polarization is labeled h (for horizontal) inside the glass.

The calculation of how the glass affects the laser polarization proceeds as follows. First of all we assume that the total amount of h-polarization is small at every point, so that the v-amplitude is barely affected. In fact we assume the v-amplitude to be constant, and calculate the amount of generated h-amplitude at each point. We follow each part of the beam through the glass, calculate the stresses at each point, transform the stresses to coordinates proper to the beam, calculate the generated h-amplitude and also the phase difference that is being accumulated between the v- and h-polarizations. The h-amplitude that has been generated is then added (coherently), with the correct phase difference, to what has been generated earlier along the path of the beam.

The transformation of the stresses to beam coordinates is shown in fig. A5 . An elementary block of material internal to

the glass is depicted with the tensile and shear stresses on it. r, t and θ are the coordinates of fig A3. The only non-zero stresses are σ_r, σ_t, and τ_{zr} and their transformation is as follows[16]:

$$\sigma_h = \sigma_r \cos^2\theta + \sigma_t \sin^2\theta$$

$$\sigma_v = \sigma_r \sin^2\alpha \sin^2\theta + \sigma_t \sin^2\alpha \cos^2\theta + 2\tau_{zr} \sin\alpha \cos\alpha \sin\theta \quad \text{(A10)}$$

$$\tau_{hv} = (\sigma_r - \sigma_t) \sin\theta \cos\theta \sin\alpha + \tau_{zr} \cos\theta \cos\alpha$$

The sign of the stresses as a function of z' reverses between the two windows on either side of the target cell, as depicted in fig A4. The actual calculations have been carried on our LSI-11 computer. The Fortran code is given below.

```
FORTRAN IV      V02.6      Wed 10-Oct-84 12:13:09                PAGE 001

0001            PROGRAM STRESS
      CCCC      LINK WITH RK3:QSF
      CCCC      Calculates optical rotation of the beam as it goes
      CCCC      through the windows. Beam offsets are taken into
      CCCC      account. No offset means that the beam goes through
      CCCC      the center of the glass in the neutral (mid-)plane.
      CCCC      The window is under 10 ato of pressure, edges are
      CCCC      supported, not clamped. In reality there is some bending
      CCCC      moment applied at the edges, so this corresponds to a
      CCCC      worst case analysis. Shear forces are not negligable
      CCCC      and are taken into account.
0002            DIMENSION PHASE(81),XCOMP(81),TPHASE(81),OUT(81),XCOS(81)
0003            DIMENSION XSIN(81), TXCOMP(7,7),TX(7,7),TXPHSE(7,7)
      CCCC      Fix values for the x and z offsets
0004            DO 200 I=1,7
0005            OFFZ= -1.2+0.3*I
0006            DO 201 J=1,7
0007            OFFX= -1.2+0.3*J
0008            TYPE *,OFFZ,OFFX
      CCCC      Let the beam progress through the glass in 80 steps.
      CCCC      Calculate at each point the x,y,z and the r,theta coordinates.
      CCCC      Calculate tensile and shear stress at each point in
      CCCC      as a function of r,theta and z. Transform the stresses
      CCCC      to the beam coordinates inside the glass: p for propagation,
      CCCC      h for horizontal and v for vertical polarization. Determine
      CCCC      the phase delay of v with respect to h in each interval.
      CCCC      sin 55.62 = 0.8253 = cos 34.38
      CCCC      cos 55.62 = 0.5647 = sin 34.38
      CCCC      tan 34.38 = 0.6842
      CCCC      0.9708=3300./4./pi/5.9/9.5/9.5/9.5*(3*5.9+1.)
      CCCC      2.*pi/514.*3.5=4.2784E-2
      CCCC      3.5E-6 is the stress optical coefficient of fused silica
      CCCC      retardation of 3.5 nanometer per mm per N/mm2.
      CCCC      9.5/80./0.8253 = 0.1439
      CCCC      Shear stress:3300.*3./19./19./pi/9.5/9.5/9.5=1.0181E-2
0009            DO 100 N=1,81
0010             NN=N
0011             Z=-4.8688+9.5/80.*NN
0012             Y=-Z*0.6842 + OFFZ/0.5647
0013             R=SQRT(Y*Y + OFFX*OFFX)
0014             IF(OFFX) 350,351,352
0015  350        IF(Y) 355,358,357
0016  351        IF(Y) 360,359,361
0017  352        THETA=ATAN(Y/OFFX)
0018             GOTO 365
0019  355        THETA=ATAN(Y/OFFX)-3.1416
0020             GOTO 365
0021  357        THETA=ATAN(Y/OFFX)+3.1416
0022             GOTO 365
0023  358        THETA=3.1416
0024             GOTO 365
0025  359        THETA=0.
0026             GOTO 365
0027  360        THETA=-3.1416/2.
```

```
FORTRAN IV      V02.6      Wed 10-Oct-84 12:13:09                PAGE 002

0028            GOTO 365
0029  361       THETA=3.1416/2.
0030  365       CONTINUE
0031            SIGMAR=+0.9708*(1.-R*R/19./19.) *Z
0032            SIGMAT=+(0.9708-0.4620*R*R/19./19.)*Z
0033            TAUZR=-1.0181E-2*R*(9.5*9.5/4.-Z*Z)
0034            SIGMAH=SIGMAR*COS(THETA)*COS(THETA)+
               1            SIGMAT*SIN(THETA)*SIN(THETA)
0035            SIGMAV=SIGMAR*0.8253*0.8253*SIN(THETA)*SIN(THETA)+
               1            SIGMAT*0.8253*0.8253*COS(THETA)*COS(THETA)+
               2            2.*TAUZR*0.8253*0.5647*SIN(THETA)
0036            TAUHV=+(SIGMAR-SIGMAT)*SIN(THETA)*COS(THETA)*0.8253+
               1          TAUZR*COS(THETA)*0.5647
0037            PHASE(NN)=-4.2784E-2*(SIGMAV-SIGMAH)
0038            XCOMP(NN)=-4.2784E-2*TAUHV
0039            IF(NN-2) 320,321,322
0040  320       TPHASE(1)=0.
0041            GOTO 323
0042  321       TPHASE(2)=(PHASE(1)+PHASE(2))*0.1439/2.
0043            GOTO 323
0044  322       CALL QSF(0.1439,PHASE,OUT,NN)
0045            TPHASE(NN)=OUT(NN)
      CCCC       x-component is generated Pi/2 out of phase with local z-comp.
      CCCC       When tauhv is positive the x-comp. is 90 degrees retarded.
0046  323       XCOS(NN)=-SIN(TPHASE(NN))*XCOMP(NN)
0047            XSIN(NN)=COS(TPHASE(NN))*XCOMP(NN)
0048  100     CONTINUE
0049            CALL QSF(0.1439,XCOS,OUT,81)
0050            TXCOS=OUT(81)
0051            CALL QSF(0.1439,XSIN,OUT,81)
0052            TXSIN=OUT(81)
0053            TX(I,J)=SQRT(TXCOS*TXCOS+TXSIN*TXSIN)
0054            IF(TXCOS) 330,330,332
0055  330       IF(TXSIN) 333,333,334
0056  333       TXPHSE(I,J)=180./3.1416*ATAN(TXSIN/TXCOS)-180.
0057            GOTO 335
0058  334       TXPHSE(I,J)=180./3.1416*ATAN(TXSIN/TXCOS)+180.
0059            GOTO 335
0060  332       TXPHSE(1,J)=180./3.1416*ATAN(TXSIN/TXCOS)
0061  335       CONTINUE
0062  201       CONTINUE
0063  200       CONTINUE
0064            PRINT 1010,(-1.2+0.3*I,I=1,7)
0065  1010      FORMAT(///4X,7F9.1,6X,'X')
0066            PRINT 1011,(-1.2+0.3*1,(TX(I,J),J=1,7),I=1,7)
0067  1011      FORMAT(/X,F4.1,7F9.4)
0068            PRINT 1012
0069  1012      FORMAT (/,'   Z')
0070            PRINT 1010,(-1.2+0.3*I,1=1,7)
0071            PRINT 1013,(-1.2+0.3*I,(TXPHSE(I,J),J=1,7),I=1,7)
0072  1013      FORMAT(/X,F4.1,7F9.2)
0073            PRINT 1012
0074            END
```

Appendix B.

```
FORTRAN IV      V02.6      Tue 09-Oct-84 09:06:56                PAGE 001

0001          PROGRAM BMSIZE
0002          EXTERNAL GAUSS
0003          EXTERNAL FCT
0004          DIMENSION QX(40),QXOUT(40),Q(47),QOUT(47),AUX(10),A(15)
0005          BYTE YES
0006          COMMON R,XC,ZC,ZO,X,X1,F
0007          F=0.0001
0008    398   F=F*5.
        CCCC  Fix beam radius, x- and z-offset.
0009          DO 400 KR=1,3
0010          R=0.4+0.2*FLOAT(KR)
0011          DO 401 KX=1,5
0012          XC=-0.75+0.25*FLOAT(KX)
0013          DO 402 KZ=1,5
0014          ZC=-0.75+0.25*FLOAT(KZ)
0015          TYPE *,R,XC,ZC,F
        CCCC  Calculate the X-integral and the convolution over z' for
        CCCC  every Z value on the lucite face (ZO), taking the magnification
        CCCC  of 1.55 into account. After the loop has been completed, the
        CCCC  integral over the lucite face is taken between -2.3 and +2.3,
        CCCC  corresponding to a 7.1 mm high aperture.
0016          DO 100 NN=1,47
0017           N=NN
0018           ZO=-2.4+0.1*N
        CCCC  Establish X-values,avoid X=0
        CCCC  Inside a radius of about 4 mm
0019           DO 200 MM=1,20
0020             M=MM
0021             X=-4.1+0.2*M
0022             X1=0.27*X
        CCCC  For every X, integrate over a circle in the Y-Z plane
0023             CALL QATR(X1,-X1,5.E-1,15,GAUSS,QX(M),IER,AUX)
0024             IF(IER .NE. 0) GOTO 900
0026    200     CONTINUE
0027           DO 201 MM=21,40
0028             M=MM
0029             X=-4.1+0.2*M
0030             X1=0.27*X
0031             CALL QATR(-X1,X1,5.E-1,15,GAUSS,QX(M),IER,AUX)
0032             IF(IER .NE. 0) GOTO 900
0034    201     CONTINUE
        CCCC  Now do the integration over X.
0035           CALL QSF(0.2,QX,QXOUT,40)
        CCCC  Normalize the intensity distribution to 1., if the integration
        CCCC  were between + and - infinity for X and ZO.
0036           Q(N)=5.56*QXOUT(40)/R/R
0037           TYPE *, N, Q(N)
0038    100   CONTINUE
0039          CALL QSF(0.1,Q,QOUT,47)
        CCCC  Since the height of the lucite is finite , the integral
        CCCC  over the normalized intensity distribution will be less
        CCCC  than 1. The total intensity on the lucite is estimated
        CCCC  here by a shortcut: assume that the image is sharp everywhere
        CCCC  the smearing out by the defocussing is neglected.
```

```
FORTRAN IV      V02.6      Tue 09-Oct-84 09:06:56                PAGE 002

      CCCC  For R=1.00 the table gave 1.00000, while this
      CCCC  approximation gives 0.9998.
0040        CALL QATR(-2.3,2.3,1.E-5,15,FCT,FLUX,IER,A)
0041        FLUX=FLUX/R*SQRT(2./3.1416)
0042        TYPE *,QOUT(47),FLUX
0043        DQQ=QOUT(47)/FLUX
0044        PRINT 1050,R,XC,ZC,F,DQQ
0045        TYPE 1050, R,XC,ZC,F,DQQ
0046  1050  FORMAT(' RADIUS',F5.2,'  OFFSETS(X,Z)',2F6.2,'   F=',F6.4,
     1 '  DQQ',F6.1)
0047  402   CONTINUE
0048  401   CONTINUE
0049  400   CONTINUE
0050        IF(F .LT. 0.05) GOTO 398
0052        GOTO 901
0053  900   TYPE *,N,M,IER
0054  901   CONTINUE
0055        END


0001        FUNCTION GAUSS(Z)
      CCCC  The units in this subroutine have been chosen such that
      CCCC  when all dimensions are in mm, the final resullt of the
      CCCC  calculation in the main program (DQQ) is in ppm.
0002        COMMON R,XC,ZC,ZO,X,X1,F
0003        Y=69.*X+12.*(Z+ZO)*(Z+ZO)-14*X*X
0004        Y=Y-SQRT(F)*486.*(X+0.96*(Z+ZO))
0005        Y=Y-40000.*(X-XC)/R/R
0006        GAUSS=EXP(-((X-XC)*(X-XC)+(ZO-ZC+Z)*(ZO-ZC+Z))*2./R/R)
0007        GAUSS=GAUSS/X/X*Y*SQRT(X1*X1-Z*Z)
0008        RETURN
0009        END


0001        FUNCTION FCT(Z)
0002        COMMON R,XC,ZC,ZO,X,X1
0003        FCT=EXP(-(Z-ZC)*(Z-ZC)*2./R/R)
0004        RETURN
0005        END
```

Appendix C.

```
      PROGRAM BDPASS
CCCC  Calculates transmission of the interference filter as a function
CCCC  of the tilt angle of the filter. The effective depolarization
CCCC  ratio, that is, the part that is transmitted by the filter
CCCC  because that depends on wavelength, is also calculated. The
CCCC  light coming out of the fibers is collimated by the 50 mm focal
CCCC  length Nikon lenses.
CCCC
      DIMENSION T(80),TT(80),RHOT(80)
      REAL LAMBDA,INTAZI,NORM
      PI=3.141593
      OPEN (UNIT=20,TYPE='OLD',NAME='FIL16.DAT')
      READ (20,*) RHO,B,NQ,T,R,TT,RHOT,BH,NQH,E,LAMBDA
CCCC  The file contains the filter transmission data at normal incidence
CCCC  and some data on the gas. RHO is the depolarization ratio, B is
CCCC  the rotational constant, NQ is the location of the Q-branch origin
CCCC  relative to the filter transmission maximum at normal incidence,
CCCC  T contains the transmission characteristic at 5 cm-1 intervals.
CCCC  The transmission maximum is at T(31). LAMBDA is Q-branch wavelength
CCCC  in nm. R is the radius of the fiber bundle (inches).  BH, NQH are
CCCC  the same as B and NQ, but then for the first "hot band", transitions
CCCC  originating on the first excited vibrational state. E is the
CCCC  vibrational energy in cm-1 of that state.
CCCC  TT and RHOT are initialized by reading in zeroes for every element
      RHOQ=RHO/4./(1.-RHO)
      Q1=RHO/(3.-4.*RHO)
      QS=7.*Q1/(1.+7.*Q1)
      Q=1.-QS*3./4.
      A=5./4./B
      AH=5./4./BH
CCCC  The gas temperature effects the extent of the side branches.
      TEMP=300.
      B=B/(0.695*TEMP)
      BH=BH/(0.695*TEMP)
      P=EXP(-E/(0.695*TEMP))
CCCC  0.695 is Boltzmann's constant in cm-1.
CCCC  A scales the distance between neighboring rotational lines (4B)
CCCC  to the distance between neighboring points on the filter
CCCC  transmission curve ( 5 cm-1). Nuclear spin degeneracy factors are
CCCC  neglected and the rotational quantum number J will be treated
CCCC  as a continuous variable in the expression for the intensity of
CCCC  the Q- and S-branch. Pressure broadening will in effect merge the
CCCC  separate lines.
      TYPE *, RHOQ,Q,B,A,NQ,Q1,QS,NQH,E
      TYPE 1011
      TYPE *,T
      TYPE 1011
      TYPE *,R,P,LAMBDA
      TYPE 1012
1011  FORMAT (/)
1012  FORMAT(///)
      PRINT 1010
1010  FORMAT(' TRANSMISSION AND DEPOLARIZATION RATIO AS A FUNCTION OF',
     1 /,' PASSBAND WAVELENGTH SHIFT IN INCREMENTS OF 5 CM-1',
     2 /,' CM-1      TRANSMISSION  DEPOLARIZATION')
CCCC  TT is going to contain the transmission for the entire ro-vibratl.
CCCC  band as a function of the shift of the filter passband at 5 cm-1
CCCC  intervals. RHOT will store the same for the effective depol. ratio.
CCCC  First calculate the normalization factor for the thermal (Boltzmann)
CCCC  distribution of rotational states.
      NORM=0.
      DO 310 N=1,40
      RJ=FLOAT(N)*A
```

```
      NORM=NORM+(2.*RJ+1.)*EXP(-B*RJ*(RJ+1.))
310   CONTINUE
      DO 200 M=1,60
CCCC  Placement of the Q-branch with respect to the filter transmission
      NQS=NQ+M-1
      TT(M)=T(NQS+31)*Q*(1.-P)
      RHOT(M)=TT(M)*RHOQ/(1.+RHOQ)
CCCC  Calculate O-branch contribution
        DO 300 N=1,40
        RJ=FLOAT(N)*A-1.5
        IF(RJ .LT. 0.) GOTO 300
        NFILTR=NQS+31-N
        IF (NFILTR .LT. 1) GOTO 301
        ADD=OS*3.*(RJ+1.)*(RJ+2.)/2./(2.*RJ+3.)*T(NFILTR)
        ADD=ADD*EXP(-B*(RJ+2.)*(RJ+3.))*(1.-P)/NORM
        TT(M)=TT(M)+ADD
        RHOT(M)=RHOT(M)+ADD*3./7.
CCCC  Calculate S-branch contribution
301     NFILTR=NQS+31+N
        IF (NFILTR .GT. 65) GOTO 300
        ADD=OS*3.*(RJ+1.)*(RJ+2.)/2./(2.*RJ+3.)*T(NFILTR)
        ADD=ADD*EXP(-B*RJ*(RJ+1.))*(1.-P)/NORM
        TT(M)=TT(M)+ADD
        RHOT(M)=RHOT(M)+ADD*3./7.
300     CONTINUE
CCCC  Calculate hot band contribution
      NQHS=NQH+M-1
      TT(M)=TT(M)+T(NQHS+31)*Q*P
      RHOT(M)=RHOT(M)+T(NQHS+31)*Q*P*RHOQ/(1.+RHOQ)
        DO 350 N=1,40
        RJ=FLOAT(N)*AH-1.5
        IF(RJ .LT. 0.) GOTO 350
        NFILTR=NQHS+31-N
        IF (NFILTR .LT. 1) GOTO 351
        ADD=OS*3.*(RJ+1.)*(RJ+2.)/2./(2.*RJ+3.)*T(NFILTR)
        ADD=ADD*EXP(-BH*(RJ+2.)*(RJ+3.))*P/NORM
        TT(M)=TT(M)+ADD
        RHOT(M)=RHOT(M)+ADD*3./7.
351     NFILTR=NQHS+31+N
        IF (NFILTR .GT. 65) GOTO 350
        ADD=OS*3.*(RJ+1.)*(RJ+2.)/2./(2.*RJ+3.)*T(NFILTR)
        ADD=ADD*EXP(-BH*RJ*(RJ+1.))*P/NORM
        TT(M)=TT(M)+ADD
        RHOT(M)=RHOT(M)+ADD*3./7.
350     CONTINUE
CCCC  Rho has so far been calculated as the ratio between horizontal
CCCC  polarization and total scattering (horizontal+vertical). Now
CCCC  we have to convert back to the ratio of horizontal to vertical.
      RHOT(M)=RHOT(M)/TT(M)
      RHOT(M)=RHOT(M)/(1.-RHOT(M))
      PRINT 1000 , (M-1)*5, TT(M),RHOT(M)
1000  FORMAT(I6,6X,2F10.5)
200   CONTINUE
      DO 201 M=61,80
      TT(M)=0.0001
      RHOT(M)=0.75
201   CONTINUE
      PRINT 1012
      PRINT 1013
1013  FORMAT(' TILT  TRANSMISSION DEPOLARIZATION')
CCCC  Convert R from inches to mm
      R=R*25.4
      DO 400 I=1,25
```

```
CCCC    PHI is the filter tilt angle in steps of 0.5 degrees.
        PHI=FLOAT(I-1)/2./57.3
        TOTAL=0.
        TDEPOL=0.
        DENOM=0.
          DO 500 J=1,20
          RADIUS=R/20.*FLOAT(J-1)+R/40.
          DENOM=DENOM+RADIUS
          THETA=RADIUS/50.
CCCC    The focal length of the Nikon lens is 50 mm.
CCCC    Integrate over azimuthal angles first.
          INTAZI=0.
          DEPOL=0.
            DO 600 K=1,50
            AZIMU=2.*PI*FLOAT(K)/50.
            PSI=COS(THETA)*COS(PHI)+SIN(THETA)*SIN(PHI)*SIN(AZIMU)
CCCC    To find the angle we can convert with arctan of the half-angle.
            PSI=SQRT((1.+1.E-7-PSI)/(1.+PSI))
            PSI=2.*ATAN(PSI)
CCCC    Calculate the wavelength shift in cm-1 of the filter transmission
CCCC    bandpass when the light hits at an angle PSI.
            SHIFT=(1./SQRT(1.-SIN(PSI)*SIN(PSI)/2.1/2.1)-1.)/LAMBDA
            NTRUNC=INT(SHIFT/5.)
            TRANS=TT(NTRUNC+1)
     C      +AMOD(SHIFT,5.)/5.*(TT(NTRUNC+2)-TT(NTRUNC+1))
            DPOL=RHOT(NTRUNC+1)
     C      +AMOD(SHIFT,5.)/5.*(RHOT(NTRUNC+2)-RHOT(NTRUNC+1))
CCCC    Linear interpolation between adjacent TT and RHOT values.
        IF(MOD(K,10) .EQ. 1) TYPE *, SHIFT,NTRUNC,PSI*57.3,TRANS,DPOL
            INTAZI=INTAZI+TRANS
            DEPOL=DEPOL+DPOL
600         CONTINUE
        TYPE 1012
          TOTAL=TOTAL+INTAZI*RADIUS/50.
          TDEPOL=TDEPOL+DEPOL*RADIUS/50.
500       CONTINUE
        TOTAL=TOTAL/DENOM
        TDEPOL=TDEPOL/DENOM
        TYPE 1001,PHI*57.3,TOTAL,TDEPOL
        PRINT 1001,PHI*57.3,TOTAL,TDEPOL
400     CONTINUE
1001    FORMAT(F6.1,F10.5,5X,F10.5)
        END
```

Appendix D.

```
CCCCCCCCCCCCCCCCCCCCCCCCCCCCCCCCCCCCCCCCCCCCCCCCCCCCCCCCCCCCCCCCCCCCCCC
C
CCCCC   OXYV6
CCCCC
CCCCC   PROGRAM FOR OXYGEN-TO-NITROGEN ANALYSIS
CCCCC   WITH 36 HZ PHILAMON TUNING FORK CHOPPERS
 CCCC   AND FIBEROPTIC BEAM SPLITTER WITH FOUR OUTPUT PORTS.
CCCCC
CCCCC   BY PIETER TANS AND PAUL WEINSTEIN, VERSION 02, APRIL 82
CCCCC   MODIFIED TO VERSION 03 BY DANIEL LASHOF, JULY 82
CCCCC   VERSION 04 BY DANIEL LASHOF, SEPTEMBER 83
CCCCC   VERSION TO RUN NEW CHOPPER DRIVER, FEBRUARY 84
CCCCC   VERSION 5, TO RUN UNIBLITZ SHUTTER FOR DARKNOISE, MAY 84
CCCCC   VERSION 6, FOR 4 OUTPUT CHANNELS, APRIL 85
CCCCC
CCCCC   LINK WITH OXYLB6,CMCLIB
CCCCC
C       CRATE AND TPG MUST BE INITIALIZED BEFORE EXECUTION.
C       IF NECESSARY, RUN TIME1 TO INITIALIZE.
C
C       Data are gathered during the innermost ('DO 100') loop.
C       This loop is nested inside the middle ('DO 200') loop which
C       obtains dark-noise data every 2 seconds.
C       The outer ('DO 300') loop contains both of these loops and
C       the beam position control.
C       Finally, Input/Output is controlled in the outer shell.  Summary
C       data is written to disk to conclude each 'update.'
C
C
C
C
^CCCC
 CCCC   VARIABLES FOR CONSTRUCTING A FILENAME FROM RUN DATE AND HOUR
        LOGICAL*1 YES
        LOGICAL*1 D1,D2,P1,M1,M2,M3,P2,Y1,Y2,H1,H2,P3,MI1,MI2,P4,S1,S2
        LOGICAL*1 STRNGD(18)
        LOGICAL*1 DOT,HOUR,DAT(4),NUL
        LOGICAL*1 DATFIL(15),FILE(20)
        LOGICAL*1 STRTIM(8)
CCCCC
CCCCC   CHOPPER AND TIMING VARIABLES
        INTEGER UPDNR,REG,SYNC,SWITCH,SWNORM,SHUTAD
        INTEGER COUNT1,COUNT2,PIKUP1,PIKUP2
        INTEGER TIMEAD(3)
        INTEGER TO1,TG1,TC1,TD2,TO2,TG2,TC2,TD1
CCCCC
CCCCC   COUNTING VARIABLES.
        INTEGER SCLRAD(6)
        INTEGER   JCOUNT(2,6),JDARK(6)
        REAL      ACOUNT(2,6),A1(6),ADARK(6)
        REAL*8    DCOUNT(2,6)
CCCCC
        INTEGER POLAD(4)
        REAL POLTOT(6)
        REAL DT(6)
CCCCC
        COMMON/G/ICR24,SCLRAD
        COMMON/WAIT/REG
        COMMON/UPDATE/ DCOUNT,ADARK
        COMMON/ALPHA/SYNC,PIKUP1,PIKUP2,UPDNR,STRTIM,DATFIL
        COMMON/ADC/IX1D,IX1S,IX2D,IX2S,IY1D,IY1S,IY2D,IY2S
        COMMON/DAC/IM1X,IM3X,IM4X,IM1Y,IM3Y,IM4Y,ID1R
        COMMON/DACDAT/ITEN,RDAC,VGAIN,VMAX
```

```
      COMMON/POS1/ DX1S, DX2S, DY1S, DY2S, S1, S2
      COMMON/POS2/PTOT,PSQ,X1TOT,X1SQ,X2TOT,X2SQ,Y1TOT,Y1SQ,Y2TOT,Y2SQ
      COMMON/MIR/XM1,YM1,NXT,NYT,NXTR,NYTR
      COMMON/ROK1/IRK,IPOW,IDUM1,IRAN1,IRAN2
      COMMON/ROK2/RDUM1,RDUM2,RDUM3,RDUM4,RDUM5
      COMMON/TEMP/ITEM,TTOT,POLAD,POLTOT
CCCC
      EQUIVALENCE (FILE(5),DATFIL(1))
CCCCC
CCCCC INITIALIZE VARIABLES.
C           Filename variables.
      DATA FILE/'O','X','Y',':',16*' '/
      DATA DOT/'.'/
      DATA NUL /'0'/
c           Beam control variables.
      DATA IRK/0/
      DATA NXT,NYT,NXTR,NYTR/4*0/
C           Program control variables.
      DATA UPDNR,MPAUSE/2*0/
CCCCC
CCCCC TIMING DATA
C     TC1     3915    OPEN COUNTING WINDOW 1
C     TG1     8390    GATE FOR PRIMARY PICKUP
C     TC1     12915   CLOSE COUNTING WINDOW 1
C     TD2     13890   DRIVE SECONDARY CHOPPER
C     TC2     17805   OPEN COUNTING WINDOW 2
C     TG2     22280   GATE FOR SECONDARY PICKUP
C     TC2     26805   CLOSE COUNTING WINDOW 2
C     TD1     27780   DRIVE PRIMARY CHOPPER, RECYCLE TPG,
C             i.e., TD1 = CHOPPER PERIOD.
C     Timing based on delay between drive and pickup of 8.415 msec
C     for both primary and secondary.
      Timing is established by program TIME1, which must be run each
C     time the CRATE is powered up or initialized. Timing gates can
C     be modified by running TIMTST.
C
CCCCC
CCCCC DEAD-TIME DATA
C     DT = (dead-time)*(prescale factor)*(1/0.009sec)
C     Prescale factor = 40. for channels 1 and 2, 1. for channels 3 and 4,
C     and 4. for channels 5 and 6.
      DATA DT/8667.E-9,9444.E-9,1111.E-9,1111.E-9,866.7E-9,944.4E-9/
CCCC
CCCCC DEFAULT RUN PARAMETER DATA
      DATA NCLOSE,NPOS,NTOT,YES,NPAUSE /2,60,600,'Y',0/
CCCCC
CCCC  DAC AND PIEZO POWER SUPPLY DATA
CCCCC ITEN IS ACTUALLY 7V FOR RUNNING THE STEPPER DRIVER
CCCCC 10 BIT DAC, ORTEC POWER SUPPLY (2.95V IN = 1000V OUT)
CCCCC VOLTAGE DIVIDER WITH 5.11K AND 1.96K RESISTOR
      DATA ITEN,RDAC,VGAIN,VMAX/716,102.3,93.2,931./
      DATA IFIVE/512/
CCCCC
CCCCC
CCCCC CONSTRUCT THE FILENAME FOR THIS RUN AND OPEN THE FILE
      CALL DATE (STRNGD)
      CALL TIME (STRNGD(10))
      DECODE (17,1081,STRNGD) D1,D2,P1,M1,M2,M3,P2,Y1,Y2,H1,H2,P3,MI1,
     1 MI2,P4,S1,S2
      ENCODE (9,1081,DATFIL) M1,M2,M3,D1,D2,DOT,H1,H2,MI1
1081  FORMAT (20A1)
      OPEN (UNIT=20,NAME=FILE,FORM='UNFORMATTED')
      TYPE 1090,(STRNGD(N),N=1,9)
```

```
      TYPE 1091,(STRNGD(N),N=10,17)
1090  FORMAT (1X,'START OF RUN OXYGEN/NITROGEN RATIO',15X,9A1)
1091  FORMAT (1X,'TIME',5X,8A1)

CCCCC GENERATE CAMAC ADDRESS VARIABLES  CCCCCCCCCCCCCCCCCCCCCCCCCCCC
      CALL CDREG(ICR24,,2,24,0)
      CALL CDREG(ISCAN,,2,19,0)
CCCCC
CCCCC SCALER ADDRESSES.
C     Variable #      Scaler #        Function
c     1               1               Oxygen detector
c     2               3               Nitrogen detector
c     3               5               Carbon Dioxide detector
c     4               7               Background detector
c     5               9               Oxygen giant pulses
c     6               11              Nitrogen giant pulses
c
      DO 10 I=1,5
10    CALL CDREG(SCLRAD(I),,2,1,2*I-1)
      CALL CDREG(SCLRAD(6),,2,1,11)
CCCCC
CCCCC QUADRANT DETECTOR (ADC) ADDRESSES.
      CALL CDREG(IY1S,,2,19,8)
      CALL CDREG(IY1D,,2,19,9)
      CALL CDREG(IX1S,,2,19,10)
      CALL CDREG(IX1D,,2,19,11)
      CALL CDREG(IY2S,,2,19,12)
      CALL CDREG(IY2D,,2,19,13)
      CALL CDREG(IX2S,,2,19,14)
      CALL CDREG(IX2D,,2,19,15)
      CALL CDREG(POLAD(1),,2,19,1)
      CALL CDREG(POLAD(2),,2,19,2)
      CALL CDREG(POLAD(3),,2,19,6)
      CALL CDREG(POLAD(4),,2,19,7)
      CALL CDREG(ITEM,,2,19,3)
CCCCC
CCCCC DAC ADDRESSES.
      CALL CDREG(IM1X,,2,18,0)
      CALL CDREG(IM1Y,,2,18,1)
      CALL CDREG(IM3X,,2,18,2)
      CALL CDREG(IM3Y,,2,18,3)
      CALL CDREG(IM4X,,2,18,4)
      CALL CDREG(IM4Y,,2,18,5)
      CALL CDREG(IDIR,,2,18,6)
      CALL CDREG(SHUTAD,,2,18,7)
CCCCC
CCCCC TIMING PULSE GENERATOR ADDRESSES.
      DO 50 I=1,8
50    CALL CDREG(TIMEAD(I),,2,3,I-1)
      CALL CDREG(LAM,,2,3,13)
      CALL CDREG(REG,,2,3,12)
CCCCC
      CALL CDREG(KENBOX,,2,4,0)
      CALL CDREG(COUNT1,,2,16,0)
      CALL CDREG(COUNT2,,2,16,1)
      CALL CDREG(SWITCH,,2,6,7)
      CALL CDREG(SWNORM,,2,6,5)
 CCCC
CCCCC INITIALIZE RUN CONFIGURATION
      CALL CSSA(25,ISCAN)     ! TURN ON ADC SCANNING
      CALL CSSA(17,LAM,0) ! SET NO LOOK-AT-ME'S FROM TPG.
      CALL CSSA(16,SHUTAD,IFIVE) ! OPEN BEAM SHUTTER.
CCCCC
```

```
CCCCC   MIRROR MONITOR VARIABLES.
CCC             READ PIEZO VOLTAGES
        CALL CSSA(0,IM1Y,IPZY)
        CALL CSSA(0,IM1X,IPZX)
        XM1=FLOAT(IPZX)*VGAIN/RDAC
        YM1=FLOAT(IPZY)*VGAIN/RDAC
 CCCC
CCCCC
CCCCC   OBTAIN PARAMETERS FOR THIS RUN.  CCCCCCCCCCCCCCCCCCCCCCCCCCCCCC
        TYPE 1011
1011    FORMAT(/,'ORUN PARAMETERS.  TYPE / FOR (DEFAULT) VALUES.')
        TYPE 1015
1015    FORMAT(/,'$ENTER NUMBER OF CYCLES FOR DARK-NOISE COUNTING'
     A   ,' PER 72 CYCLES (2): ')
        ACCEPT *,NCLOSE
        NOPEN=72-NCLOSE
1000    TYPE 1001
1001    FORMAT('$ENTER NUMBER OF SECONDS BETWEEN BEAM POSITION '
     1  ,'ADJUSTMENTS (60): ')
        ACCEPT *,NPOS
        NPOS=NPOS/2
        NPOS=NPOS*2
        TYPE 1002
1002    FORMAT('$ENTER NUMBER OF SECONDS PER UPDATE (600): ')
        ACCEPT *,NTOT
        NUPD=NTOT/NPOS
        NTOT=NUPD*NPOS
        TYPE 1003,NTOT,NUPD
1003    FORMAT('$EACH UPDATE WILL TAKE ',I4,' SEC., AND CONTAIN ',
     A          I3,' MIRROR MOVES. OK? (Y/N): ')
        ACCEPT 1004,YES
1004    FORMAT(A1)
        IF(YES.NE.'Y')GO TO 1000
        TYPE 1005
1005    FORMAT('$PAUSE AFTER N UPDATES. N=? (0 FOR NO PAUSE): ')
        ACCEPT *, NPAUSE
CCCCC
CCCCC
        WRITE(20)NTOT,NPOS,NOPEN,NCLOSE
CCCCC
CCCCC
CCCCC   START UPDATE CYCLE    CCCCCCCCCCCCCCCCCCCCCCCCCCCCCCCCCCCCCCCCCCC
CCCCC
400     UPDNR=UPDNR+1
        MPAUSE=MPAUSE+1
CCCCC   CLEAR PICKUP COUNTS FOR BOTH CHOPPERS
        CALL CSSA(2,COUNT1,PIKUP1)
        CALL CSSA(2,COUNT2,PIKUP2)
CCCCC
        SYNC=0
CCCCC   BEAM MONITOR VARIABLES.
        PTOT=0.0
        PSQ=0.0
        X1TOT=0.0
        X1SQ=0.0
        X2TOT=0.0
        X2SQ=0.0
        Y1TOT=0.0
        Y1SQ=0.0
        Y2TOT=0.0
        Y2SQ=0.0
        DO 405 I=1,6
405     POLTOT(I)=0.0
```

```
CCCCC
      TTOT=0.0 ! TEMPERATURE MONITOR VARIABLE.
CCCCC COUNTING VARIABLES.
      DO 410 I=1,6
      ADARK(I)=0.
      DO 410 J=1,2
 10   DCOUNT(J,I)=0.DO
CCCCC
CCCCC OUTER LOOP.  ONE BEAM POSITION ADJUSTMENT PER PASS.
      DO 300 M=1,NUPD
            DO 310 I=1,6
            DO 310 J=1,2
310         ACOUNT(J,I)=0.0
       DX1S=0.
       DX2S=0
       DY1S=0
       DY2S=0
       S1=0
       S2=0
      NRP=0
      NRN=0
CCCCC
CCCCC ESTABLISH PHASE LOCK TO CHOPPERS AND CLEAR SCALERS.
      CALL CSSA(11,REG) ! CLEAR LAM STATUS
      CALL WAIT(7) ! WAIT FOR UNK WINDOW TO CLOSE.
      CALL CSSA(11,REG) ! CLEAR LAM STATUS
      CALL CSSA(9,SCLRAD(6)) ! CLEAR SCALERS
CCCCC
CCCCC MIDDLE LOOP.  TWO SECONDS PER PASS.
      DO 200 N=1,NPOS/2
CCCCC
CCCCC INNER LOOP.  ONE CHOPPER CYCLE PER PASS.
            DO 100 K=1,NOPEN
101         CALL WAIT(3) ! WAIT FOR STD WINDOW TO CLOSE
CCCCC             READ STANDARD
                  DO 110 I=1,6
110               CALL CSSA (2,SCLRAD(1),JCOUNT(1,I) )
CCCCC
            CALL CSSA(1,REG,LSR) ! READ LAM STATUS
            CALL CSSA(11,REG) ! CLEAR LAM STATUS
            NP=IAND(16,LSR) ! CHECK FOR PULSE 5
            IF(NP.NE.0) GO TO 180 ! SYNC ERROR IF UNK COUNTS STARTED
CCCCC
            CALL POSRD
CCCC
CCCC         DEAD-TIME CORRECTION
                  DO 115 I=1,6
                  A1(I)=JCOUNT(1,I)
115               A1(I)=A1(I)/(1.-A1(I)*DT(I))
CCCCC
            CALL WAIT(7) ! WAIT FOR UNK WINDOW TO CLOSE
CCCCC             READ UNKNOWN
                  DO 120 I=1,6
120               CALL CSSA( 2, SCLRAD(I), JCOUNT(2,I) )
CCCCC
            CALL CSSA(1,REG,LSR) ! READ LAM STATUS
            CALL CSSA(11,REG) ! CLEAR LAM STATUS
            NP=IAND(1,LSR) ! CHECK FOR PULSE 1
            IF(NP.NE.0) GO TO 180 ! SYNC ERROR IF STD COUNTS STARTED
CCCCC
      IF (K.EQ.NOPEN) CALL CSSA(16,SHUTAD,0) ! CLOSE SHUTTER IN BEAM.
CCCCC
            CALL POSRD
```

```
CCCC
CCCC            SUM UP AND DEAD-TIME CORRECTION
                      DO 130 I=1,6
                      A2=FLOAT(JCOUNT(2,I))
                      A2=A2/(1.-A2*DT(I))
                      ACOUNT(1,I)=ACOUNT(1,I)+ A1(I)
 30                   ACOUNT(2,I)=ACOUNT(2,I)+ A1(I)-A2
                GO TO 100
CCCCC
CCCCC           SYNC ERROR
180             SYNC=SYNC+1
                CALL WAIT(7) ! WAIT FOR UNK WINDOW TO CLOSE
                CALL CSSA(14,REG) ! CLEAR LAM STATUS
                CALL CSSA(9,SCLRAD(6)) ! CLEAR SCALERS
                GO TO 101
100             CONTINUE
CCCCC
CCCC
CCCCC           DARKNOISE COUNTING
                DO 150 K=1,NCLOSE
                CALL WAIT(3)
                CALL CSSA(11,REG) ! CLEAR LAM STATUS
151             CALL WAIT(7) ! WAIT FOR UNK WINDOW TO CLOSE
CCCC                  READ DARK COUNTS
                      DO 140 I=1,6
140                   CALL CSSA(2,SCLRAD(I),JDARK(I))
                CALL CSSA(1,REG,LSR) ! READ LAM STATUS
                CALL CSSA(11,REG) ! CLEAR LAM STATUS
                NP=IAND(1,LSR) ! CHECK FOR PULSE 1
                IF(NP.NE.0) GO TO 185 ! SYNC ERROR IF STD COUNTS STARTED.
        IF(K.EQ.NCLOSE) CALL CSSA(16,SHUTAD,IFIVE) ! OPEN SHUTTER
                DO 160 I=1,6
                      A2=JDARK(I)
                      A2=A2/(1.-A2*DT(I))
160                   ADARK(I)=ADARK(I) + A2
                GO TO 150
CCC
CCCC                  SYNC ERROR
185                   SYNC=SYNC+100
                      CALL WAIT(7) ! WAIT FOR UNK WINDOW TO CLOSE
                      CALL CSSA(11,REG) ! CLEAR LAM STATUS
                      CALL CSSA(9,SCLRAD(6)) ! CLEAR SCALERS
                      GO TO 151
150             CONTINUE
CCCCC
CCCC
200     CONTINUE
CCCCC
CCCCC   REPOSITION MIRRORS AFTER NPOS CYCLES.
250     CALL MIRPOS(NOPEN*NPOS)
        CALL POWOPT
        DO 260 I=1,2
        DO 260 J=1,6
260     DCOUNT(I,J)=DCOUNT(I,J) + DBLE(ACOUNT(I,J))
300     CONTINUE
CCCCC
CCCCC   END OF UPDATE. WRITE RESULTS TO SCREEN AND DISK.
 CCCC   READ AND CLEAR PICKUP COUNTS FOR BOTH CHOPPERS
        CALL CSSA(2,COUNT1,PIKUP1)
        CALL CSSA(2,COUNT2,PIKUP2)
CCCCC
        CALL UPDEND(FLOAT(NUPD))
        CALL TIME(STRTIM)
```

```
      TTOT=TTOT/FLOAT(NUPD)
      DO 305 I=1,6
305   POLTOT(I)=POLTOT(I)/FLOAT(NUPD)
CCCCC OXYDSK MUST PRECEED OXYTYP BECAUSE COUNTING VARIABLES ARE MODIFIED
CCCCC         IN OXYTYP.
      CALL OXYDSK
      CALL OXYTYP(NTOT,NOPEN,NCLOSE)
CCCCC
CCCCC START NEXT UPDATE IF SWITCH ON KENBOX IS TRUE.
      IF(MPAUSE.NE.NPAUSE) GO TO 499
      MPAUSE=0
      TYPE 1005
      ACCEPT *, NPAUSE
499   IF (CSSA(27,KENBOX,0)) GOTO 400
CCCCC END RUN IF SWITCH ON KENBOX IS SET TO FALSE.

500   TYPE 1050
1050  FORMAT(' RUN STOPPED')
      CALL TIME(STRTIM)
      TYPE 1051,STRTIM
1051  FORMAT (' TIME IS   ',3A1)
      END
```

```
      SUBROUTINE POSRD
CCCCC READS ADC TO MONITOR BEAM POSITION AND POWER AND KEEPS
CCCCC A RUNNING SUM.
CCCCC
      COMMON/ADC/IX1D,IX1S,IX2D,IX2S,IY1D,IY1S,IY2D,1Y2S
      COMMON/POS1/DX1S,DX2S,DY1S,DY2S,S1,S2
  CCC
CCCCC READ QUADRANTS
      CALL CSSA(0,IX1D,IDX1)
      CALL CSSA(0,IX1S,ISX1)
      CALL CSSA(0,IX2D,IDX2)
      CALL CSSA(0,IX2S,ISX2)
      CALL CSSA(0,IY1D,IDY1)
      CALL CSSA(0,IY1S,ISY1)
      CALL CSSA(0,IY2D,IDY2)
      CALL CSSA(0,IY2S,ISY2)
CCCCC
CCCCC DIFFERENCE VARIABLES
      DX1S = DX1S + IDX1
      DX2S = DX2S + 1DX2
      DY1S = DY1S + IDY1
      DY2S = DY2S + IDY2
CCCCC
CCCCC SUM VARIABLES
      S1 = S1 + (ISX1+ISY1)
      S2 = S2 + (ISX2+ISY2)
      RETURN
      END
```

```
      SUBROUTINE STEPS(NHTILT,NHTRAN,NVTILT,NVTRAN)
CCCCC TURNS THE STEPPER MOTOR MIRRORS #3 AND #4 AND THE PIEZO
CCCCC MIRROR #1 TO REPOSITION THE BEAM.
CCCCC ASSUMES DAC IS 0-10V ALL CHANNELS.
CCCCC The positive direction is up and to the left when looking toward
ccccc the laser from behind the Burleigh mount.
 cccc Positive voltage contracts the piezos.
ccccc Contracting the piezos tilts the normal to the mirror up and
ccccc to the left (defined as above).  This is required for NEGATIVE TILT
ccccc and POSITIVE TRANSLATION (when a curved reflector is used).
ccccc Piezo control voltages are calculated for a reflector with R=600cm.
ccccc See p.53 of log book starting May 1984.
ccccc
      COMMON/DAC/IM1X,IM3X,IM4X,IM1Y,IM3Y,IM4Y,IDIR
      COMMON/DACDAT/ITEN,RDAC,VGAIN,VMAX
      COMMON/MIR/XM1,YM1,NXT,NYT,NXTR,NYTR
CCCC
      DATA IMAX/1023/ !  Assumes 10 BIT DAC.
CCCC  LIMIT NUMBER OF STEPS
      IF (NHTILT.GT.10)NHTILT=10
      IF (NHTRAN.GT.35)NHTRAN=35
      IF (NVTILT.GT.10)NVTILT=10
      IF (NVTRAN.GT.50)NVTRAN=50
      IF (NHTILT.LT.-10)NHTILT=-10
      IF (NHTRAN.LT.-35)NHTRAN=-35
      IF (NVTILT.LT.-10)NVTILT=-10
      IF (NVTRAN.LT.-50)NVTRAN=-50
CCCC  IF OUTSIDE OF RANGE OF PIEZOS, SET TILT TO MAX OF PIEZO RANGE
      XX=XM1-10.21*FLOAT(NHTILT)
      YY=YM1-7.22*FLOAT(NVTILT)
      IF (XX .GT. VMAX) NHTILT=-IFIX((VMAX-XM1)/10.21)
      IF (XX .LT. 0.) NHTILT=-IFIX((0.-XM1)/10.21)
      IF (YY .GT. VMAX) NVTILT=-IFIX((VMAX-YM1)/7.22)
      IF (YY .LT. 0.) NVTILT=-IFIX((0.-YM1)/7.22)
      IF (NHTILT .EQ. 0) GOTO 101
CCCC  HORIZONTAL TILT
      IF (NHTILT .LT. 0) CALL CSSA(16,IDIR,ITEN)
      IF (NHTILT .GT. 0) CALL CSSA(16,IDIR,0)
      DO 110 M=1,60
110   CONTINUE
      DO 100 N=1,IABS(NHTILT)
      CALL CSSA(16,IM4X,ITEN)  !  STEPPER MOTOR CONTROL
      DO 111 M=1,60
111   CONTINUE
      CALL CSSA(16,IM4X,0)  !  STEPPER MOTOR CONTROL
      IF(NHTILT .GT. 0) XM1=XM1-10.21
      IF(NHTILT .LT. 0) XM1=XM1+10.21
      IXM1=IFIX( (XM1/VGAIN)*RDAC + 0.5 )
      IF(IXM1.LT.0) IXM1=0
      IF(IXM1.GT.IMAX) IXM1=IMAX
      CALL CSSA(16,IM1X,IXM1)  !  PIEZO MIRROR CONTROL
      DO 90 M=1,500
90    CONTINUE
100   CONTINUE
101   IF (NHTRAN .EQ. 0) GOTO 201
CCCC  HORIZONTAL TRANSLATION
      IF (NHTRAN .GT. 0) CALL CSSA(16,IDIR,ITEN)
      IF (NHTRAN .LT. 0) CALL CSSA(16,IDIR,0)
      DO 210  M=1,60
210   CONTINUE
      DO 200 N=1,IABS(NHTRAN)
      CALL CSSA(16,IM3X,ITEN)  !  STEPPER MOTOR CONTROL
      DO 211 M=1,60
```

```
211     CONTINUE
        CALL CSSA(16,IM3X,0)   !  STEPPER MOTOR CONTROL
        CALL CSSA(16,IM4X,ITEN)   !  STEPPER MOTOR CONTROL
        DO 212 M=1,60
212     CONTINUE
        CALL CSSA(16,IM4X,0)   !  STEPPER MOTOR CONTROL
        DO 190 M=1,500
190     CONTINUE
200     CONTINUE
        XM1=XM1 + 1.12*FLOAT(NHTRAN)
        IF(XM1.GT.VMAX)XM1=VMAX
        IF(XM1.LT.0.)XM1=0.
        IXM1=IFIX( (XM1/VGAIN)*RDAC + 0.5)
        IF(IXM1.LT.0) IXM1=0
        IF(IXM1.GT.IMAX) IXM1=IMAX
        CALL CSSA(16,IM1X,IXM1)
201     IF (NVTILT .EQ. 0) GOTO 301
CCCC  VERTICAL TILT
        IF (NVTILT .LT. 0) CALL CSSA(16,IDIR,ITEN)
        IF (NVTILT .GT. 0) CALL CSSA(16,IDIR,0)
        DO 310 M=1,60
310     CONTINUE
        DO 300 N=1,IABS(NVTILT)
        CALL CSSA(16,IM4Y,ITEN)   !  STEPPER MOTOR CONTROL
        DO 311 M=1,60
311     CONTINUE
        CALL CSSA(16,IM4Y,0)   !  STEPPER MOTOR CONTROL
        IF(NVTILT .GT. 0) YM1=YM1-7.22
        IF(NVTILT .LT. 0) YM1=YM1+7.22
        IYM1=IFIX( (YM1/VGAIN)*RDAC + 0.5 )
        IF(IYM1.LT.0) IYM1=0
        IF(IYM1.GT.IMAX) IYM1=IMAX
        CALL CSSA(16,IM1Y,IYM1)   !  PIEZO MIRROR CONTROL
        DO 290 M=1,500
290     CONTINUE
300     CONTINUE
301     IF (NVTRAN .EQ. 0) RETURN
        IF(NVTRAN .LT. 0) GOTO 450
CCCC  VERTICAL TRANSLATION -- POSITIVE
        DO 400 N=1,NVTRAN
        CALL CSSA(16,IDIR,0)
        DO 410 M=1,60
410     CONTINUE
        CALL CSSA(16,IM3Y,ITEN)   !  STEPPER MOTOR CONTROL
        DO 411 M=1,60
411     CONTINUE
        CALL CSSA(16,IM3Y,0)   !  STEPPER MOTOR CONTROL
        DO 412 M=1,60
412     CONTINUE
        CALL CSSA(16,IDIR,ITEN)
        DO 413 M=1,60
413     CONTINUE
        CALL CSSA(16,IM4Y,ITEN)   !  STEPPER MOTOR CONTROL
        DO 414 M=1,60
414     CONTINUE
        CALL CSSA(16,IM4Y,0)   !  STEPPER MOTOR CONTROL
        DO 387 M=1,500
387     CONTINUE
400     CONTINUE
        RETURN
CCCC  VERTICAL TRANSLATION -- NEGATIVE
450     DO 470 N=1,IABS(NVTRAN)
        CALL CSSA(16,IDIR,ITEN)
```

```
      DO 420 I=1,60
420   CONTINUE
      CALL CSSA(16,IM3Y,ITEN)   !  STEPPER MOTOR CONTROL
      DO 421 M=1,60
421   CONTINUE
      CALL CSSA(16,IM3Y,0)   !  STEPPER MOTOR CONTROL
      DO 422 M=1,60
422   CONTINUE
      CALL CSSA(16,IDIR,0)
      DO 423 M=1,60
423   CONTINUE
      CALL CSSA(16,IM4Y,ITEN)   !  STEPPER MOTOR CONTROL
      DO 424 M=1,60
424   CONTINUE
      CALL CSSA(16,IM4Y,0)   !  STEPPER MOTOR CONTROL
      DO 466 M=1,500
466   CONTINUE
470   CONTINUE
      YM1=YM1+0.792*FLOAT(VTRAN)
      IF(YM1.GT.VMAX)YM1=VMAX
      IF(YM1.LT.0.)YM1=0.
      IYM1=IFIX( (YM1/VGAIN)*RDAC + 0.5 )
      IF(IYM1.LT.0) IYM1=0
      IF(IYM1.GT.IMAX) IYM1=IMAX
      CALL CSSA(16,IM1Y,IYM1)   !  PIEZO MIRROR CONTROL
      RETURN
      END
```

```
      SUBROUTINE MIRPOS(NPOS)
CCCCC MOVE MIRRORS TO CORRECT FOR THE AVERAGE BEAM DISPALCEMENT
CCCCC FROM THE CENTER OF THE QUADRANT DETECTORS DURING THE LAST
CCCCC NPOS CYCLES.
CCCCC
      INTEGER POLAD(4),IPOL(4)
      REAL POL(6),POLTOT(6)
CCCCC
      COMMON/POS1/ DX1S, DX2S, DY1S, DY2S, S1, S2
      COMMON/POS2/PTOT,PSQ,X1TOT,X1SQ,X2TOT,X2SQ,Y1TOT,Y1SQ,Y2TOT,Y2SQ
      COMMON/DAC/IM1X,IM3X,IM4X,IM1Y,IM3Y,IM4Y,IDIR
      COMMON/DACDAT/ITEN,RDAC,VGAIN,VMAX
      COMMON/MIR/XM1,YM1,NHT,NVT,NHTR,NVTR
      COMMON/TEMP/ ITEM,TTOT,POLAD,POLTOT
CCCCC
      DATA C1/0.00244141/
CCCCC
CCCCC NORMALIZE POSITION VARIABLES
CCCCC MULTIPLY BY C1 TO CONVERT ADC VALUES TO VOLTS
CCCCC SUBTRACT TO CORRECT FOR 5 VOLT OFFSET
      D=FLOAT(NPOS)
      S1 =  S1*C1 - 10.*D
      S2 =  S2*C1 - 10.*D
      PAV = (S1+S2)/D
      X1AV = -( DX1S*C1 - 5.0*D)/S1
      X2AV = -( DX2S*C1 - 5.0*D)/S2
      Y1AV = -( DY1S*C1 - 5.0*D)/S1
      Y2AV = -( DY2S*C1 - 5.0*D)/S2
CCCCC
CCCCC READ TEMPERATURE
      CALL CSSA(0,ITEM,ITMP)
      TEMP=ITMP*0.00244141-5.0
      TEMP=20.0 - TEMP/0.260
CCCCC
CCCCC READ POLARIZATION PICKUP
      DO 5 I=1,4
      CALL CSSA(0,POLAD(I),IPOL(I))
5     POL(I)=(IPOL(I)*0.00244141 - 5.0)/PAV
      POL(5)=SQRT( (POL(1))**2 + (POL(2))**2 )
      POL(6)=SQRT( (POL(3))**2 + (POL(4))**2 )
CCCCC
CCCCC SKIP MIRROR MOVES IF POWER IS LOW
      IF(PAV.LT.0.5) GO TO 100
CCCCC
CCCCC CALCULATE MIRROR STEPS
      NHTILT = IFIX(-10.*(X1AV-X2AV))
      NVTILT = IFIX(-14.*(Y1AV-Y2AV))
      NHTRAN = IFIX(-15.*X2AV)
      NVTRAN = IFIX(-21.*Y2AV)
CCCCC
      CALL STEP5(NHTILT,NHTRAN,NVTILT,NVTRAN)
CCCCC
      NHT=NHT+NHTILT
      NVT=NVT+NVTILT
      NHTR=NHTR+NHTRAN
      NVTR=NVTR+NVTRAN
CCCCC
100   PAV=PAV*14.1 ! GIVE POWER IN WATTS.
      X1AV=X1AV/.012 ! GIVE POSITION IN MICRONS
      X2AV=X2AV/.012
      Y1AV=Y1AV/.012
      Y2AV=Y2AV/.012
      TYPE 9,PAV,X1AV,X2AV,Y1AV,Y2AV
```

```
9       FORMAT(' POWER= ',F6.2,'W  X1= ',F7.2,' X2= ',F7.2,' Y1= ',F7.2,
     1  ' Y2= ',F7.2,' MICRONS')
        TYPE 10,NHT,NVT,NHTR,NVTR
10      FORMAT(' SUM OF STEPS: HTILT: ',I4,' VTILT: ',I4,
     1  ' HTRAN: ',I4,' VTRAN: ',I4)
        TYPE 12,XM1,YM1,TEMP
 ?      FORMAT(' PIEZO VOLTAGES: X= ',F7.3,' Y= ',F7.3,
     1'  TEMPERATURE= ',F5.2)
        TYPE 13, POL
13      FORMAT(' POLARIZATION: STD X,Y; UNK X,Y: ', 4(F6.3,X),/
     1  ' STD POL: ',F7.3, ' UNK POL: ',F7.3,//)
CCCCC
CCCCC   KEEP UPDATE TOTALS
        PTOT=PTOT+PAV
        X1TOT=X1TOT+X1AV
        X2TOT=X2TOT+X2AV
        Y1TOT=Y1TOT+Y1AV
        Y2TOT=Y2TOT+Y2AV
        TTOT=TTOT+TEMP
        DO 15 I=1,6
15      POLTOT(I)=POLTOT(I) + POL(I)
CCCCC
        PSQ=PSQ+PAV*PAV
        X1SQ=X1SQ+X1AV*X1AV
        X2SQ=X2SQ+X2AV*X2AV
        Y1SQ=Y1SQ+Y1AV*Y1AV
        Y2SQ=Y2SQ+Y2AV*Y2AV
CCCCC
        POLD = PAV
        RETURN
        END
```

```
      SUBROUTINE WAIT(N)
CCCCC WAIT FOR PULSE N FROM TIMING PULSE GENERATOR.
      COMMON/WAIT/IREG
      MASK=2**(N-1)
1     CALL CSSA(1,IREG,LSR)
      NP=IAND(MASK,LSR)
      IF(NP.EQ.0) GO TO 1
      RETURN
      END
```

```
      SUBROUTINE UPDEND(X)
CCCCC SUBPROGRAM TO COMPUTE POSITION STATISTICS
CCCCC PART OF OXYLIB
CCCCC
      COMMON/POS2/PTOT,PSQ,X1TOT,X1SQ,X2TOT,X2SQ,Y1TOT,Y1SQ,Y2TOT,Y2SQ
CCCCC
      SD(TOT,SQ) = SQRT(ABS((SQ-X*TOT*TOT))/(X-1.))
CCCCC
      PTOT=PTOT/X
      X1TOT=X1TOT/X
      X2TOT=X2TOT/X
      Y1TOT=Y1TOT/X
      Y2TOT=Y2TOT/X
CCCCC
      PSQ=SD(PTOT,PSQ)
      X1SQ=SD(X1TOT,X1SQ)
      X2SQ=SD(X2TOT,X2SQ)
      Y1SQ=SD(Y1TOT,Y1SQ)
      Y2SQ=SD(Y2TOT,Y2SQ)
CCCCC
      RETURN
      END
```

```
      SUBROUTINE OXYDSK
CCCCC
CCCCC   WRITING UPDATE RESULTS ON LOGICAL UNIT NO 20
CCCCC   MAIN PROGRAM HAS TO OPEN A FILE ON THAT UNIT
CCCCC
      LOGICAL*1 STRTIM(8)
      LOGICAL*1 DATFIL(15)
      INTEGER UPDNR,SYNC,PIKUP1,PIKUP2,POLAD(4)
      REAL ADARK(6),PT(6)
      REAL*8 DCOUNT(2,6)
CCCCC
      COMMON/UPDATE/DCOUNT,ADARK
      COMMON/ALPHA/SYNC,PIKUP1,PIKUP2,UPDNR,STRTIM,DATFIL
      COMMON/POS2/PFIN,PSD,X1FIN,X1SD,X2FIN,X2SD,Y1FIN,Y1SD,Y2FIN,Y2SD
      COMMON/MIR/XM1,YM1,NXT,NYT,NXTR,NYTR
      COMMON/TEMP/ITEM,TTOT,POLAD,PT
CCCCC
      WRITE(20) UPDNR,STRTIM,SYNC,PIKUP1,PIKUP2,TTOT
      WRITE(20) DCOUNT
      WRITE(20) ADARK
CCC***  TEMPORARY CHANGE TO STORE ALL POLARIZATION DATA ***
C***    WRITE(20) PFIN,PSD,X1FIN,X1SD,X2FIN,X2SD,Y1FIN,Y1SD,
C***     1 Y2FIN,Y2SD
      WRITE(20) PFIN,PSD,X1FIN,PT(1),X2FIN,PT(2),Y1FIN,PT(3),
     1 Y2FIN,PT(4)
C***
      WRITE(20) XM1,YM1,NXT,NYT,NXTR,NYTR
      WRITE(20) PT(5),PT(6)
      RETURN
      END
```

```
      SUBROUTINE OXYTYP(NTOT,NOPEN,NCLOSE)
      LOGICAL*1 DATFIL(15)
      LOGICAL*1 STRTIM(8)
      INTEGER UPDNR,SYNC,PIKUP1,PIKUP2,POLAD(4)
      REAL ADARK(6),ADRK(4),ADRKGN(2),POLTOT(6)
      IMPLICIT REAL*8 (D)
      REAL*8 DCOUNT(2,6),DSTD(4),DUNST(4),DGAIN(2)
CCCCC
      COMMON/UPDATE/ DCOUNT,ADARK
      COMMON/ALPHA/SYNC,PIKUP1,PIKUP2,UPDNR,STRTIM,DATFIL
      COMMON/POS2/PFIN,PSD,X1FIN,X1SD,X2FIN,X2SD,Y1FIN,Y1SD,Y2FIN,Y2SD
      COMMON/MIR/XM1,YM1,NXT,NYT,NXTR,NYTR
      COMMON/TEMP/ITEM,TTOT,POLAD,POLTOT
CCCCC
      TYPE 2000,UPDNR,STRTIM,SYNC,PIKUP1,PIKUP2,TTOT
2000  FORMAT(////,' UPDATE ',I3,X,8A1,X,'SYNC ERRS=',I5,
     C X,'PICKUP PULSES=',I5,', ',I5,' TEMP=',F7.3)
CCCCC
      DO 5 I=1,2
      DO 10 J=1,6
10    IF(DCOUNT(I,J) .EQ. 0.D0) DCOUNT(I,J)=0.5D0
5     IF(ADARK(I).EQ.0.) ADARK(I)=1.
CCCCC
CCCCC DARKNOISE SUBTRACTION
CCCC  NOPEN/(2*NCLOSE) = LIGHT/DARK COUNTING TIME
      DO 15 I=1,6
15    DCOUNT(1,I)=DCOUNT(1,I)-(FLOAT(NOPEN)/(2.*FLOAT(NCLOSE)))*ADARK(I)
CCCCC
      DO 20 I=1,4
20    DUNST(I)=-DCOUNT(2,I)/DCOUNT(1,I)
CCCCC
CCCC  CONVERT TO RATES PER SECOND
 CCCC       0.009*NOPEN*NTOT/2.=ACTIVE COUNTING TIME
      DO 30 I=1,2
      ADRK(1)=ADARK(I)*40./(0.009*NCLOSE*NTOT)
30    DSTD(I)=DCOUNT(1,I)*40./(0.009*NOPEN*NTOT/2.)
      DO 35 I=3,4
      ADRK(I)=ADARK(I)/(0.009*NCLOSE*NTOT)
35    DSTD(I)=DCOUNT(1,I)/(0.009*NOPEN*NTOT/2.)
CCCCC
      DO2N2=DCOUNT(1,2)*(DCOUNT(1,1)-DCOUNT(2,1))/
     A       (DCOUNT(1,1)*(DCOUNT(1,2)-DCOUNT(2,2))) - 1.
      DCO2N2=( (DCOUNT(1,3)-DCOUNT(2,3))/(DCOUNT(1,2)-DCOUNT(2,2)) -
     A       DCOUNT(1,3)/DCOUNT(1,2) )*4.25
CCCCC
      DO 40 I=1,2
      ADRKGN(I)=0.1*ADARK(I+4)/ADARK(I)
40    DGAIN(I)=0.1*(DCOUNT(1,I+4)+DCOUNT(2,I+4))/
     A               (DCOUNT(1,I)+DCOUNT(2,I))
CCCC
      DO 50 I=5,6
50    POLTOT(I)=POLTOT(I)*0.325/150. ! F for 150 psi.
CCCC
      TYPE 2001, DO2N2*1.E6,DCO2N2*1.E6
2001  FORMAT(X,'O2N2= ',F10.1,'     CO2N2= ',F10.1)
      TYPE 2002, DSTD
2002  FORMAT(X,'STD COUNTS/SEC., A,B,C,D: ',4(F10.1,X))
      TYPE 2003, DUNST
2003  FORMAT(X,'UN/ST - 1,        A,B,C,D: ',4(F10.6,X))
      TYPE 2004, DGAIN
2004  FORMAT(X,'GAIN (HIGH/NORM),  A,B: ',2(F10.6,X))
      TYPE 2005, ADRK
2005  FORMAT(X,'DARK-NOISE,       A,B,C,D: ',4(F10.1,X))
```

```
      TYPE 2055, ADRKGN
2055  FORMAT(X,'DARK GAIN,          A,B: ',2(F10.6,X))
      TYPE 2006
2006  FORMAT('  POWER     S.D.       X1     S.D.       X2     S.D.')
      TYPE 2007,PFIN,PSD,X1FIN,X1SD,X2FIN,X2SD
2007  FORMAT(6F8.2)
      TYPE 2008
2008  FORMAT(16X,'      Y1     S.D.       Y2     S.D.')
      TYPE 2009,Y1FIN,Y1SD,Y2FIN,Y2SD
2009  FORMAT(16X,4F8.2)
      TYPE 2010, POLTOT
2010  FORMAT(' POLARIZATION, STD X,Y; UNK X,Y: ', 4(F6.3,X),/
     A  ' STD F: ',F5.2,' UNK F: ',F5.2,////)
      RETURN
      END
```

```
      SUBROUTINE POWOPT
C             Routine to optimize power by turning mirror 3 by 50 steps
C     in each direction for both horizontal and vertical.  The mirror
C     setting is optimized by fitting a cubic to the power distribution.
C
      INTEGER ADDR, ADCADD(8), IPOW(101)
      INTEGER ISAVE(4)
      REAL X(101,4),XBAR(4),STD(4),D(10),SUMSQ(4)
      REAL RX(3,3),RY(3),DUM1(3),DUM2(3)
      REAL CUBIC(3),SB(3),T(3),ANS(10)
      COMMON/ADC/ ADCADD
      COMMON/DAC/ IM1X,IM3X,IM4X,IM1Y,IM3Y,IM4Y,IDIR
      DATA ITEN/716/
      DATA ISAVE/1,2,3,4/
CC
      ADDR=IM3X ! SET AXIS TO HORIZONTAL
      DO 1000 IAXIS=1,2
      NSTEP=1
1     CALL CSSA(16,IDIR,0) ! SET DIRECTION TO POSITIVE.
CCC
            DO 10 I=1,101
10          IPOW(I)=0
CCC
            DO 100 I=51,101
            DO 100 ISTEP=1,NSTEP
                  DO 110 M=1,500 ! PAUSE 12.5 ms (25 micro-s/null loop)
110               CONTINUE       ! WAIT FOR POWER TO SETTLE
CC
CC          READ POWER
            DO 120 J=2,8,2
            CALL CSSA(0,ADCADD(J),IP)
120         IPOW(I)=IPOW(I)+IP-2048 ! SUBTRACT 5 V OFFSET
CC
            CALL CSSA(16,ADDR,ITEN)
                  DO 130 M=1,60 ! PAUSE 1.5 ms.
130               CONTINUE      ! WAIT FOR DAC VOLTAGE TO SETTLE.
            CALL CSSA(16,ADDR,0) ! TAKE ONE POSITIVE STEP
100         CONTINUE
CCC
            DO 140 I=1,60
140         CONTINUE
CCC
      CALL CSSA(16,IDIR,ITEN) ! SET DIRECTION TO NEGATIVE.
CCC
            DO 200 I=1,101
            DO 200 ISTEP=1,NSTEP
            II=102-I
CC
            CALL CSSA(16,ADDR,ITEN)
                  DO 230 M=1,60
230               CONTINUE
            CALL CSSA(16,ADDR,0) ! TAKE ONE NEGATIVE STEP
CC
                  DO 210 M=1,500
210               CONTINUE
CC
CC          READ POWER
            DO 220 J=2,8,2
            CALL CSSA(0,ADCADD(J),IP)
220         IPOW(II)=IPOW(II) + IP -2048
200         CONTINUE
CC
CC
```

```
      CALL CSSA(16,IDIR,0) ! SET DIRECTION TO POSITIVE.
              DO 300 I=1,50
              DO 300 ISTEP=1,NSTEP
                      DO 310 M=1,500
310                   CONTINUE
CC
CC            READ POWER
              DO 320 J=2,8,2
              CALL CSSA(0,ADCADD(J),IP)
320           IPOW(I)=IPOW(I) + IP -2048
CC
              CALL CSSA(16,ADDR,ITEN)
                      DO 330 M=1,60
330                   CONTINUE
              CALL CSSA(16,ADDR,0) ! TAKE ONE POSITIVE STEP
300           CONTINUE
CC
CC
CCC     FIT A CUBIC TO THE POWER DISTRIBUTION.
      IFLAG=0
              DO 500 I=1,101
              IF(IPOW(I).NE.IPOW(1) .AND. IPOW(I).GT.0) IFLAG=1
              X(I,1) = I-51.
500           X(I,4) = IPOW(I)
      IF(IFLAG.NE.0) GO TO 501
CC
CC            IF THE BEAM IS OUT (ALL READINGS THE SAME), DOUBLE
CC            THE NUMBER OF STEPS TAKEN AND TRY AGAIN
              NSTEP=2*NSTEP
              IF(NSTEP.GE.8) GO TO 1000
              GO TO 1
CC
501   CALL GDATA(101,3,X,XBAR,STD,D,SUMSQ)
      CALL ORDER(4,D,4,3,ISAVE,RX,RY)
      CALL MINV(RX,3,DET,DUM1,DUM2)
      CALL MULTR(101,3,XBAR,STD,SUMSQ,RX,RY,ISAVE,CUBIC,SB,T,ANS)
      IMAX=0
      FMAX=0.
              DO 505 I=1,101
              XX=I-51.
              FX = CUBIC(1)*(XX) + CUBIC(2)*(XX)**2 + CUBIC(3)*(XX)**3
              IF(FX.LE.FMAX) GO TO 505
              FMAX=FX
              IMAX=I-51
505           CONTINUE
CCC
              TYPE *,IMAX
              TYPE *
      IF(IMAX)510,450,420
510   CALL CSSA(16,IDIR,ITEN) ! SET DIRECTION TO NEG. IF IMAX<0.
      IMAX=-IMAX
CC
420   DO 450 I=1,IMAX
      DO 450 ISTEP=1,NSTEP
              DO 430 M=1,60
430           CONTINUE
      CALL CSSA(16,ADDR,ITEN)
              DO 435 M=1,60
435           CONTINUE
      CALL CSSA(16,ADDR,0) ! STEP.
450   CONTINUE
CC
CC


450   ADDR=IM3Y ! SET AXIS TO VERTICAL
1000  CONTINUE
      RETURN
      END
```

References

and

Figures

References

1. W. C. Clark, ed. Carbon Dioxide Review: 1982. Oxford University Press, NY, 1982.

2. G. Marland and R. M. Rotty. Carbon Dioxide Emissions from Fossil Fuels: A Procedure for Estimation and Results for 1950-1981. DOE report TR003, NTIS (U. S. Dept. of Commerce, Springfield, Virginia 22161), 1983.

3. B. Bolin. "Changes in Land Biota and Their Importance for the Carbon Cycle." Science 196 (1977). p. 613.

4. G. M. Woodwell et al. "Global Deforestation: Contribution to Atmospheric Carbon Dioxide." Science 222 (1983). p. 1081.

5. W. Seiler and P. J. Crutzen. "Estimates of Gross and Net Fluxes of Carbon Between the Biosphere and the Atmoshpere From Biomass Burning." Climatic Chjange 2 (1980). p. 207.

6. S. Brown, ed. Global Dynamics of Biospheric Carbon. DOE report 019, NTIS, 1982.

7. W. S. Broecker et al. "Fate of Fossil Fuel Carbon Dioxide and the Global Carbon Budget." Science 206 (1979). p. 409.

8. L. Machta and E. Hughes. "Atmospheric Oxygen in 1967 to 1970." Science 168 (1970). p. 1582.

9. R. L. Schwiesow and V. E. Derr. "A Raman Scattering Method for Precise Measurement of Atmospheric Oxygen Balance. JGR 75 (1970). p. 1629.

10. S. P. S. Porto. "Angular Dependence and Depolarization Ratio of the Raman Effect." J. Opt. Soc. Am. 56 (1966). p. 1585.

11. M. Born. Optik. Springer Verlag, Berlin, 1933. p. 349.

12. J. M. Cherlow & S. P. S. Porto. Laser Raman Spectroscopy of Gases, Chapter 4 in Laser Spectroscopy of Atom and Molecules. H. Walther, ed. Springer Verlag, Berlin, 1976.

13. A. R. Adamson. Physical Chemistry of Surfaces 4th Edition. John Wiley & Sons, New York, 1982. p. 537.

14. E. A. Brandes, ed. Smithell's Metals Reference Book 6th Edition, Butterworths, London, 1983. Ch. 12.

15. R. A. Hill and D. L. Hartley. "Focused, Multiple-Pass Cell for Raman Scattering." Applied Optics 13 (1974). p. 186.

16. R. J. Roark and D. Young. Formulas for Stress and Strain. 5th Edition. McGraw Hill, New York, 1975.

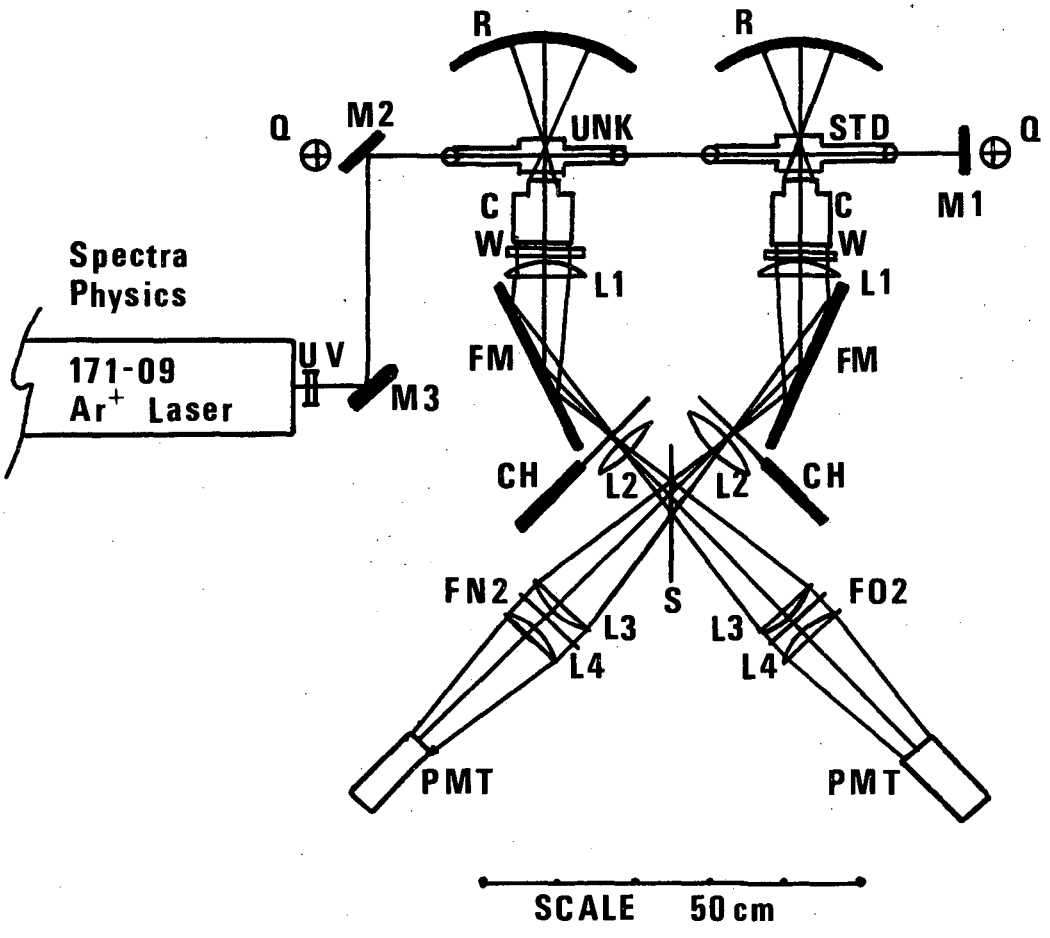

Figure 1. Original set-up with central beamsplitter. UV: BK-7 glass flat, blocking UV light from laser plasma; M1, 2, 3: flat beam steering mirrors, M1 defines the end of the laser cavity; Q: quadrant detectors; R: spherical mirrors; C: Canon lenses; W: half wave plates; FM: flat mirrors for steering beam of scattered light; CH: tuning fork light choppers; S: 50/50 dielectric beamsplitter; F: bandpass interference filters.

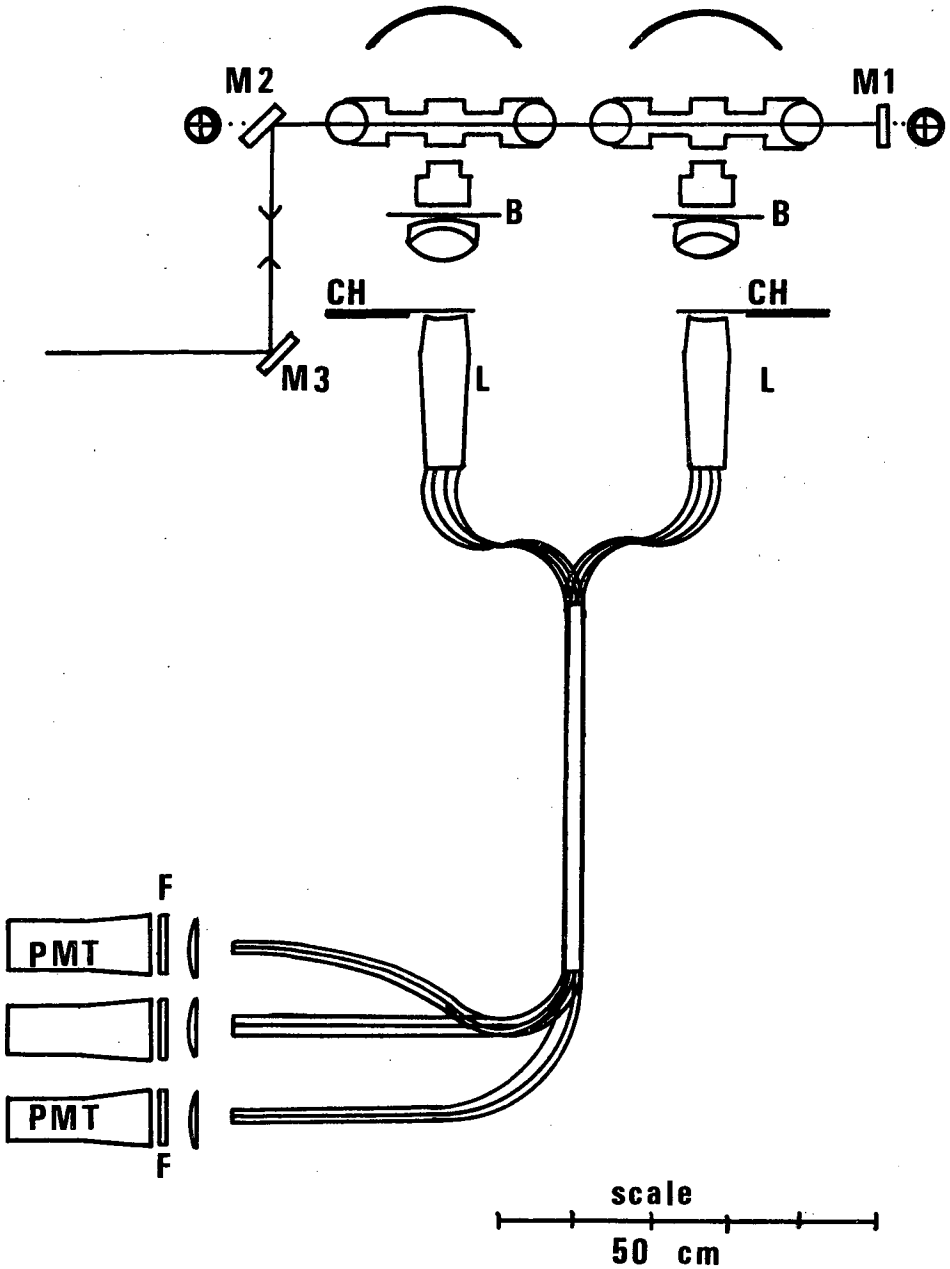

Figure 2. Fiberoptic light collection and mixing scheme. Additional symbols are: B: Rayleigh light blocking filters; L: lucite entrance cones.

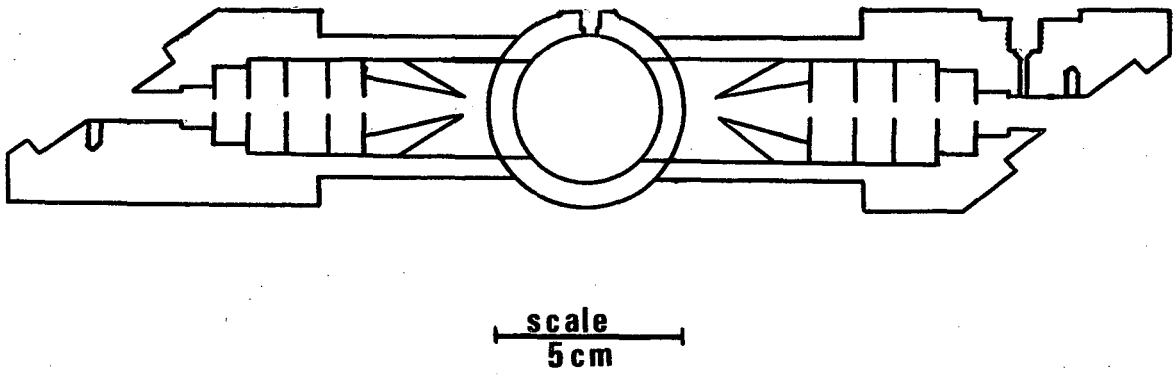

Figure 3. Side view of intra-cavity target cell. The beam enters and exits through the side arms outfitted with Brewster angle windows. Each arm contains a set of internal apertures to block and trap the very bright scattering generated where the beam goes through the window. Raman scattered light is collected through the front and back window of the central cylindrical cell. A narrow peekhole is provided on top to monitor the polarization of the beam.

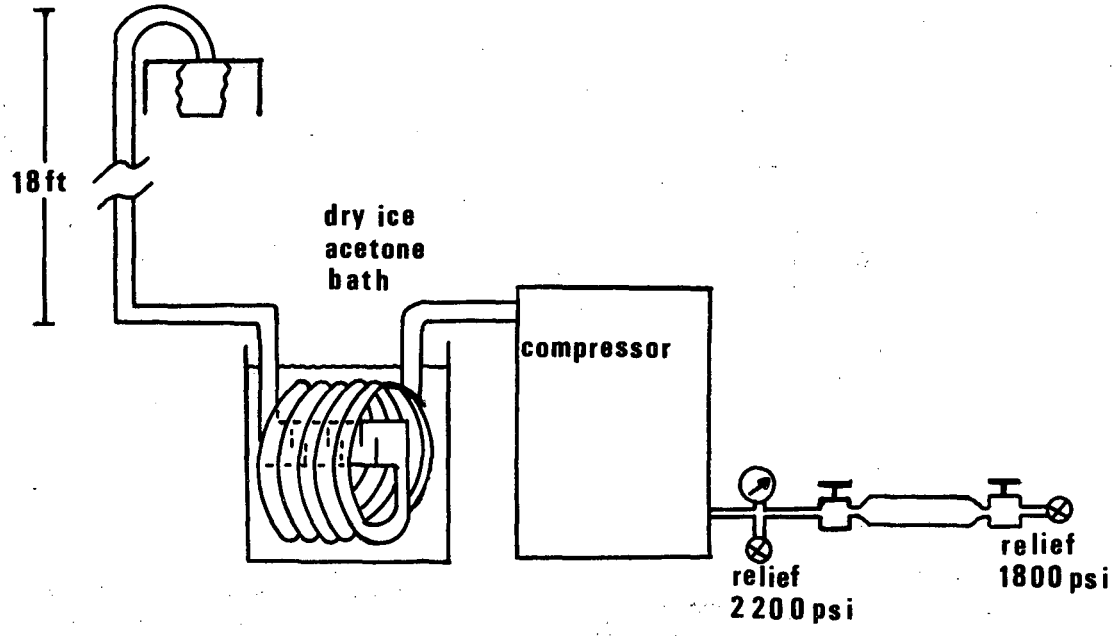

Figure 4. Schematic sample collection system. The intake tower consists of 3 6-foot sections of stainless steel tubing fitted together with swagelok connectors. A glass fiber dust filter is mounted on the intake. Before entering the compressor the air is dried cryogenically.

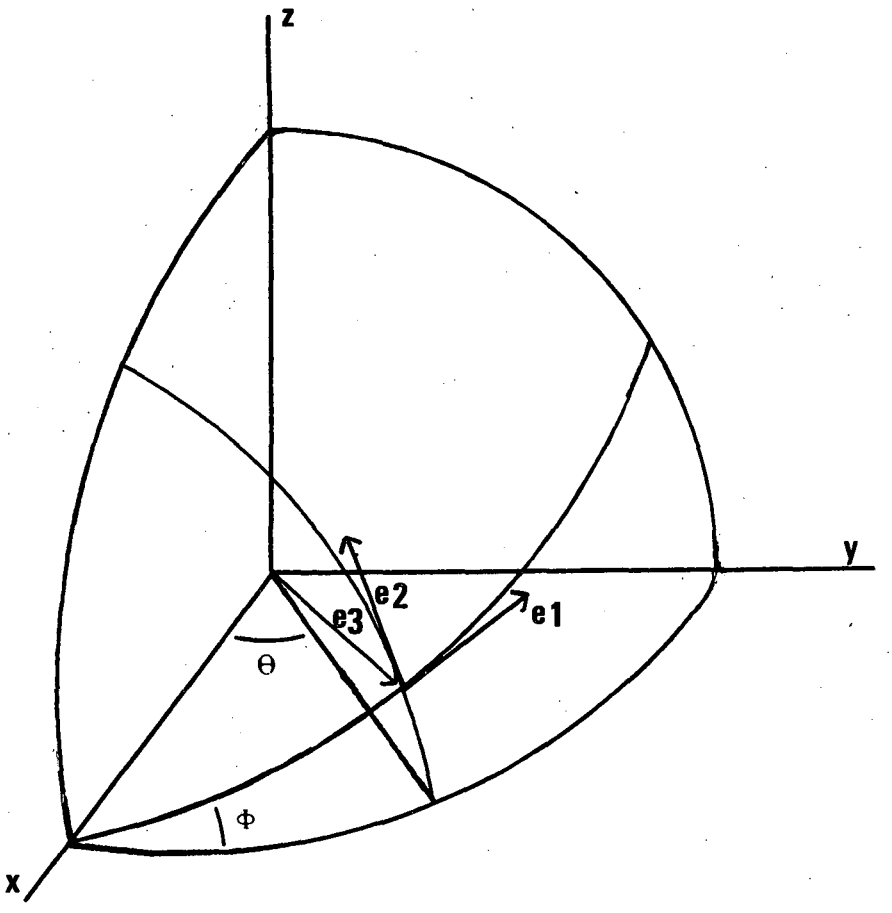

Figure 5. Scattering coordinates. The laser beam travels along the Y-axis. Raman light is collected inside a cone centered on the X-axis. Z is the vertical axis along which the polarization of the laser is directed.

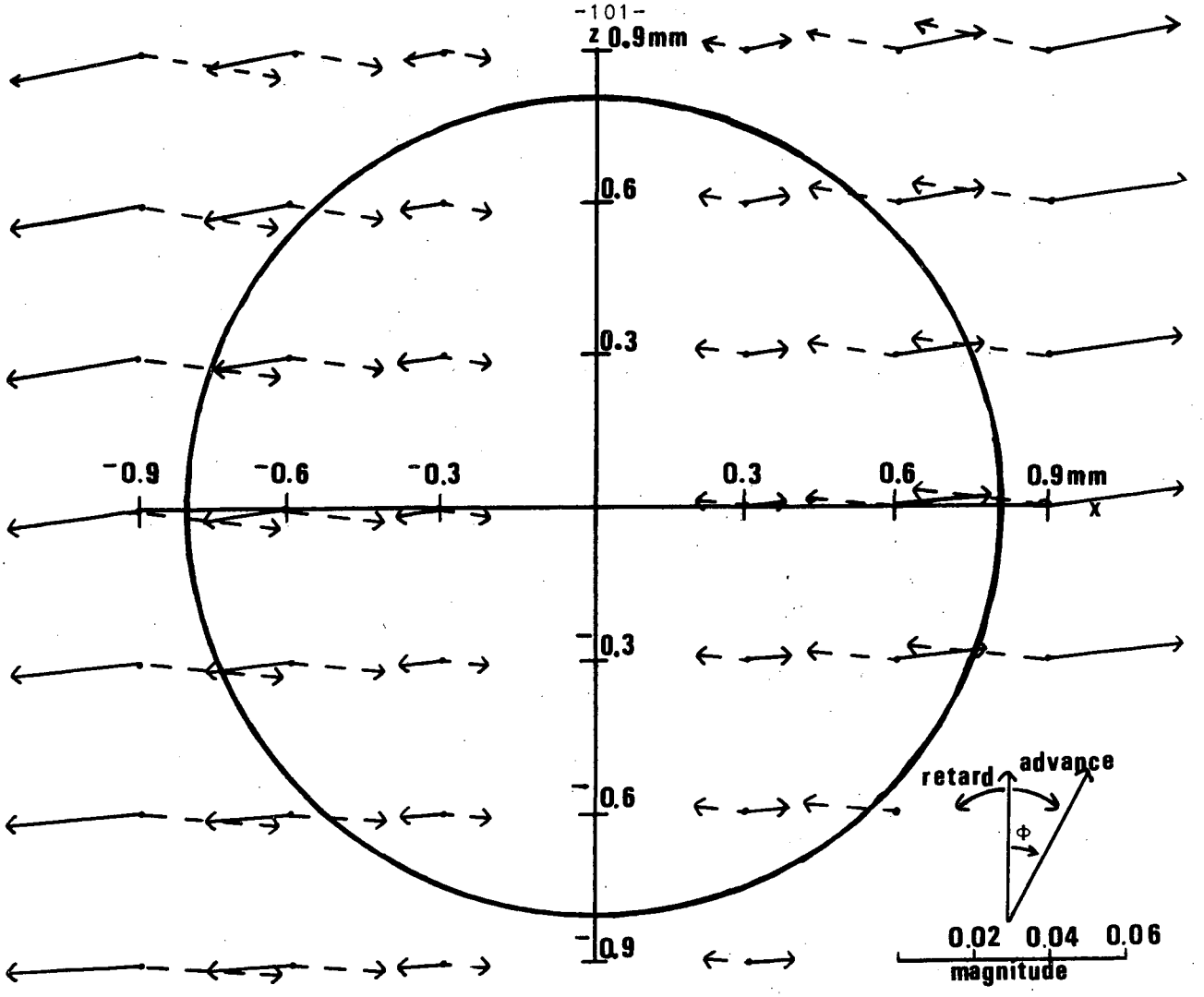

Figure 6. Generation of a horizontal polarization component in the Brewster window under stress. The $1/e^2$ intensity contour of the laser beam is indicated by the circle. The length of the arrow gives the amplitude of the X-component as a fraction of the Z-component amplitude. The angle from the vertical indicates the phase difference from the Z-component, with a phase advance in the clockwise direction. The main effect of the window is the generation of elliptically polarized light, although there is also some turning of the linear polarization away from the Z-axis. The broken lines represent the effect due to the opposite window on the other arm of the target cell.

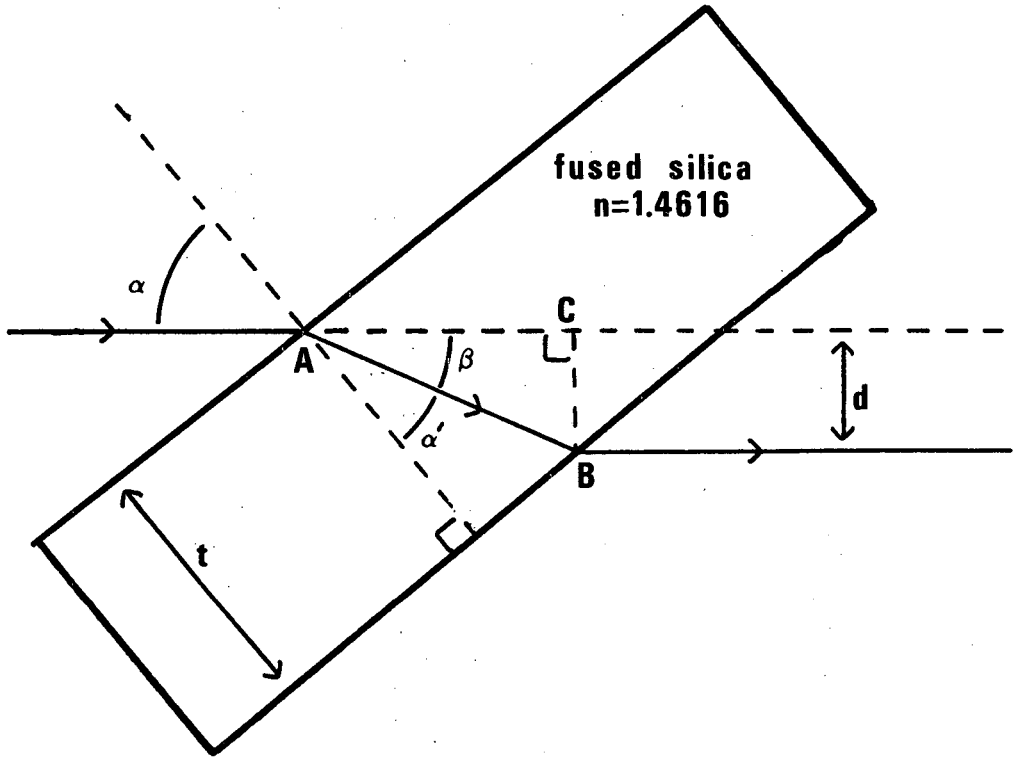

Figure 7. Beam offset through fused silica Brewster's window.

d = offset

α = 55.62°, (55°37'), Brewster's angle

β = α - α' = 21.24°

α'= 34.38°

t = window thickness

AB= t/cosα'

d = BC = ABsinβ = tsin(α - α')/cosα'

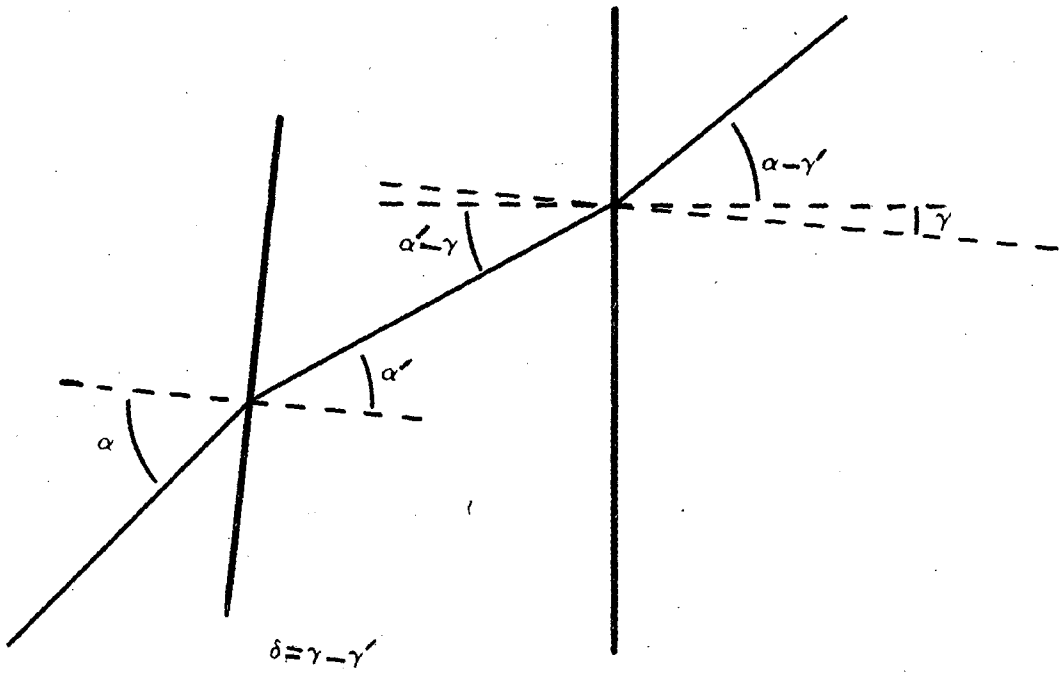

Figure 8. Beam angle deviation, δ, caused by wedge angle γ of the two faces of the Brewster's window.

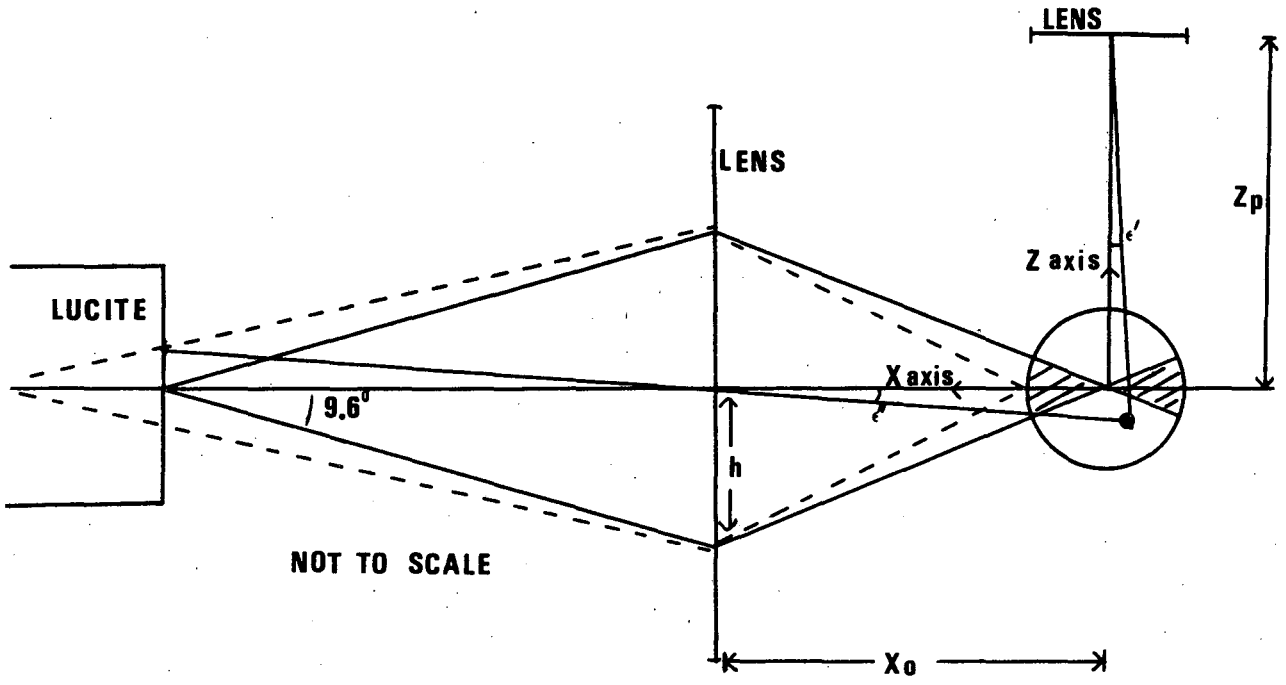

Figure 9. Imaging of a finite beam onto the lucite entrance sheet of the fiber optics. The coordinate origin is where the beam should be centered; it is imaged exactly on the center of the lucite. Light originating from a point $x > 0$ away from the origin is imaged inside the lucite, at a depth of 2.5 mm (if index n=1 in lucite) for every mm of translation in the object space (broken line). The opening angle is 9.6° so that the radius of the blur spot is $2.5 \times (\tan 9.6°) = 0.42$ mm. In the object space this corresponds to 0.42/1.55 (magnification) = 0.27 mm. A point at x=1 on the radius 0.27 mm in object space will then just contribute the edge of its blur spot on the lucite to the intensity at the center.

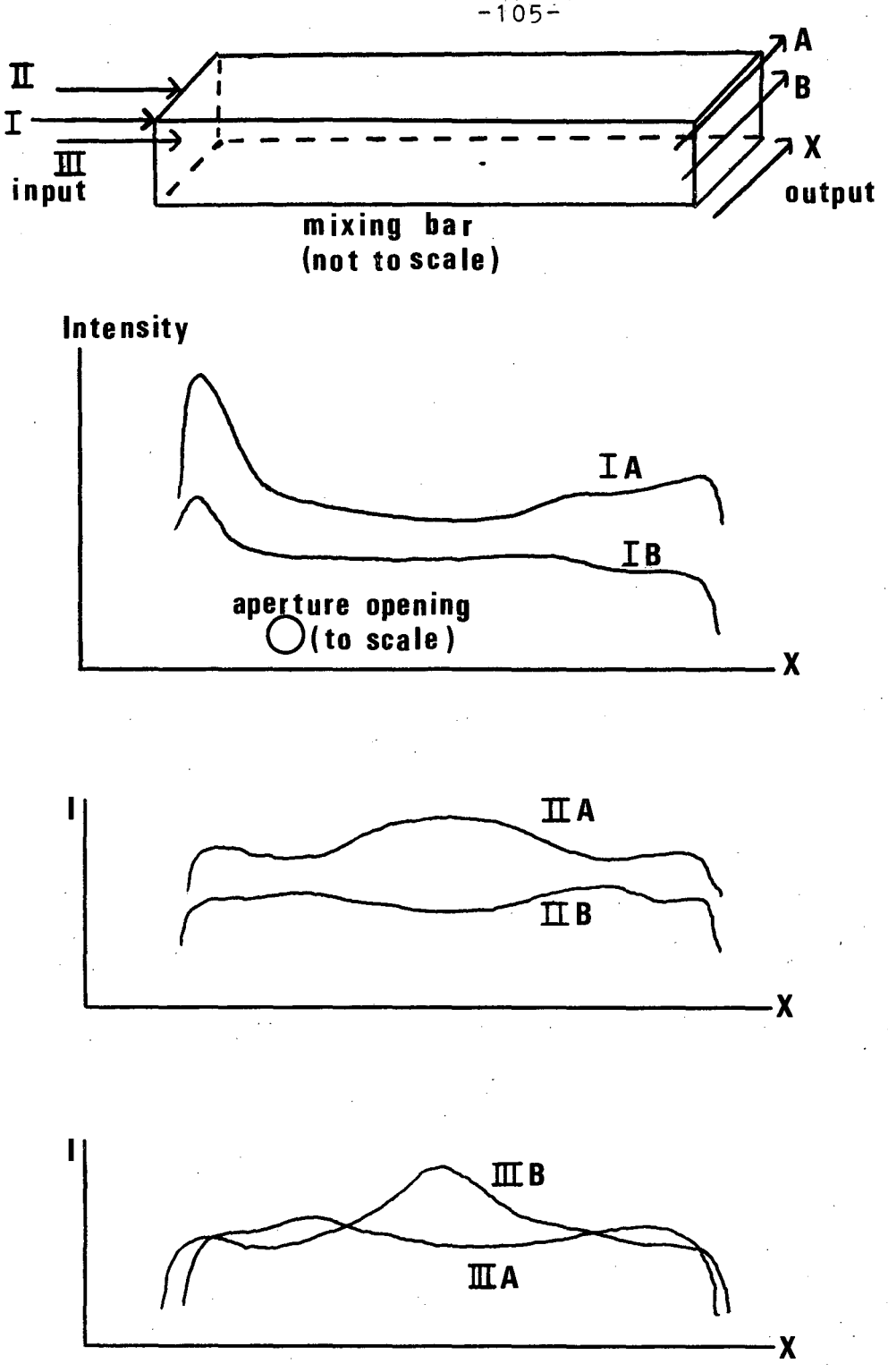

Figure 10. Transmission through the central lucite mixing bar. The test beam (He-Ne) was pointed at points I (corner), II (middle of upper edge) and III (center of bar). The output was scanned by a 1 mm circular aperture along tracks A and B. The three graphs display the intensity as a function of the horizontal scan distance.

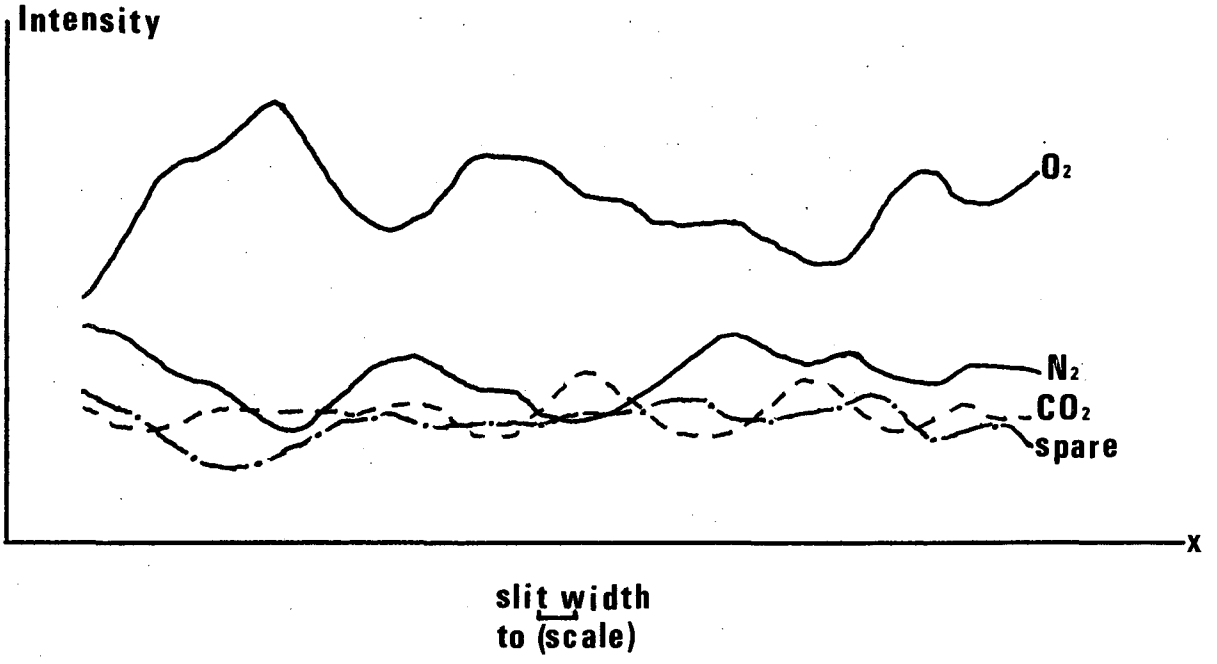

Figure 11. Transmission through output fiber bundles. The front end which abuts the lucite mixing bar is illuminated through a vertical slit of 0.025" width. The outputs of each of the 4 prongs are recorded while the slit moves in the horizontal direction.

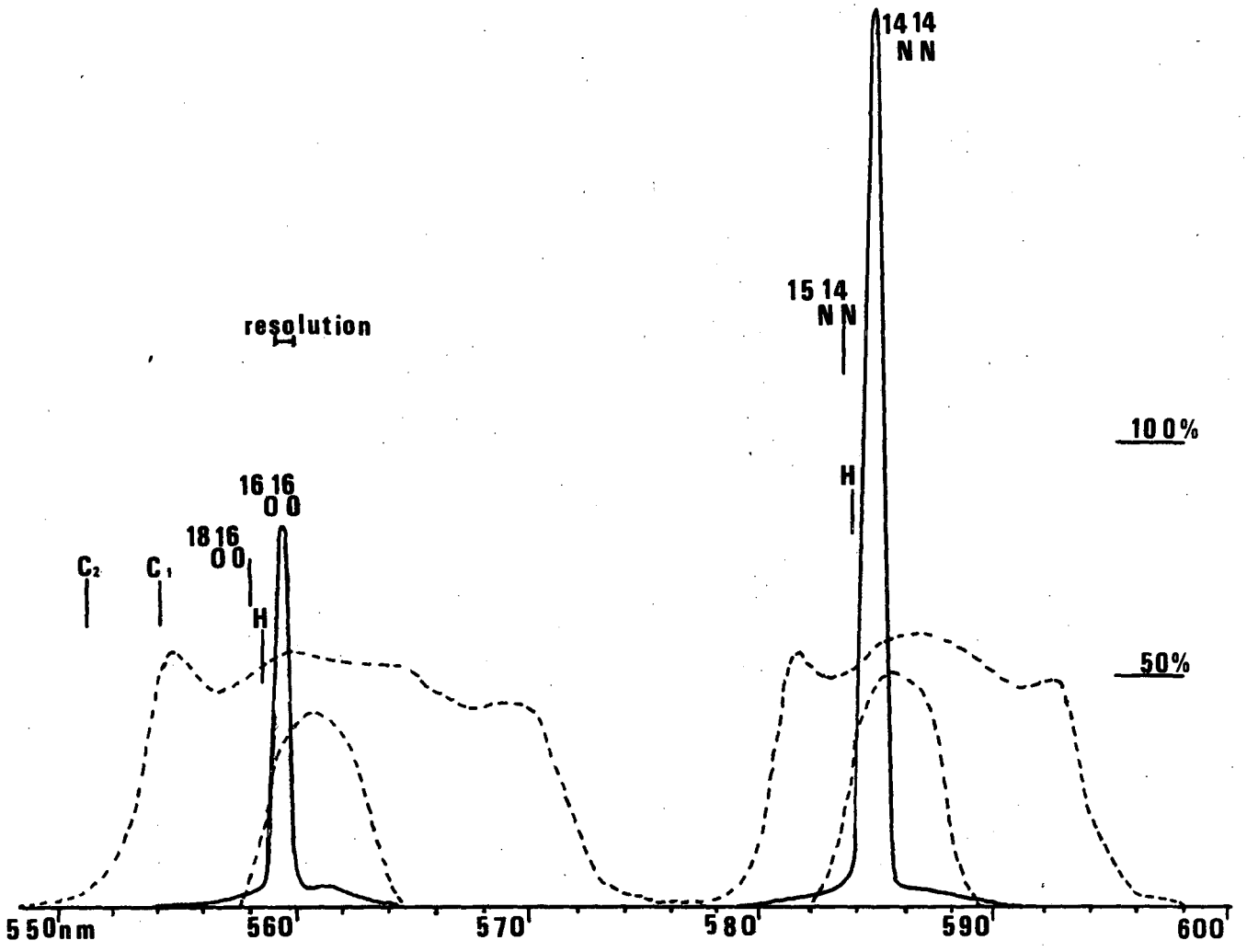

Figure 12. Raman bands of oxygen and nitrogen and filter transmission characteristics. The Raman bands are the full curves labeled $^{16}O^{16}O$ and $^{14}N^{14}N$ as measured on our spectrometer (SPEX 1672, resolution 10 A) with laser excitation at 514.5 nm. The pedestals are the O- and S-rotational side branches on either side of the vibrational Q-branch. The locations of the Q-branch centers for the isotopic molecules and the vibrational hot band are indicated by arrows. The two arrows labeled C_1 and C_2 point to the location of the CO_2 Raman line pair at 1388 cm^{-1} and 1286 cm^{-1} respectively. The broken lines display the transmission characteristics for the various filters as measured by the manufacturer.

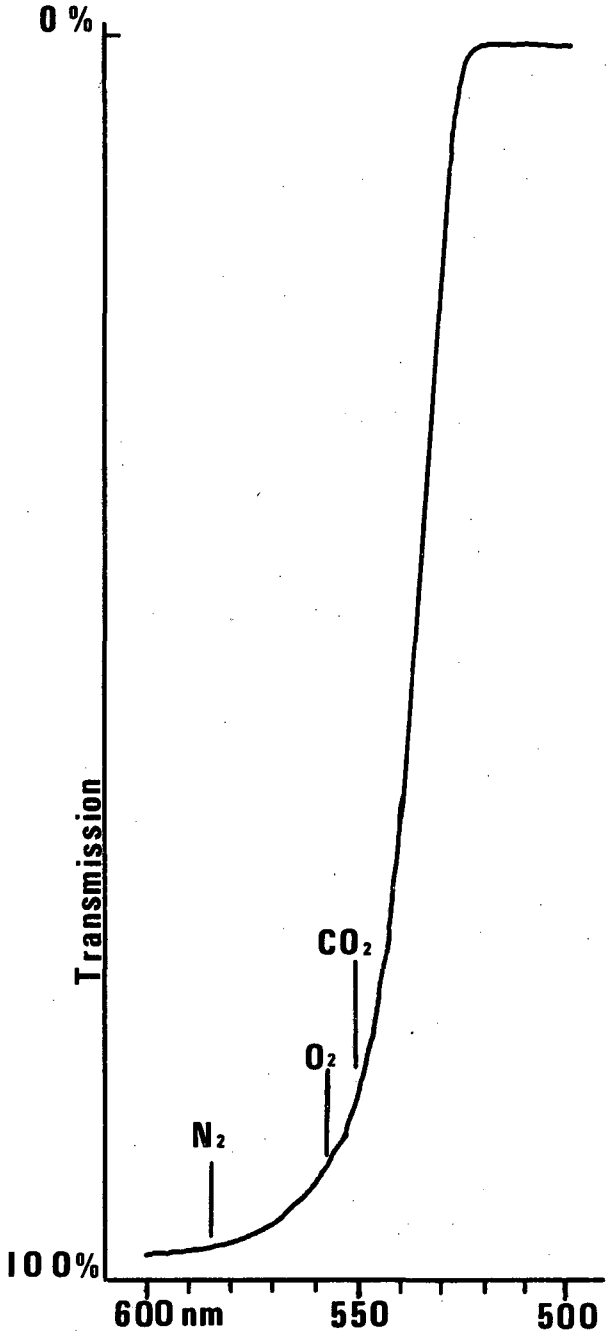

Figure 13. Transmission through the Schott glass OG 530 (6 mm thick).

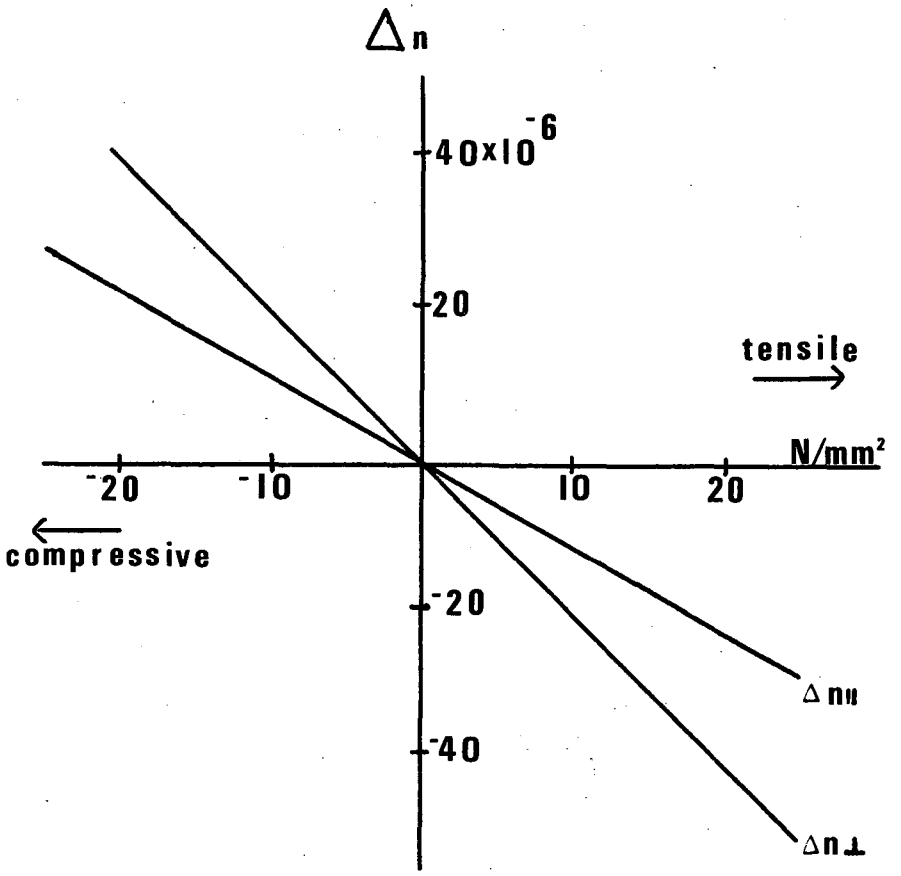

Figure A1. Birefringence in glass. The values are typical for many glasses. Depicted is the change in index for light polarized parallel and perpendicular to the direction of stress. Specifications for glasses usually give the difference between parallel and perpendicular index as the stress optical coefficient.

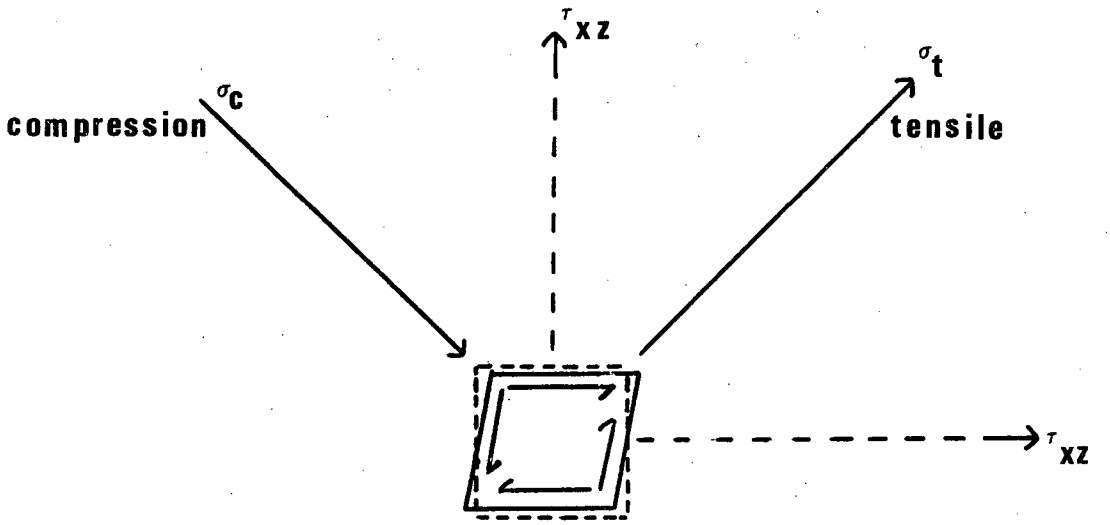

Figure A2. Transformation of a pair of shear stresses into a tension-compression pair along different axes.

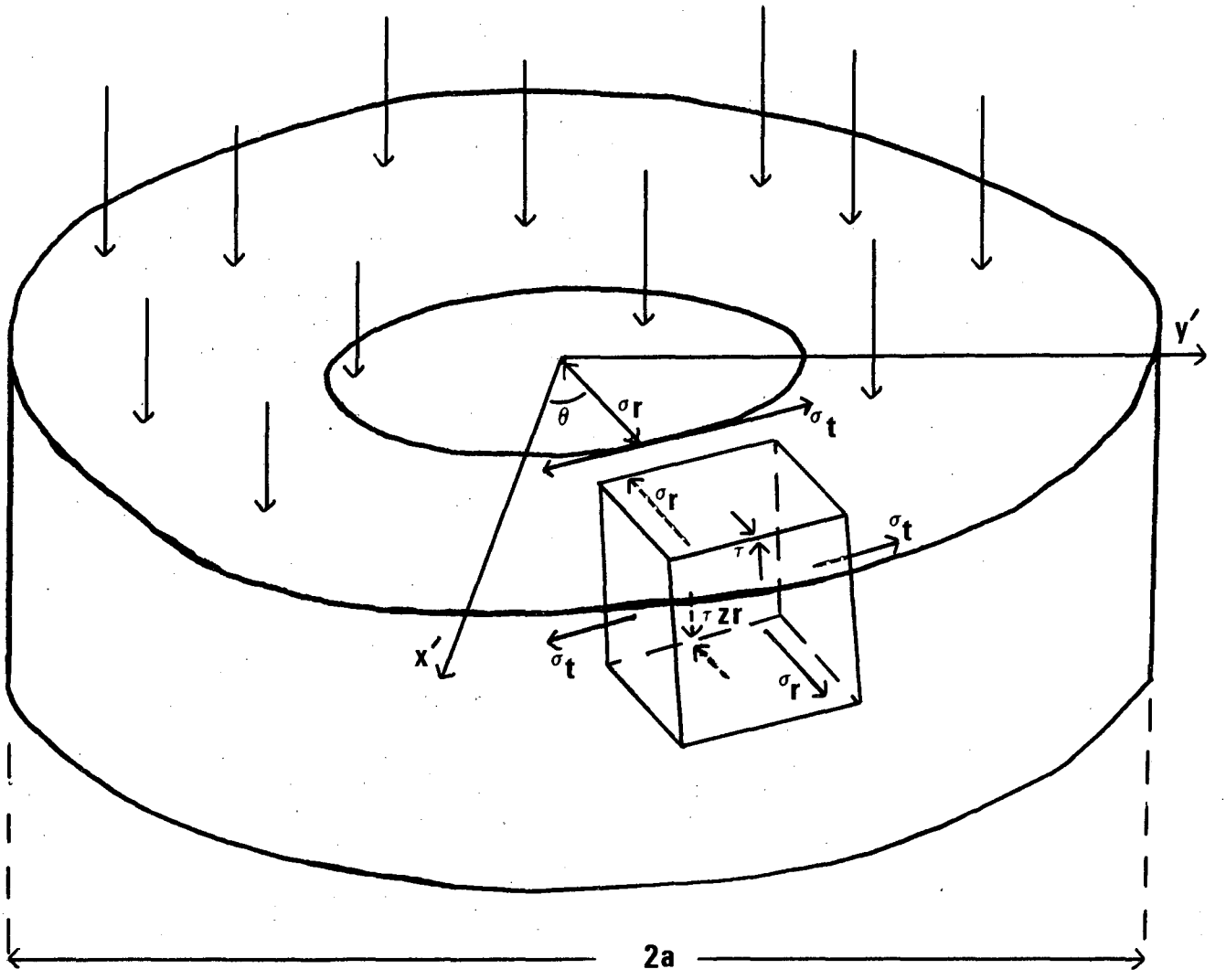

Figure A3. Coordinates in a window. σ_r is the radial, σ_t the tangential stress. θ is the angle from the horizontal (x') coordinate axis on the surface of the window. Because the window is tilted at Brewsters angle (α) with respect to the beam, its coordinate system (x', y', t') has been rotated by $(90 - \alpha)°$ around the horizontal axis x. Also shown is a block of internal material with σ_r, σ_t and the shear stresses τ_{zr}. z = 0 is the midplane of the window.

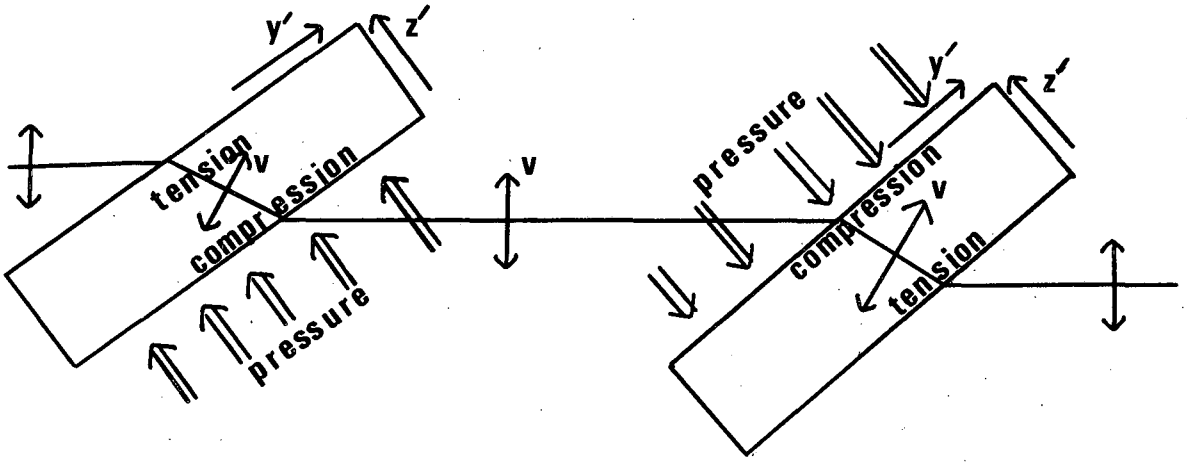

Figure A4. Coordinates of two windows on either side of a target cell.

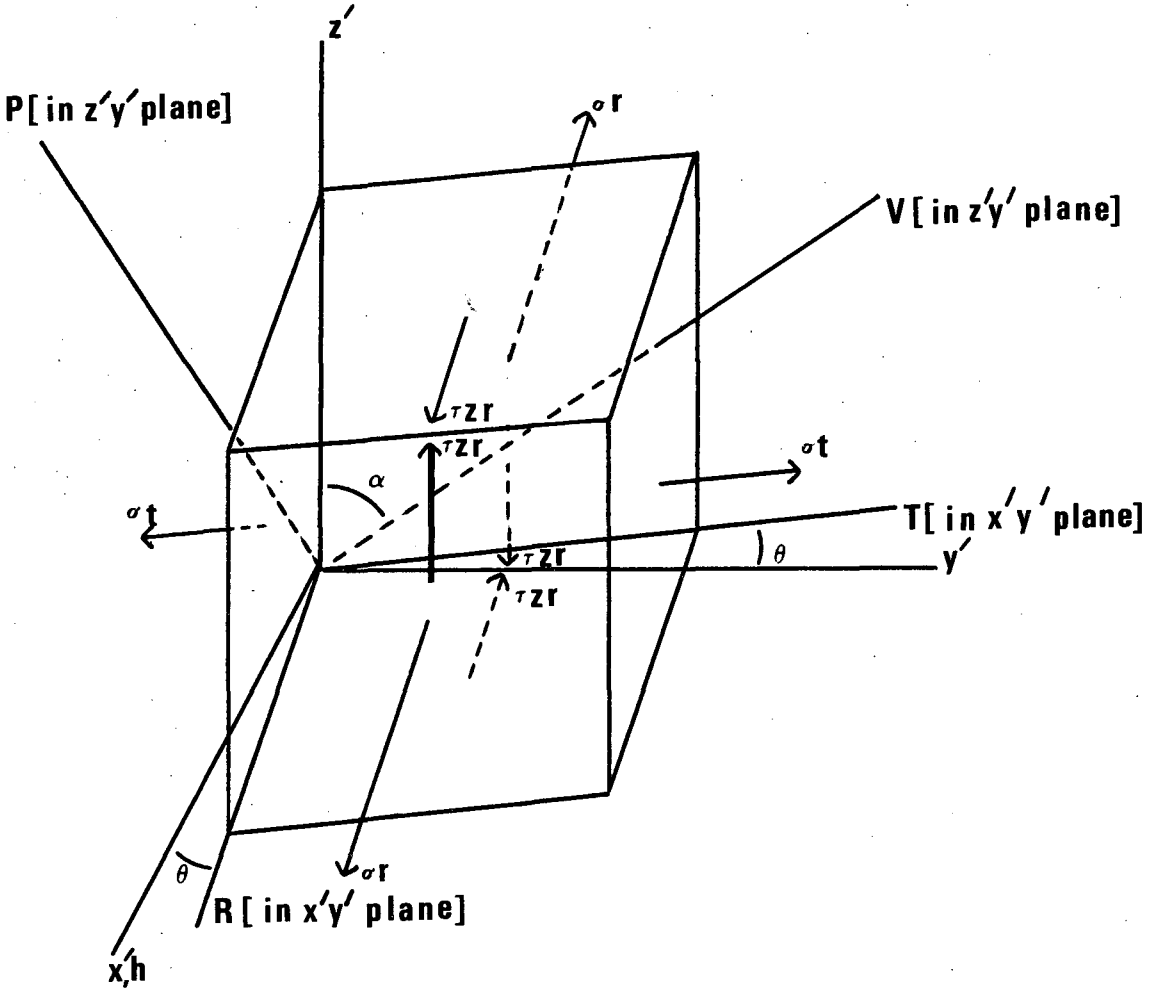

Figure A5. Transformation of stresses to beam coordinates in an elementary block of material inside the glass.

This report was done with support from the Department of Energy. Any conclusions or opinions expressed in this report represent solely those of the author(s) and not necessarily those of The Regents of the University of California, the Lawrence Berkeley Laboratory or the Department of Energy.

Reference to a company or product name does not imply approval or recommendation of the product by the University of California or the U.S. Department of Energy to the exclusion of others that may be suitable.

LAWRENCE BERKELEY LABORATORY
TECHNICAL INFORMATION DEPARTMENT
UNIVERSITY OF CALIFORNIA
BERKELEY, CALIFORNIA 94720